



University of
Stavanger

Faculty of Science and Technology

MASTER'S THESIS

Study program/ Specialization:
Petroleum Engineering/Drilling
Technology

Spring semester, 2014

Open

Writer:
Su Wai Aung Khaing

.....
(Writer's signatures)

Faculty supervisors:

Bernt Aadnøy and Mesfin Belayneh

Thesis title:

“Characterization and Performance of 70/30 and 90/10 OBM mud systems”

Credits (ECTS): 30

Key words:

OBM, Bridging, Rheology, Hydraulics, ANSYS
Wellplan/Landmark

Pages: 102

+enclosure:16

Stavanger, 16.06.2014

Acknowledgements

First of all, I would like to express my deepest appreciation and gratitude to my supervisor Mesfin Belayneh, who gave me substantial amounts of his time and excellent guidance throughout the entire thesis work. And I would like to thank him for his tireless support and providing me immense knowledge through the learning process of this master thesis. I also would like to give a special gratitude to Professor Bernt S. Aadnøy for providing me the project, for discussion and guidance during the thesis work.

Special thanks to my parents for being supportive and for their encouragement in my academic life ever since my childhood. And thanks to my brother, Phyo N. Aung Khaing, and my fiancé, Naw Wai W. Aung, for being supportive and their help.

Furthermore I also would like to thank to Eng. Sivert B. Drangeid for helping me with practical guidance in experiment with High Pressure High Temperature Filtration Test. I would also like to thank Eng. Kim Andre for helping me with Visco-elasticity tests. And I also would like to thank my friend Mahmoud Sami Alaassar who helped me a guidance of using ANSYS Simulation for my thesis.

Finally, I would like to thank MI-Swaco for providing us 70/30 and 90/10 OBM drilling fluids and for technical discussion with Richard Gyland during the 70/30 ES modification.

Stavanger, June 2014

Abstract

Drilling fluid is an essential part of drilling operation. The main functions of the drilling fluid are to transport cutting, to maintain well pressure and cooling formation and drill-bit. The detail knowledge of drilling fluid is very important to design safe and proper drilling operations.

This thesis presents the characterization and performance evaluation of 70/30 and 90/10 Oil Water Ratio of Oil Based Mud systems. The characterization is through direct experimental measurements and the performance is through simulation and experimental studies as well.

Table of Contents

ACKNOWLEDGEMENTS	1
ABSTRACT.....	2
1 INTRODUCTION	6
1.1 Background	6
1.2 Problem Formulation	8
1.3 Objective	9
2 LITERATURE STUDY	10
2.1 Well Program	10
2.2 Well fracture models	11
2.2.1 Non-penetrating fracture model	11
2.2.2 Penetrating fracture model	12
2.3 Well Collapse.....	13
2.4 Stress Cage Theory	14
2.4.1 Alberty’s Interpretation of Stress Cage.....	14
2.4.2 Aadnøy’s Interpretation of Bridging and Fracture Propagation Process	17
2.5 Visco-elasticity	19
2.5.1 Fundamental Viscoelastic Theory.....	20
2.5.2 Linear Viscoelastic Region (LVER)	21
2.5.3 Oscillatory Test: Amplitude Sweep	21
2.5.4 Oscillatory Test: Frequency Sweep	22
2.6 Lost Circulation	23
2.7 Drilling Fluid, Rheology and Hydraulics.....	25
2.7.1 Drilling Fluid Types.....	25
2.7.2 Drilling Fluid Rheology Model.....	26
2.7.2.1 Newtonian Model	27
2.7.2.2 Bingham Plastic Model.....	27
2.7.2.3 Power Law Model.....	28
2.7.2.4 Herschel-Buckley.....	28
2.8 Hydraulics Models	29

3 EXPERIMENTAL DRILLING FLUID CHARACTERIZATION	33
3.1 Fann 35 - Viscometer ES and Density Measurement of 70/30 & 90/10 OBM.....	33
3.2 HPHT Static Filtration and ES Measurement	36
3.2.1 Rheology Modeling and Analysis of 70/30 OBM	40
3.2.2 Rheology Modeling and Analysis of 90/10 OBM	42
3.2.3 Temperature Dependent Plastic Viscosity Modeling of 70/30 & 90/10 OBM	43
3.2.4 Temperature Dependent Yield Stress Modeling of 70/30 & 90/10 OBM.....	45
3.2.5 Hydraulic Simulation and Analysis	46
3.2.5.1 Experimental arrangement	46
3.2.5.2 Simulation result	48
3.3 Flow in Sand Pack Porous Media of 70/30 & 90/10 OBM.....	51
3.4 Visco-elasticity Test.....	53
3.4.1 Oscillatory Amplitude Sweep Tests-70/30 OBM and 90/10 OBM	54
3.4.2 Oscillatory Frequency Sweep Test 90/10 OBM	56
4 DRILLING FLUID PERFORMANCE EVALUATIONS.....	57
4.1 Bridging Experimental Study	57
4.1.1 Experimental Arrangements and Test Procedure.....	57
4.1.2 Description of Drilling Fluids	59
4.1.3 Description of Particle – LC-lube	60
4.1.4 Bridging Test Results and Analysis	62
4.1.4.1 Bridging Test Result Summary.....	62
4.1.4.2 Test with 70/30 OBM vs 90/10 OBM.....	62
4.1.4.3 Comparison and Analysis of the Experimental data.....	65
4.2 Hole Cleaning Efficiency of the 90/10 and 73/30 OBM systems.....	68
4.2.1 Simulation Setup	68
4.2.2 Simulation Performance Result and Analysis.....	70
4.3 Hydrodynamic Force Effect of 90/10 & 73/30 OBM Systems on Hook Load	74
5 SIMULATION AND ANALYSIS OF MUD SYSTEMS	76
5.1 Numerical Bridging Simulation	76

5.2 Model Generation Loading and Material Properties.....	77
5.2.1 Model Scenario 1-Refernce model.....	77
5.2.2 Model Scenario 2-Model based on Alberty’s interpretation.....	82
5.2.3 Model Scenario 3-Model based on Aadnøy’s interpretation	85
6 SUMMARY AND DISCUSSION.....	90
7 CONCLUSION	95
8 FUTURE WORK.....	98
REFERENCE.....	99
APPENDIX	103
Appendix A: Rheology Models and Model Parameters	103
Appendix B: Bridging Tests70/30 & 90/10 OBMs after 10, 15 & 20 min.....	106
Appendix C: Thermal conductivity of drilling fluid.....	108
Appendix D: Hydrodynamic Force Effect on Hook Load – Tripping In.....	112
Appendix E: Hole and drill string data for simulating §4.2 & §4.3.....	114
LIST OF FIGURES	115
LIST OF TABLES	117
NOMENCLATURE.....	118

1 Introduction

This thesis presents the characterization and performance of the 90/10 and the 70/30 oil water ratio (OWR) of Oil-Based Mud systems. The characterization and comparisons are based on direct measurement and indirectly based on their performances.

Measurement and modeling

- The temperature dependent rheological properties, HPHT filtrate, Flow in porous media, the physical, and the viscoelastic properties will be measured.
- Based on the measurement, hydraulics simulation and rheology modeling will be performed.

Performance evaluation:

The performance of the drilling fluid depends on its properties. The performance evaluation of the two drilling fluid systems will be investigated through experimental and simulation studies such as:

- Bridging experiment
- Hole cleaning simulation and
- Torque and drag simulation

In addition, a finite element simulation studies will be performed in order to analyze the stress cage interpretations presented by Alberty et al [9] and Aadnøy et al [13].

1.1 Background

An oil or gas well simply cannot be drilled without continuous circulation of the drilling fluid to facilitate drilling the hole. The functions of drilling-fluid are to (a) Transport drilled cuttings to the surface, and b) Maintain well pressures. Additionally, to cool and lubricate the bit and drill string, buoy the weight of the drill string and casing, and help obtain information on subsurface formations [2][19][23].

While providing these functions, the drilling fluid should not cause side effects. The productive formations are not caused damage by the drilling fluid. Filtration control additives in drilling minimize formation damage [2].

Lost circulation is the most common problem in the drilling industry [3] [4]. The loss of drilling fluid occurs through excessive mud pressures induced fracture and also through a pre-existing open fracture. The problem can be minimized by loss circulation material additives in a drilling fluid [4] [10].

Due to drilling fluid and formation physicochemical interaction the wellbore might be unstable. For instance due to the fluid filtrate into the formation may cause pore pressure build up and weaken the formation strength. The temperature and pressure affects the rheology and the physical properties of the drilling fluid. This as a result affects the hydraulics of the drilling fluid.

Wellbore stability is a complex subject, which integrate mechanical, thermodynamic and fluid mechanical and chemistry [2]. Since the introduction of wellbore stability, several researches through experimental, modeling and numerical means have been performed. Despite the efforts, still the problem of well stability is not a completely solved subject.

One of the backgrounds this thesis is the experimental study performed on 80/20 and 60/40 OBM mud systems [11]. The studies show that the mechanical and petro-physical properties of mud cake determine the strength of mud cake, which indirectly determine the bridging and wellbore strengthening performances.

This thesis tries to characterize the properties of the 90/10 and 70/30 Oil-Based Mud (OBM) systems. In addition, the thesis will look into analyzing the performance the drilling fluid fluids.

1.2 Problem Formulation

In reference [9], the authors have presented a stress cage theory stating that the particles increase the hoop stress and therefore the well is strengthening. In reference [13], the authors have presented the process of cylindrical bridge forming at the mouth of a fracture and carrying well pressure and increasing the well strength. As the bridge collapse the communication between the well and the fracture further allow fracture growth. This is because the stress concentration will be increasing due to the pressure on the face of the fracture. Bridging is a key factor for hindering the possible stress field increase at the tip of the fracture and hence hinders the fracture propagation. Reference [11] presented bridging experimental study of the comparisons of 80/20 and 60/40 OMB systems with respect to bridging performances at various fracture widths. However the work didn't study characterize the drilling fluid properties in detail.

Having the mentioned works earlier as background, this thesis work is to study further with more detail to characterize the properties of the 90/10 and 70/30 OBM mud system through directly and indirectly performances. Figure 1.1 shows the picture of the mud systems. As shown, the 90/10 consists of about three times more filtrate than the 70/30 OBM.



Figure 1.1: Illustration of the 70/30 & 90/10 Oil Based Mud systems

This thesis addresses issues such as:

- What is the temperature effect on the rheology of the drilling fluids?
- What is the filtrate of the two mud systems at higher temperature?
- What are the thermo-physics parameters of the 90/10 and 70/30 mud systems?
- What are the visco-elastic behavior of the 91/10 and 70/30 mud systems?
- What is the stress distribution as the particle plug at the mouths and tip of a fracture?
- What are the bridging performance of the 90/10 and 70/30 mud systems?
- What are filtrate behaviors of the 90/10 and 70/30 mud systems in porous media?

1.3 Objective

In this thesis, the performance of 90/10 and 73/30 Oil-Based Mud systems are characterized and evaluated by using experimental and numerical methods. The activities are:

- Literature study to be used to analyze the mud systems.
- Experimental measurement and modelling of measured data
- Finally performance evaluation of the mud system through simulation studies

2 Literature Study

Drilling fluid is associated with several drilling operations such as hole cleaning, well stability, torque and drag. The rheology, density and visco-elasticity properties determine the performance of drilling operations. This section presents the theories associated with the problems mention above. Later the stress case phenomenon will be analyzed with ANSYS finite element numerical study in order to learn more about the stress conditions at a tip of a fracture and around a wellbore.

2.1 Well Program

Wellbore instability is one of the major problems encountered during drilling [1][3][5]. The borehole problems can be analyzed by using the stresses around the wellbore. There are two main wellbore failure mechanisms which could occur during drilling and completion operations. These are wellbore fracture and wellbore collapse failures [5][6]. The problem of well fracturing results lost circulation and the problem of well collapse results mechanical drill string sticking. The well bore instability problem alone increases the drilling budget by 10%, which is several billions per year [37].

To avoid or mitigate the problem, it is important to predict the appropriate circulation mud weight, which is between the well collapse and the well fracture profiles. The well pressure is a function of static mud weight and the friction loss. The friction loss term is a function of the drilling fluid properties. Thus characterization of drilling fluid properties is an important subject in order to predict the desired mud weight during drilling operations. The dynamics circulation pressure is given as [19]:

$$ECD = \rho + \frac{\Delta P_f}{gh} \quad (1.1)$$

Where, ρ = the static mud weight and ΔP_f = dynamic friction loss, g = acceleration due to gravity and h = True vertical depth

2.2 Well Fracture Models

Drilling fluid is lost when the minimum effective principal stress at the wellbore exceeds the tensile strength of the formation [5][6]. The following sections review non-penetrating and penetrating well fracture models.

2.2.1 Non-penetrating fracture model

The non-penetrating or impermeable well boundary condition assumes that there is no or minor communication between the well and the formation. This is due to the formation petro-physical properties and the quality of mud cake. Figure 2.1 illustrates a non-penetrating boundary condition between the borehole and the formation. This condition doesn't cause pore pressure build up, which may weaken the well strength.

For this boundary condition, among other Aadnoy and Chenvert (1987) [6] have derived a fracture model. The model assumes that the deformation is linear elastic, isotropic, and a continuous medium. The model is derived based on the Kirsch solution. The formation breakdown pressure equation reads:

$$P_{wf} = 3\sigma_h - \sigma_H - P_o + \sigma_t \quad (2.1)$$

Where

- P_{wf} = fracturing pressure
- σ_h, σ_H = minimum and maximum in-situ horizontal stresses
- P_o = pore pressure
- σ_t = tensile strength of a rock

Equation 2 is a function of in-situ rock and reservoir parameters. Experiments show that the fracturing pressure depends on the type of drilling fluids [6]. This implies that mud cake contributes to the fracturing resistance in the case of a permeable rock. This suggests the need to characterize the fluid behaviour in order to evaluate the performance on well strengthening. For this, 90/10 and 70/30 OWR mud systems will be characterized and tested for the loss circulation.

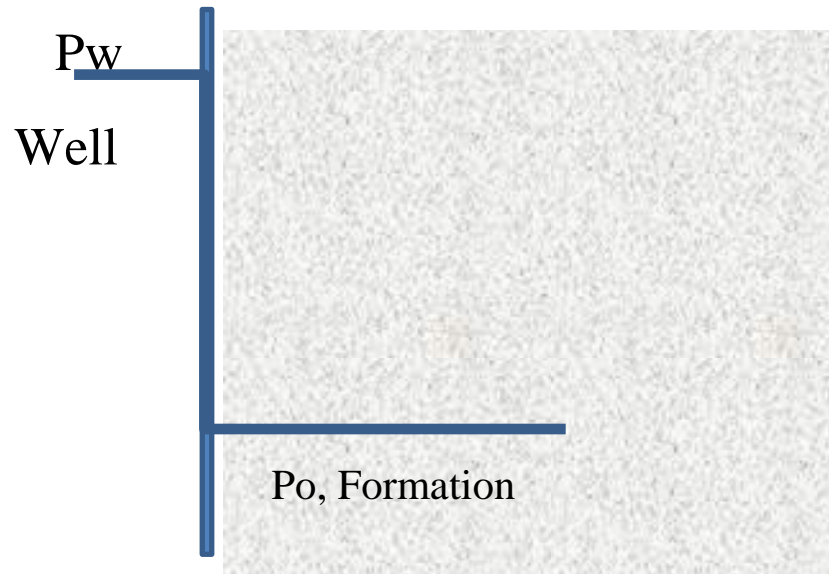


Figure 2.1: Non-penetrating borehole [8]

2.2.2 Penetrating fracture model

Because of the porous and permeable properties and micro fracture of a formation, the differential pressure causes fluid and filtrate to flow into the formation. This results formation pressure build up. Figure 2.2 illustrates the fluid flow and pressure communication between the borehole and the formation. For this case, Haimson and Fairhurst (1968) [38] among others have developed a fracture model based on the poro-elasticity theory. The hydraulic fracturing model is given as

$$P_{wf} - P_o = \frac{3\sigma'_h - \sigma'_H + \sigma_t}{2 - \frac{\alpha(1-2\nu)}{1-\nu}} \quad (2.2)$$

where:

P_{wf} = breakdown pressure, P_o = pore pressure, σ_t = tensile strength of the rock, σ'_h = minimum effective stress, σ'_H = maximum effective stress, ν = Poisson's ratio for the rock. α_o is the Biot poroelastic parameter and is defined as $\alpha_o = 1 - C_r/C_b$, where C_r is rock matrix compressibility; C_b is rock bulk compressibility

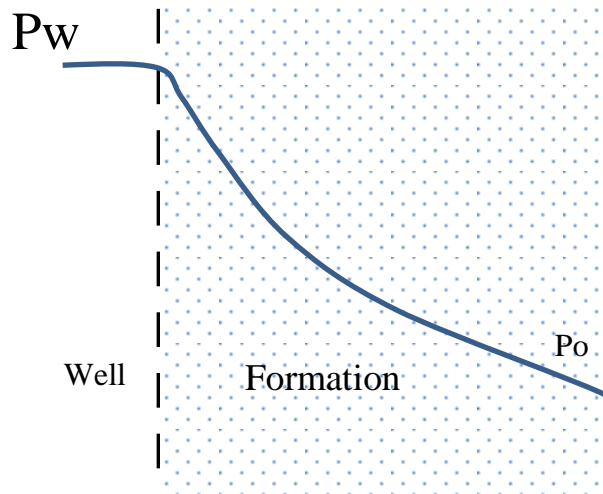


Figure 2.2: Penetrating borehole and possible pore fluid distribution [8]

2.3 Well Collapse

Borehole collapse is mainly caused by the shear failure. The well collapse results a near –wellbore breakout zone that causes spalling, sloughing, and hole enlargement. The borehole collapse is occurred at the pressure in the wellbore is low [5][6].

There are a number of failure criteria to determine well collapse pressure. The most commonly used failure criterion is Mohr-Coulomb. Considering a vertical hole with an impermeable wall, drilled in an anisotropic horizontal stress ($\sigma_H > \sigma_h$) field. The minimum mud weight required in order to prevent shear failure by excessive hoop (tangential) stress is then [3][36].

$$\rho_{\min} gH = \frac{3\sigma_H - \sigma_h - C_o + \alpha P_o (\tan^2 \beta - 1)}{1 + \tan^2 \beta} \quad (2.3)$$

Where C_o = Uniaxial compressive strength, and β is the failure angle, α is Biot coefficient and P_o is the pore pressure, g is acceleration due to gravity, and H is the Vertical depth.

2.4 Stress Cage Theory

Stress caging is the wellbore strengthening method by increasing the fracture resistance of a formation. As illustrated in Figure 2.3, the mechanism of stress cage theory is that particles (LCM eg, Graphite, Quartz, Feldspar, CaCO₃) propped into the fracture and deposited at the mouth of the fracture [4]. This as a result isolated the communication between the well pressure the fracture tip. Since the tip of the fracture doesn't grow hence the mud loss will be stopped.

Aston et al presented that the solid particles plugged the fracture keep it open, and near wellbore tangential stress increases [4]. However this thesis will analyze the claim proposed by reference about the increase in tangential stress at the wellbore or the fracture tip will be investigate through numerical finite element simulation.

2.4.1 Alberty's Interpretation of Stress Cage

Alberty et al presented a finite element model and their study interpretation shows that high stresses can be developed in the near well bore region by inducing fractures and plugging and sealing them with particles [9]. The amount of stress trapped is a function of the stiffness of the formation, the width of the fracture, the position of the bridge within the fracture, the length of the fracture, and the compressive strength of the bridging material. Figure 2.3 illustrates the stress cage concept. According to Aston et al, the stress cages result in a wellbore strengthening with the help of changing the stress state in the vicinity of the well. The equation for a penny shaped fracture is given as [4]:

$$\Delta P = \frac{\pi w E}{8R(1-\nu^2)} \quad (2.4)$$

Where, w- width of the fracture, ν - Poisson Ratio, R- Distance from the center of the wellbore and E- Young's Modulus

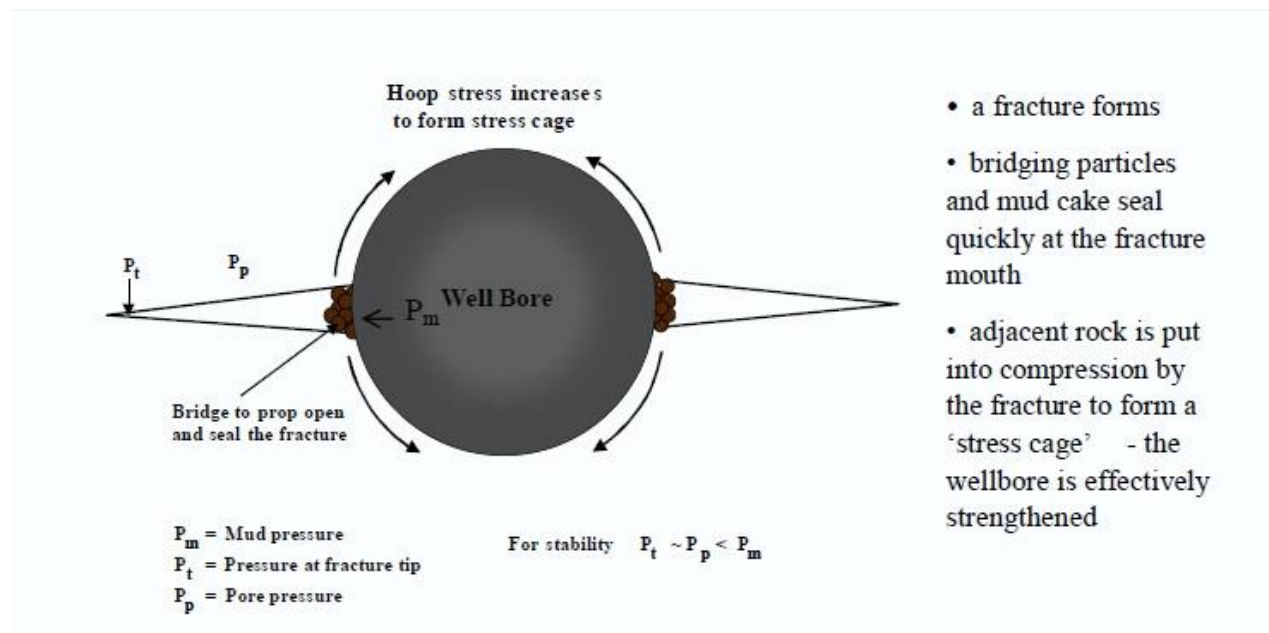


Figure 2.3: Stress cage concept to enhance wellbore strength [4]

The lost circulation particles should hold the fracture open near the fracture mouth and to seal efficiently to provide pressure isolation to prevent the propagation of the opening. In case when the induced opening is created and sealed at or close to the wellbore, the hoop stress is established in the vicinity of the well [10].

Figure 2.4 illustrates a poor bridging which allows well pressure communicating with the fracture. In this case if the formation is porous and permeable, the fluid is then leak into the wings of the fracture. Figure 2.5 illustrates a good bridging which doesn't allow well pressure communicating with the fracture. In addition, one can observe that if in case the fluid is communicating due to low permeable nature of the formation, the fluid is not leak into the wings of the fracture [4].

In permeable formations such as sands the bridge can be imperfect as pressure can leak away into the rock:

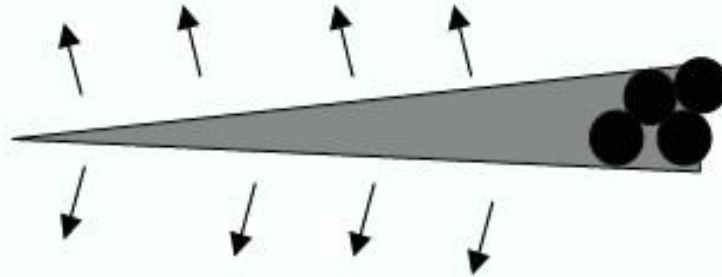


Figure 2.4: Fracture sealing in permeable rocks [4]

In shales the bridge must be virtually impermeable to avoid fracture propagation:

Impermeable/no leak off

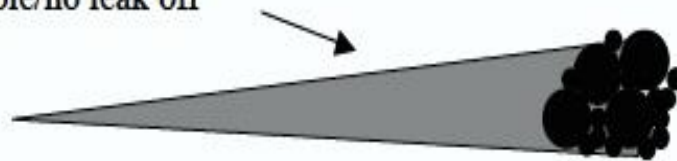


Figure 2.5: Fracture sealing in low-permeability rocks [4]

2.4.2 Aadnøy's Interpretation of Bridging and Fracture Propagation Process

It is experimentally investigated that the fracturing pressure depends on the types of drilling fluid used. Drilling fluid forms a mud cake on the wall of the fracture. The mud cake is then used as a part of the well bore and carries well pressure. Good quality of mud cake increase the wellbore strengthens. The quality of mud cake is determined by the particle deposited in the mud cake and the type of drilling fluid used. Aadnøy et al have presented a theory that describe the bridging phenomenon and fracture propagation. According to the paper, in the mud cake, there exists a bridge that carries a well pressure [12] [13].

As shown on the Figure 2.6(B) the fracture propagates only after the bridging has been collapse. This shows that the bridging disconnects the communication between the well the fracture and hence it is the bridging that reduces stress field from being increased at the tip of the fracture. In chapter 5 the theory presented by [13] will be evaluated through finite element numerical simulation. In addition the bridging performance of the 70/30 and 90/10 will be investigated through bridging experiment and presented in chapter 4.

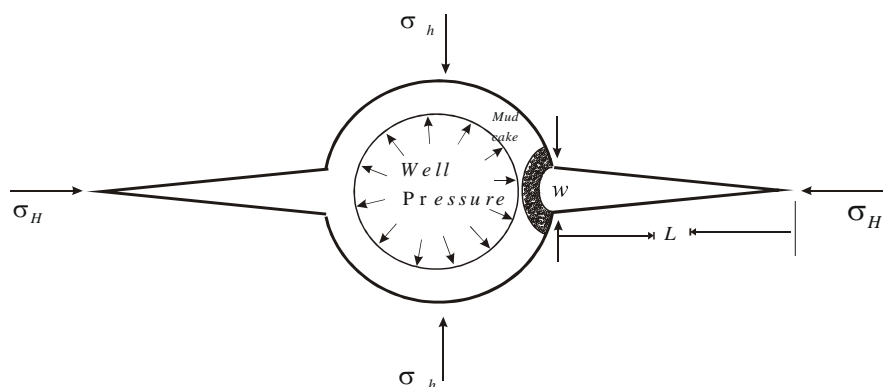


Figure 2.6 A: Cylindrical bridge at the mouth of the fracture [12]

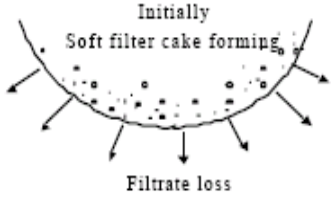
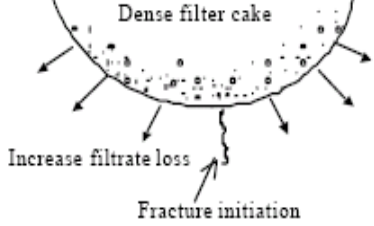
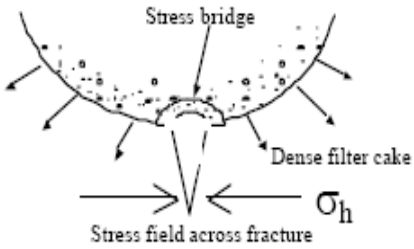
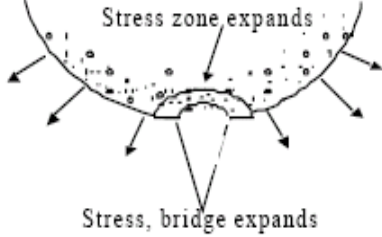
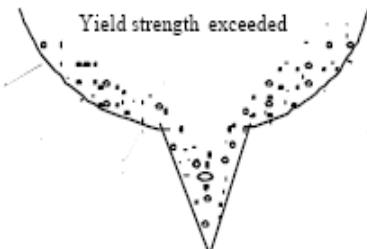
Event	Fig	Main controlling parameters
Filter cake formation		Filtrate loss
Fracture initiation		Filtrate loss, Stress
Fracture growth		Bridge stress Rock stress
Further fracture growth		Bridge/rock stress Particle strength
Filter cake collapse		Particle strength

Figure 2.6 B: Description of the fracture process [13]

2.5 Visco-elasticity

Viscoelastic is a time-dependent property of the materials. Drilling fluids exhibit both viscous and elastic responses under deformation. The viscoelastic properties of drilling fluids are very important to evaluate gel structure, gel strength, barite sag, hydraulic modeling, and solid suspension [15].

Viscoelastic properties are usually measured as responses to an instantaneously applied or removed constant stress or strain or a dynamic stress or strain.

The elastic property of drilling fluids has a strong effect on the flow behavior and pressure drop. The pressure transient, pressure peak and pressure delay is a clear evidence of viscoelasticity and gel structure formation of drilling fluids.

Normally gel formation occurs when fluid is at rest. Heavy solid components such as weighting additives, cuttings may result in severe operational problems. The gel structure of a drilling fluid holds solids in suspension and hinders particles from settling. The dynamic condition help to enhance cutting carrying capacity and reduce barite sag.

Measurement of drilling fluids elastic modulus (G') and viscous modulus (G'') is the most common method of quantifying the viscoelastic properties of fluids. The elastic modulus, G' is also known as the storage modulus since elastic energy is stored. The viscous modulus G'' is refer to the loss modulus since the viscous energy is lost [16]. Since viscoelasticity cannot be measured in the steady, uniform flow field found in viscometers, oscillatory methods of measurement must be used [16]. This section presents the basic theories of viscoelasticity and later in chapter 3 the properties of the 70/30 and 90/10 OMB mud systems will be measured.

2.5.1 Fundamental Viscoelastic Theory

Steady-shear viscosity provides useful rheological properties of drilling fluids under large deformation or shear flow. Under infinitesimal strain in transient gel formation, gel breakage and at rest, drilling fluids show significant viscoelastic response to the deformation [15][16].

Drilling fluids are not strongly viscoelastic. In the linear viscoelastic range, the viscous property is dominant. The test method used to determine visco-elastic properties are called dynamic test. The two major categories of the tests are a) transient and b) oscillatory [15][16].

During an oscillatory experiment, drilling fluid specimen is subjected to a sinusoidal deformation and the resulting fluid response stress is measured.

Shear stress can be written in term of strain as [15][16]:

$$\tau(t) = \gamma_o \left[\left(\frac{\tau_o}{\gamma_o} \cos \delta \right) \sin(\omega t) + \left(\frac{\tau_o}{\gamma_o} \sin \delta \right) \cos(\omega t) \right]$$

$$\tau(t) = \gamma_o [G' \sin(\omega t) + G'' \cos(\omega t)] \quad (2.5)$$

$$G' = \left(\frac{\tau_o}{\gamma_o} \cos \delta \right) \quad (2.6)$$

$$G'' = \left(\frac{\tau_o}{\gamma_o} \sin \delta \right) \quad (2.7)$$

$$\tan \delta = \left(\frac{G''}{G'} \right) \quad (2.8)$$

For a purely viscous fluid, the phase angle (δ) is equal to 90. For a purely elastic material, the phase angel is equal to 0. And for a viscoelastic material, the phase angle has values between 0 and 90.

2.5.2 Linear Viscoelastic Region (LVER)

It is common practice to define the viscoelastic regions before performing detailed dynamic measurements to investigate the sample's microstructure. The linear viscoelastic region (LVER) is determined by an amplitude sweep test. The LVER can also be used to determine the stability of a suspension. The stability of the sample structure can be measured by the length of the LVER of the elastic modulus (G'). The sample having a long LVER is an indication that the system is well-dispersed and stable system. The stress or strain obtained from the amplitude test must of selected from the LVER and used to oscillation test [39].

2.5.3 Oscillatory Test: Amplitude Sweep

Amplitude test is an oscillatory test. During an amplitude sweep test the amplitude of the deformation or in other words the amplitude of the shear stress is allowed to vary while the frequency is kept constant. Figure 2.7 shows the oscillation of the motion and the amplitude is the maximum of the oscillatory motion. For the analysis the storage modulus G' and the loss modulus G'' are plotted against the deformation [15] [32].

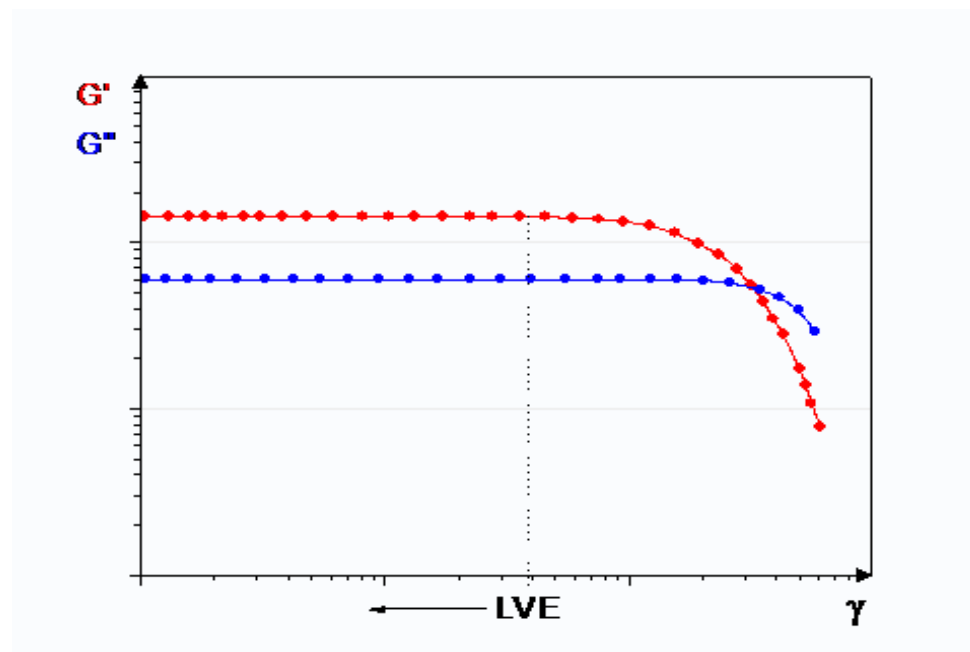


Figure 2.7: Amplitude Test G' and G'' moduli plotted against the deformation [32]

At low deformation G' and G'' are constant. This is an indication that the sample structure is undisturbed. This region is normally called linear-viscoelastic (LVE). As shown on the figure as soon as the moduli start to decrease, it is an indication that the structure is disturbed. That is to say the end of the LVE-region is reached.

As shown on Figure 2.7, the plateau value of G' in the LVE-region describes the rigidity of the sample at rest. The plateau value G'' is a measure for the viscosity of the unsheared sample [32] [39].

- If the storage modulus is larger than the loss modulus, the sample behaves more like a viscoelastic solid.
- In the opposite case - $G'' > G'$ in the LVE-region - the sample has the properties of a viscoelastic fluid.

The yield point can be determined with the amplitude sweep test. During viscoelastic study, there are two Therefore two special points can be used:

- the end of the LVE-region and
- the intersection of the curves for G' and G'' .

In most cases the intersection of G' and G'' is of more practical importance.

2.5.4 Oscillatory Test: Frequency Sweep

During the frequency sweep the frequency is varied while the amplitude of the deformation - or alternatively the amplitude of the shear stress - is kept constant. For the analysis the storage and loss modulus are plotted against the frequency. The data at low frequencies describe the behavior of the samples at slow changes of stress. Oppositional the behavior at fast load is expressed at high frequencies.

The frequency sweep is very important for polymer fluids. For dispersions (e.g. paints, cosmetics, comestible) this method can provide some information about the

sedimentation stability. Figure 2.8 shows the behavior of G' and G'' that is typical frequency sweep test result for a polymer solution [15][32].

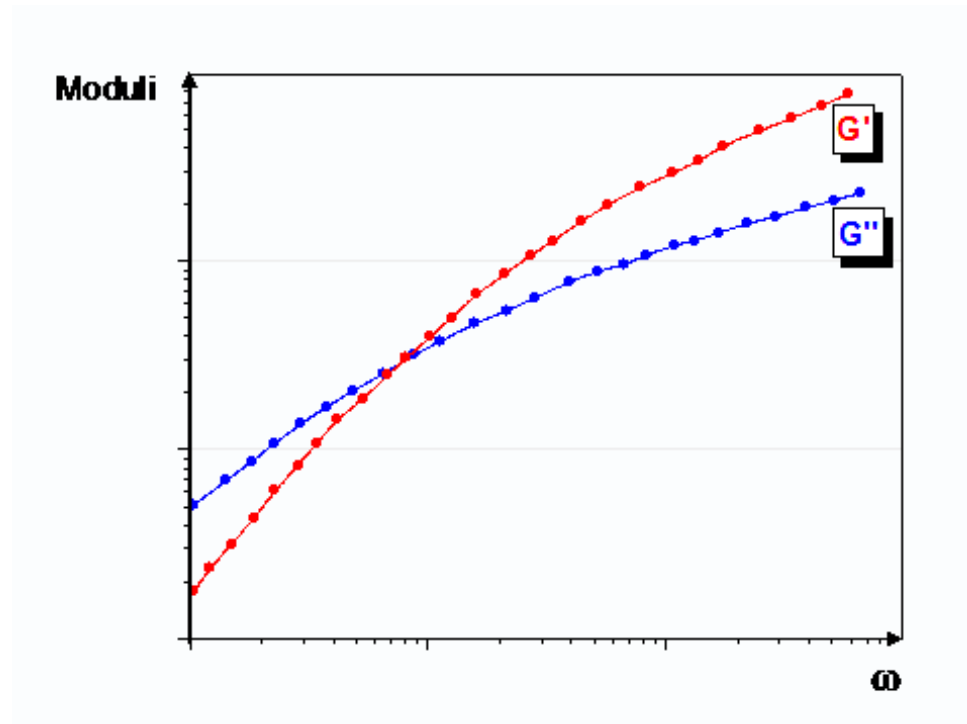


Figure 2.8: The Frequency Sweep Test [32]

2.6 Lost Circulation

Lost Circulation occurs through natural and drilling induced fracture. This causes several negative effects. The Lost Circulation can occur in formations which are [17]:

1. Unconsolidated or highly permeable formations (such as loose gravels)
2. Natural fractures
3. Drilling induced fractures
4. Cavernous formations (crevices and channels)

There are two different methods to avoid the problem of Lost Circulation. It is possible to apply “Preventive measures” during the planning phase and the second

method is “Corrective measures” which applies in during the execution phase. The choice of method between these two depends on economic and availability [29].

Types of Loss Zones

Figure 2.9 illustrates the various types of formation that experiences loss circulation.

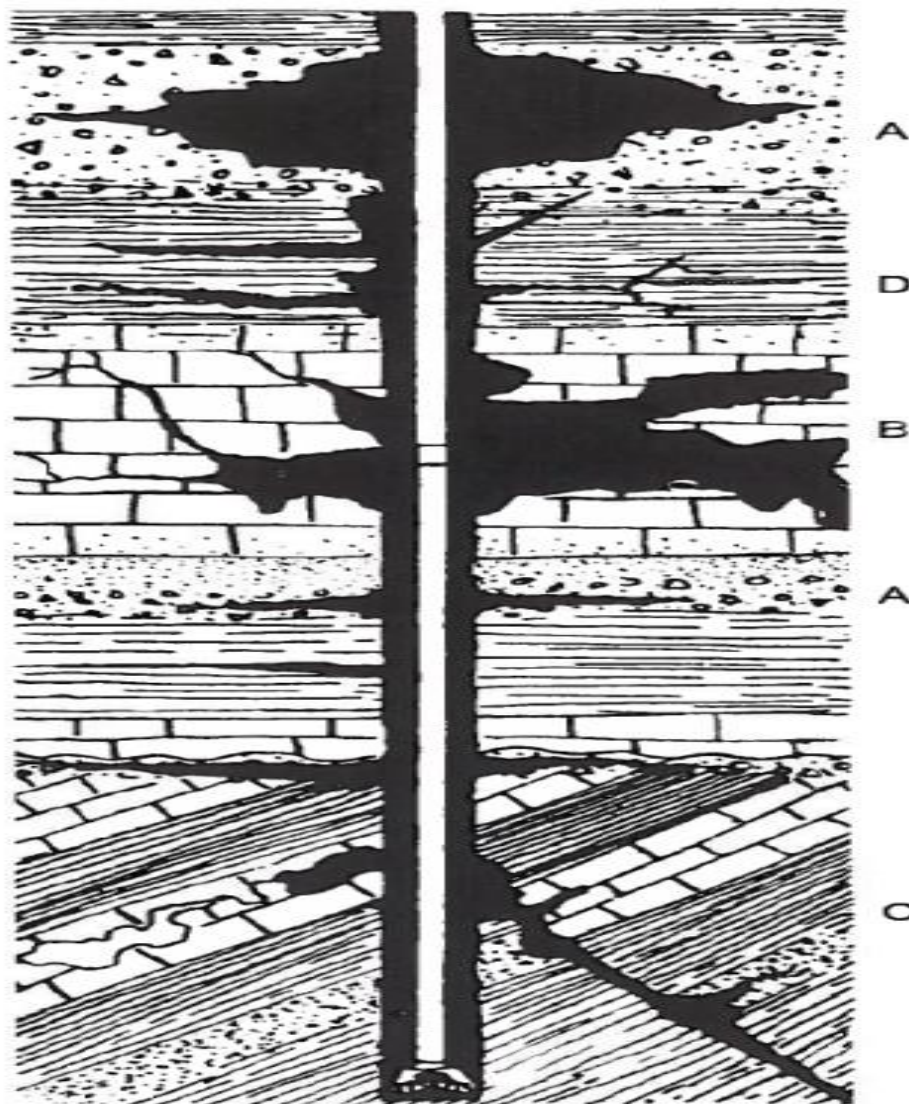


Figure 2.9: Types of Lost Circulation. A=Permeable zone, B=Caverns, C=Natural fractures and D=Induced fractures [18]

2.7 Drilling Fluid, Rheology and Hydraulics

2.7.1 Drilling Fluid Types

Due to temperature and pressure, the rheology, physical and visco-elastic properties of drilling fluid are also changes. This as a result influences the performance of the drilling fluid. There are four types of drilling fluid available in the industry. They are [2];

- Water-based muds
- **Oil-based muds**
- Synthetic-based muds
- Pneumatic drilling fluids

Oil-Based Muds

Oil-based muds provide good drilling performance by combining shale hydration inhibition and drill string lubrication. It can be used to reduce and eliminate of the drilling related problems such as reduced stuck pipe risk, low formation damage, corrosion avoidance and increased downhole temperature.

They are particularly effective for the drilling of (1) highly reactive shale (2) extended-reach wells, and (3) deep, high-pressure, high-temperature [2].

However, oil-based muds are highly toxic and can cause the risk of contamination of environment. A development of refined mineral oils for use in low-toxicity oil-based muds can reduce environmental problems and improve working conditions [2]. Effect of temperature on the rheology of drilling fluids is of particular concern in high-temperature applications and in drilling in deep water. In deep-water drilling, large variations in temperature from low at sea (around 1-2°C) to high values downhole cause significant changes in fluid rheology. This has major implications for the hydraulics of the drilling operation, including hole cleaning and hole stability [25].

2.7.2 Drilling Fluid Rheology Model

The rheology of the drilling fluid is a study of deformation of fluids such as the flow behavior of suspensions in pipes and other conduits. Frictional pressure loss is extremely important in relative to the analysis of drilling hydraulics since large viscous forces must be overcome to move the drilling fluid through the longer, slender pipes and annuli in the drilling process. Flow behavior of the fluid can also be described by the rheological model that describes the relationship between the shear rate and the shear stress. Figure 2.10 illustrate the summary of non-Newtonian fluids [40]:

1. Viscoplastic fluid,
2. Bingham fluid (Constant apparent viscosity),
3. Pseudoplastic fluid (Power law, shear thinning fluid),
4. Newtonian fluid,
5. Dilatant fluid (Shear thickenings fluid)

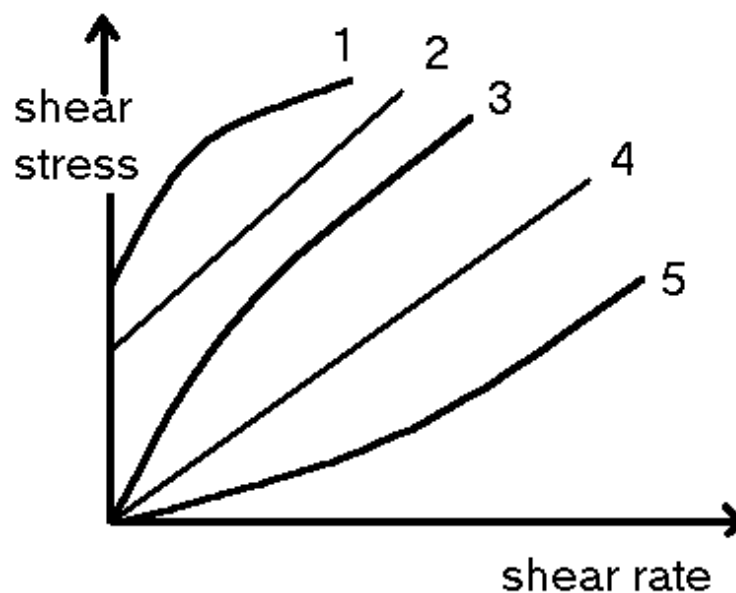


Figure 2.10: Rheology Model for different fluids [40]

2.7.2.1 Newtonian Model

Newtonian fluids exhibit a constant viscosity for any shear rate at a constant pressure and temperature. The fluid rheological model can be described by one one-parameter such that shear stress is directly proportional to the shear rate. The proportionality constant is the viscosity of the fluid. There are several Newtonian fluid systems such as glycerin, light-hydrocarbon Water, sugar solutions, oils, oils, air and other gases are Newtonian fluids. However the Newtonian fluid doesn't describe the drilling fluid and hence are they are non-Newtonian. The Newtonian fluid can be written as [19][31]:

$$\tau = \mu \gamma \quad (2.9)$$

where, τ = Shear stress, γ = Shear rate and μ = Newtonian Viscosity

2.7.2.2 Bingham Plastic Model

The Bingham model is widely used in the industry. The model describes the flow behavior of many drilling fluid types. According to the model the fluid behavior exhibits a linear shear stress and shear rate relationship. The intercept of the line is part of the fluid viscosity which is caused by an attractive force of attraction between charges or ions in the drilling fluid. This is called the yield stress. The slope of the line is called Bingham plastic. This part of the fluid resistance is due to the fluid-fluid or fluid –solid or solid-solid interaction in the drilling fluid. Bingham model is given as: [19] [31]

$$\tau = \tau_y + \mu_p \gamma \quad (2.10)$$

where, yield point (τ_y) and plastic viscosity (μ_p) can be read from a graph or can be calculated by the following equations,

$$\mu_p (cP) = R_{600} - R_{300} \quad (2.11)$$

$$\tau_y (\text{lbf}/100\text{sqft}) = R_{300} - \mu_p \quad (2.12)$$

2.7.2.3 Power Law Model

Most drilling fluid reduces the viscosity as the shear rate increase. This is also called a pseudo plastic fluid. For instance wasted based polymer drilling fluid especially shows formulated with XC polymer the power law model describe better than the Bingham plastic model. The power law model is described by two parameters and the model mathematically written as: [19][31]

$$\tau = k\gamma^n \quad (2.13)$$

where k is the consistence index and n is flow behavior index.

The Power-law parameters can be estimated from Fann 35 data as:

$$n = 3.32 \log \left(\frac{R_{600}}{R_{300}} \right) \quad (2.14)$$

$$k = \frac{R_{300}}{511^n} = \frac{R_{600}}{1022^n} \quad (2.15)$$

2.7.2.4 Herschel-Buckley

The Herschel-Buckley model defines a fluid by three-parameter and can be described mathematically as follows [22]:

$$\tau = \tau_o + k\gamma^n \quad (2.16)$$

The unit of k is $\text{lb}\cdot\text{sec}^n/100\text{sqft}$. The n and k values can be determined graphically.

Versan and Tolga approach can be used to obtain τ_o . [26]

$$\tau_o = \frac{\tau^{*2} - \tau_{\min} \times \tau_{\max}}{2 \times \tau^* - \tau_{\min} - \tau_{\max}} \quad (2.17)$$

where τ^* is the shear stress value corresponding to the geometric mean of the shear rate, γ^* and given as:

$$\gamma^* = \sqrt{\gamma_{\min} \times \gamma_{\max}} \quad (2.18)$$

From Eq. 2.18, $\gamma^* = 72.25 \text{ sec}^{-1}$. Using this value, we need to interpolate between values of shear stress to get: $\tau^* = 19.77 \text{ lbf}/100\text{ft}^2$.

2.8 Hydraulics Models

As mentioned in the introduction part, ECD is the function of static pressure and frictional pressure loss. The frictional pressure loss is a function of several factors such as:

- the rheological behavior of the drilling fluid
- the flow regime of the drilling fluid
- the drilling fluid properties such as density and viscosity;
- the flow rate of the drilling fluid;
- the wellbore geometry and drill string configuration.

The pump pressure, ΔP_p , has to overcome:

- Frictional pressure losses (ΔP_s) in the surface equipment such as Kelly, swivel, standpipe.
- Frictional pressure losses (ΔP_{ds}) inside the drillstring (drillpipe, ΔP_{dp} and drill collar, ΔP_{dc}).
- Frictional pressure losses across the bit, ΔP_b .
- Frictional pressure losses in the annulus around the drillstring, ΔP_a .

Figure 2.11: Diagram of the drilling fluid circulating system

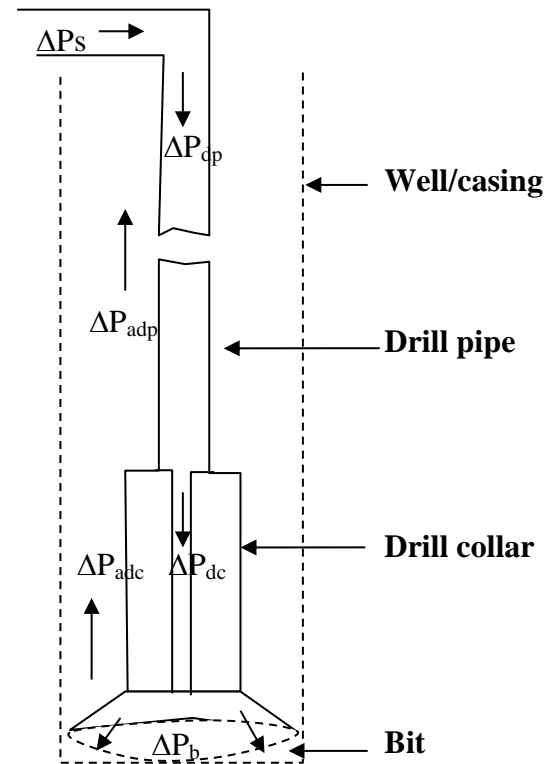
The total pressure loss is the sum of the pressure losses as illustrated on Figure 2.19 [24]:

$$\Delta P_p = \Delta P_s + \Delta P_{dp} + \Delta P_{dc} + \Delta P_b + \Delta P_{adc} + \Delta P_{adp} \quad (2.19)$$

Frictional pressure losses across the bit, ΔP_b [24]:

$$\Delta P_b = \frac{156 \cdot \rho \cdot q^2}{(D_{N1}^2 + D_{N2}^2 + D_{N3}^2)^2} \quad (2.20)$$

where D_{N1} , D_{N2} , D_{N3} are diameters of the three nozzles.



For the hydraulic evaluation of the 70/30 and

90/100BM systems a Unified model was considered. Table 2.1 shows the summary of the model in pipe and annular flow.

The unified rheology model is given as: [27] [28]

$$\tau = \tau_y + k\gamma^n \quad (2.21)$$

Where, the shear yield (τ_y), k and n values are calculated from Fann rheology data as shown in the table.

Pipe Flow	Annular Flow
$\mu_p = R_{600} - R_{300}$ $\tau_y = R_{300} - \mu_p$ $\tau_0 = 1.066(2R_3 - R_6)$	
$\mu_p = cp$	
$n_p = 3.32 \log\left(\frac{2\mu_p + \tau_y}{\mu_p + \tau_y}\right)$ $k_p = 1.066\left(\frac{\mu_p + \tau_y}{511}\right)$	$n_p = 3.32 \log\left(\frac{2\mu_p + \tau_y - \tau_y}{\mu_p + \tau_y - \tau_y}\right)$ $k_p = 1.066\left(\frac{\mu_p + \tau_y - \tau_0}{511}\right)$
$G = \left(\frac{(3-\alpha)n+1}{(4-\alpha)n}\right) \left(1 + \frac{\alpha}{2}\right) \quad \alpha = 1 \text{ for annular}$ $\alpha = 1 \text{ for pipe}$	
$v_p = \frac{24.51 q}{D_p^2}$	$v_a = \frac{24.51 q}{D_2^2 - D_1^2}$
$v = ft/min$	
$\gamma_w = \frac{1.6 * G * v}{D_R}$	
$\gamma_w = sec^{-1}$	
$\tau_w = \left[\left(\frac{4-\alpha}{3-\alpha}\right)\right] \tau_0 + k \gamma_w^n$	
$N_{Re} = \frac{\rho v_p}{19.36\tau_w}$	$N_{Re} = \frac{\rho v_e}{19.36\tau_w}$
Laminar: $f_{laminar} = \frac{16}{N_{Re}}$	Laminar: $f_{laminar} = \frac{24}{N_{Re}}$
Transient: $f_{transient} = \frac{16 N_{Re}}{(3470 - 1370n_p)}$	Transient: $f_{transient} = \frac{16 N_{Re}}{(3470 - 1370n_p)}$
Turbulent: $a = \frac{\log n + 3.93}{50}$ } $f_{turbulent} = \frac{a}{N}$ $b = \frac{1.75 - \log n}{7}$ }	Turbulent: $a = \frac{\log n + 3.93}{50}$ } $f_{turbulent} = \frac{a}{N}$ $b = \frac{1.75 - \log n}{7}$ }
$f_{partial} = (f_{transient}^{-8} + f_{turbulent}^{-8})^{-1/8}$	
$f_p = (f_{partial}^{12} + f_{laminar}^{12})^{1/12}$	$f_a = (f_{partial}^{12} + f_{laminar}^{12})^{1/12}$

$\left(\frac{dp}{dL}\right) = 1.076 \frac{f_p v_p^2 \rho}{10^5 D_p}$ <p style="text-align: right;">psl/ft</p> $\Delta p = \left(\frac{dp}{dL}\right) \Delta L$	$\left(\frac{dp}{dL}\right) = 1.076 \frac{f_a v_a^2 \rho}{10^5 (D_2 - D_1)}$ <p style="text-align: right;">psl/ft</p> $\Delta p = \left(\frac{dp}{dL}\right) \Delta L$ <p style="text-align: right;">psl</p>
$\Delta p_{Nozzles,psi} = \frac{156 \rho q^2}{(D_{N1}^2 + D_{N2}^2 + D_{N3}^2)^2}$	

Table 2.1: Summary of Unified hydraulics model

3 Experimental Drilling Fluid Characterization

This chapter presents the direct characterization of the 70/30 and the 90/10 OBMs thought measurement. These are rheology, density, HPHT filtrate, visco-elasticity, and flow in porous media. In addition, the hydraulic and rheology modeling will be presented.

3.1 Fann 35 - Viscometer ES and Density Measurement of 70/30 & 90/10 OBMs

The two drilling fluids, 70/30 and 90/10 OBMs, have been measured with the Fann35 viscometer. The drilling fluids have been heated at the desired temperature with the Tufel heating cup and the measurement was performed under controlled temperature condition and under atmospheric pressure. The measurement was performed at 80, 120 and 180 degree Fahrenheit (°F). Before the measurement the drilling fluid systems were shear for 10-min with Hamilton Beach mixer. Figure 3.1 shows the comparisons of the measured viscometer data.

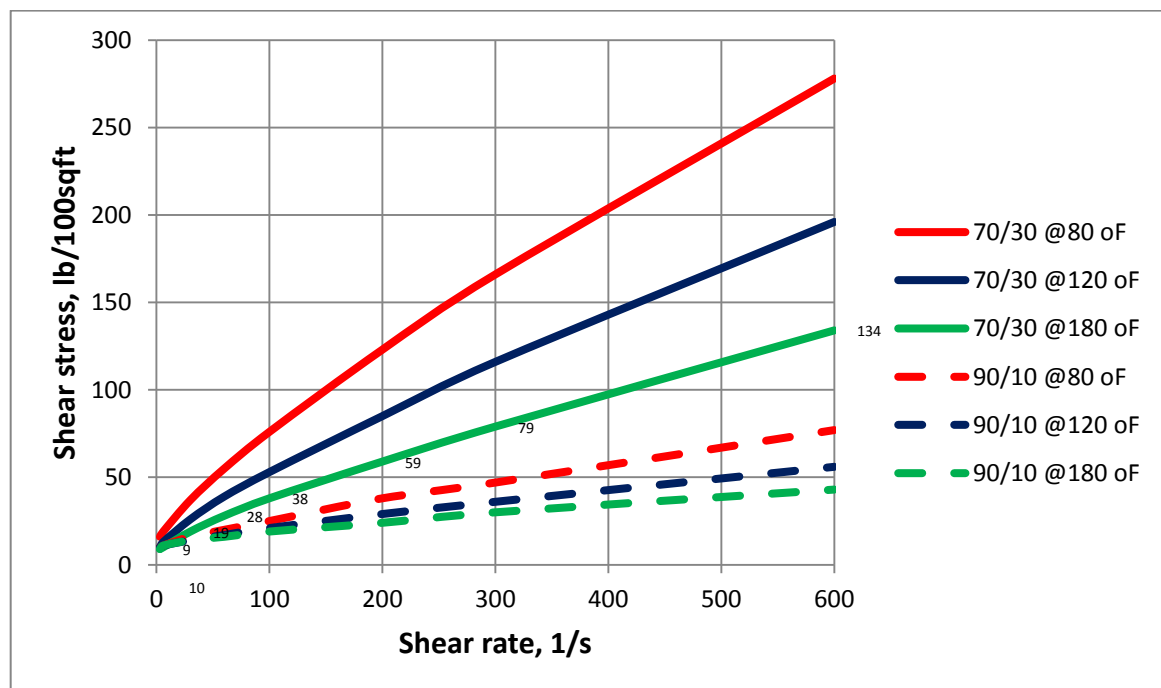


Figure 3.1: Rheology data for 70/30 and 90/10 OBMs in different temperatures

For better comparisons of the measured data shown in Figure 3.1, the relative percentage error between the two drilling fluids was calculated. Figure 3.2 presents the comparisons between the 70/30 and 90/10 OBMs at the temperature of 80, 120 and 180°F. As shown the error ranges from -18 to 140%, -18 to 154% and 20 to 186% at temperatures 80°F, 120°F and 180°F respectively. The lower and the upper limits of the error values are at 3 and 600RPM. The result exhibits that the error rate is higher at higher RPM and at lower temperature.

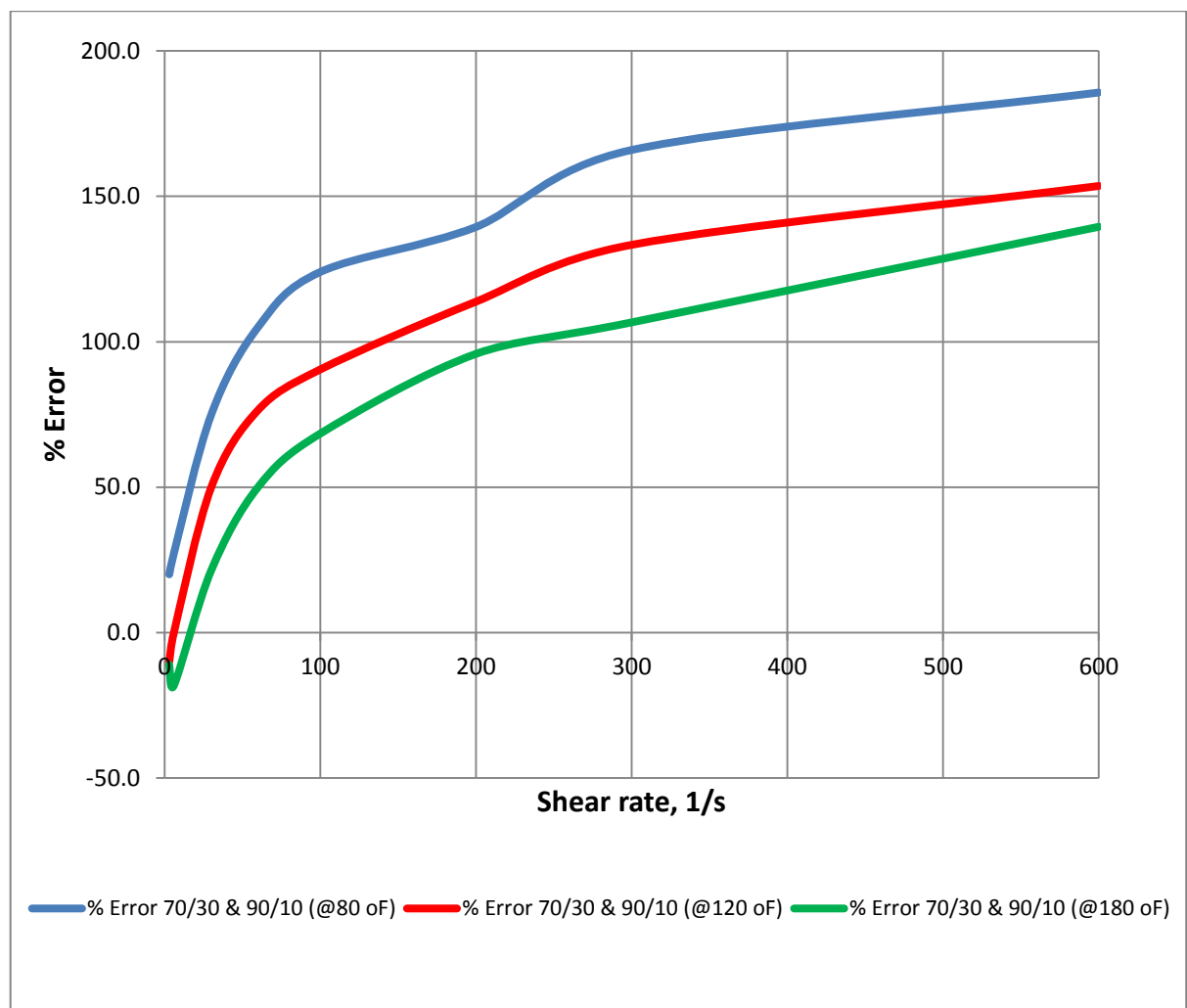


Figure 3.2: Comparison of Error % for the 70/30 and 90/10 OBMs at the 80, 120 and 180°F temperatures

The relative error comparisons of the individual mud systems (i.e 70/30 and 90/10 OBM) between (80 and 120°F) and (80 and 180°F) is shown in the Figure 3.3. The result shows that an increase in relative error is due to the increase in RPM and temperature. For the 70/30 OMB, the relative error changes ranges from 21-35% and 33-53% respectively. For the 90/10 OBM, the error range from 10-27% and 10-44% respectively. The result in general shows that the error rate is higher at higher RPM and at higher temperature.

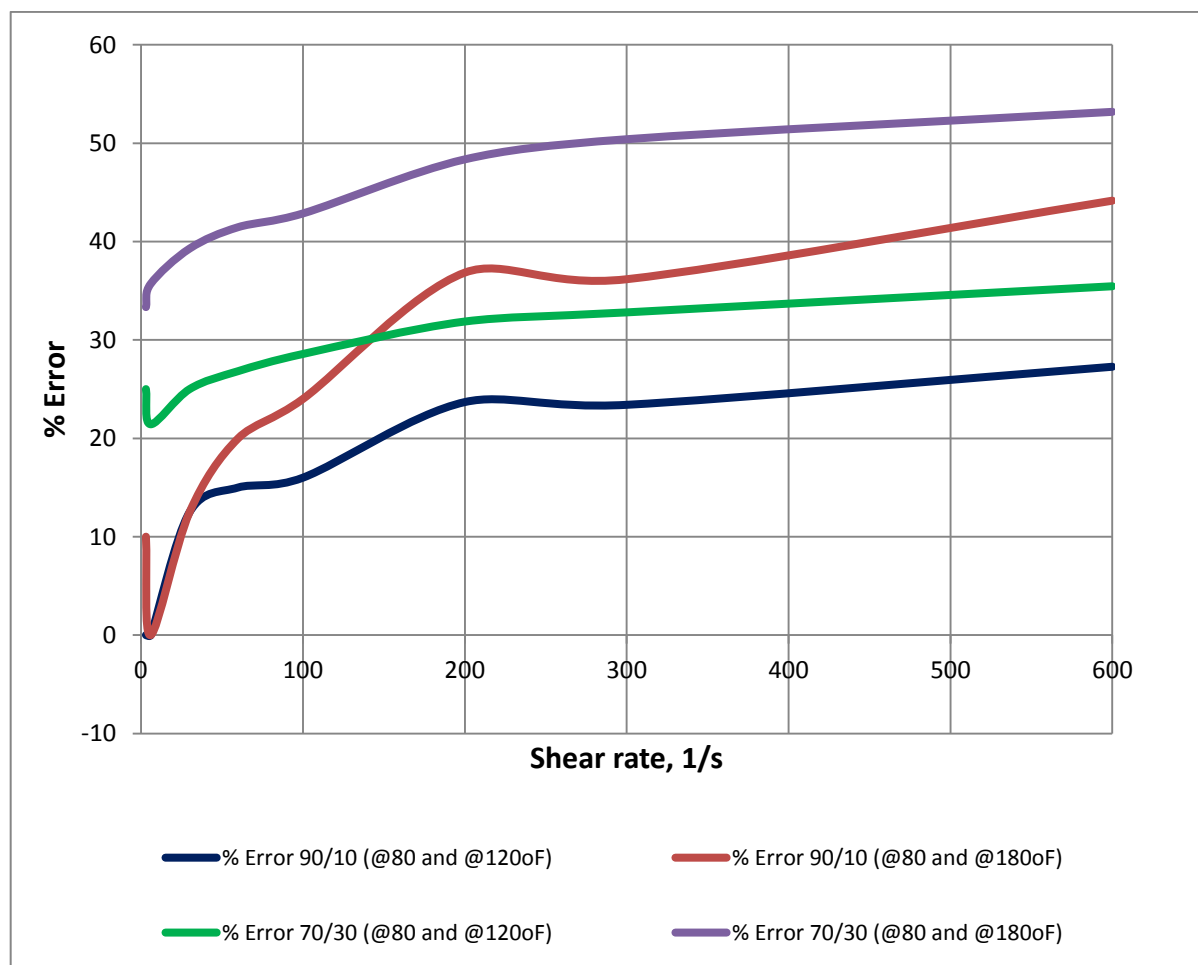


Figure 3.3: Comparison of the individual mud systems at the 80, 120 and 180 °F temperatures

3.2 HPHT Static Filtration and ES Measurement

Filtration is the diffusion of the liquid phase of the drilling fluid into a permeable formation by the applied differential pressure. The solid part of the fluid systems deposited and forming filter cake. It is important to control the filtration behavior of the drilling fluid in order to control both the volume filtrate and the quality filter cake formed on the wellbore. The quality of drilling fluid can be evaluated based on the filtrate behavior. The more the filtrate of the drilling fluid shows the more the formation damage and at the same time the drilling fluid loses its rheological and physical properties. As a result it reduces its performances with respect to cutting transport and results several undesired operational problems such as borehole instability, excessive torque and drag, pressure differential sticking, and formation damage [1][2][23].

In order to compare the two mud systems, static HPHT filtration test was performed at the temperature of 100⁰C. The differential pressure across the filter paper is maintained as 500 psi. Running time for the HPHT filtration test is set to 30 minutes [23].

The HPHT filtration test result is presented in Figure 3.4. The volume of the 90/10 OBM is recorded as 7,2 ml and the 70/30 OBM is recorded as 1,1 ml water phase out of the total filtrate volume 4,6ml oil filtrate. The water phased in the filtrate is an indication that the 70/30 is not very well emulsified.

Growcock et al (1990) studied that the Electrical Stability voltage values generally correlates well with other established measures of mud stability, such as HTHP fluid loss [30]. Thus the measurement of the Electrical Stability (ES) test is required to check the stability of the drilling fluids.

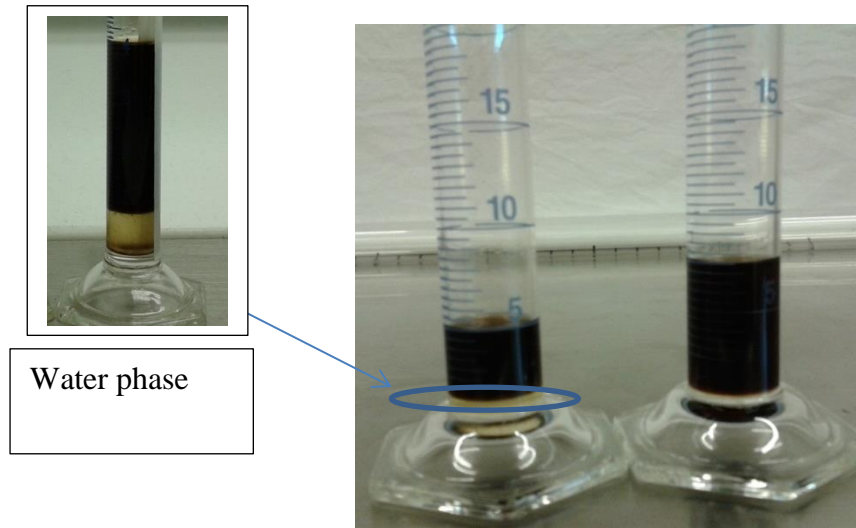


Figure 3.4: Comparison of the HPHT filtration for the 70/30 and 90/10 OBMs

The ES Measurement

Many of the physical properties of the Oil-Based Mud and Water-Based Mud are common except the Electrical Stability Test, which can only be applied on the Oil-Based Muds [23]. The measurement is critical since the Electrical Stability (ES) of an oil-based mud is considered a measure of its emulsion stability [31]. The ES measurement shows the voltage of the current to flow in the mud. The measured Electrical Stability number represents mud emulsion stability. In this section, the ES measurements of two drilling fluids are performed.

The result of the ES measurement should typically be higher than 500 volts for a good emulsified mud. However, the amount of water and solids contained in the drilling mud do have effect on the ES measurement. A typical behavior of drilling mud with a poor emulsion exhibit high viscosity, high amount of water phase in filtration and lower ES value [23].

ES measurement the 70/30 OBM and 90/10 OBM

The drilling muds of 70/30 and 90/10 OWR were performed to measure the property of ES. Both drilling muds were mixed for around 10 minutes by using a Hamilton Beach mixer before the measurement and the results of the measurement are shown in Figure 3.5.

The ES measurement result for 90/10 OWR displays that the drilling mud has a good emulsified mud. On the other hand, the ES measurement result for the 70/30 OBM is 350mV, which can be considered as lower value. The lower ES value is an indication that the drilling mud has a poor emulsion. This was the reason for the 1,1ml water phase in the HPHT filtrate. We decided to improve the emulsification of the 70/30 OBM system and re-measure the ES value and HPHT filtrate test. The comparison of the result of the ES measurement for 70/30 and 90/10 OBMs before modification and re-measurement result of the 70/30 OBM after modification is presented in the Figure 3.5 below.

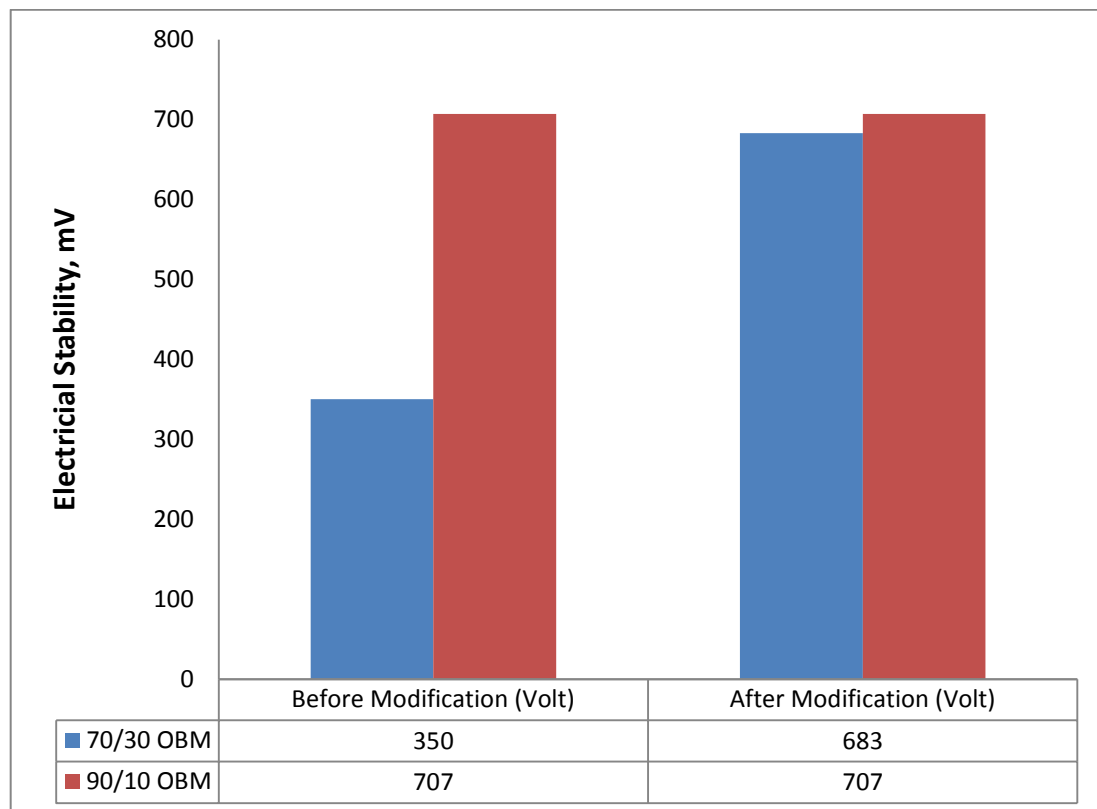


Figure 3.5: ES measurement of Before and After Modification for the 70/30 and 90/10 OBMs

ES adjustment of 70/30 OBM

The ES of the 70/30 OBM is adjusted by adding lime and emulsifier such as Paramul and Parawet into the drilling mud. The ratio of the lime and emulsifier added to the drilling fluid is 1:1. The drilling fluid was sheared very well for 40 minutes. The ES-value is then re-measured and recorded as 683mV. This indicates that the drilling fluid has attained a good emulsion.

HPHT filtrate re-measured 70/30 OBM

The HPHT filtrate test of the 70/30 OBM is carried out again after modification by adding lime and emulsifier to the drilling mud. The filtrate volume is recorded as 2,25 ml for the 70/30 OBM after modification and no water contains in the filtrate. The result shows that the modification for the 70/30 OBM is successful since it can remove the water containing in the drilling mud. Comparison between before and after modification of the 70/30 OBM is shown in Figure 3.6.

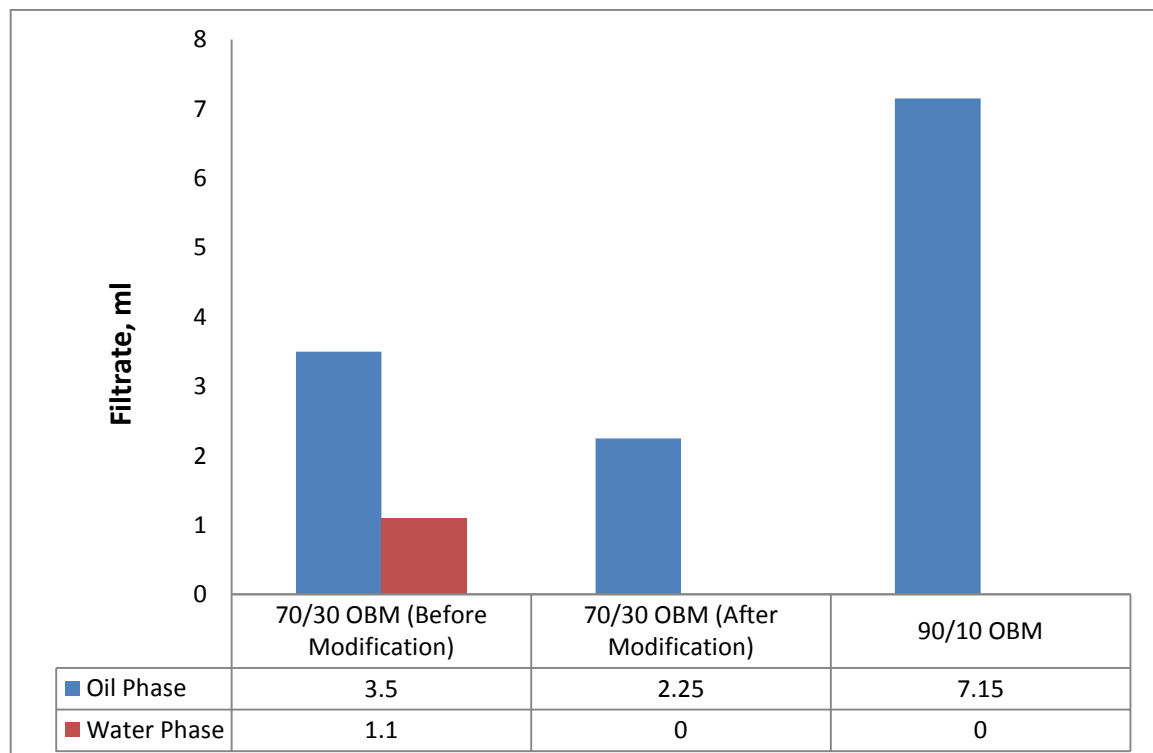


Figure 3.6: Volume of filtration test for the 70/30 OBM (Before & After Modification) and 90/10 OBM

3.2.1 Rheology Modeling and Analysis of 70/30 OBM

Rheology data is an important parameter for drill string mechanics, hydraulics ECD, hole cleaning, kick simulation and swab/surge calculation. As reviewed in section §2.6.2, there exist several rheology models. It is therefore important to raise question that which of these models can describe the behavior of the 70/30 and 90/10 OBM systems?

In order to answer the question, this section deals with modeling of the Fann 35 data with the rheology models and compare errors obtained from the analysis. In addition, temperature dependent plastic viscosity and yield stress of the mud systems will be modelled.

The Rheology prediction of the 70/30 OWR drilling fluid at normal temperature (80°F) is shown in Figure 3.7. Using different rheology models, the shear stress of the drilling fluids were calculated and compared with experimental data.

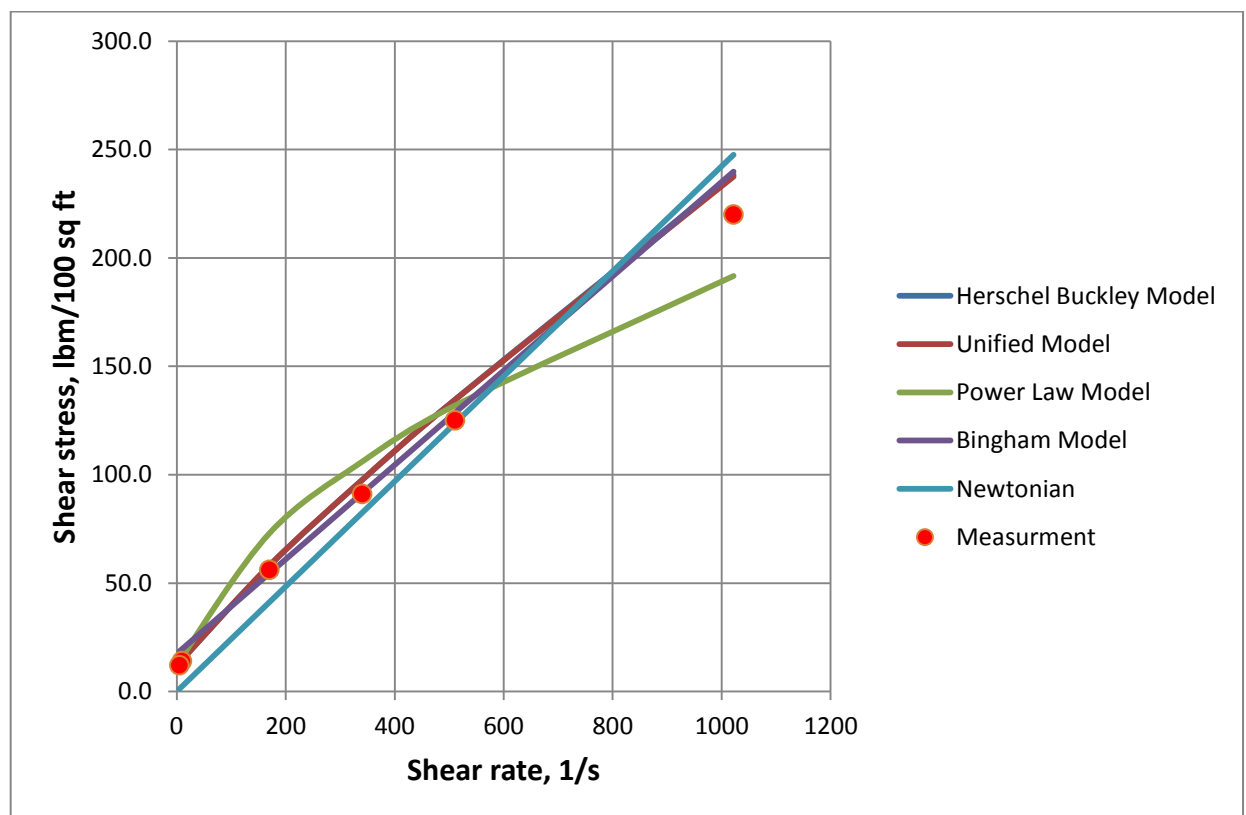


Figure 3.7: Comparison of different rheology models measurement of the 70/30 OWR at normal temperature (80 °F)

The commutative error was analyzed based on comparing the difference between the model and the experimental measured data. All the models derived for each drilling fluid are available in appendix A. Figure 3.8 shows the % error obtained from the rheology models. As can be seen, for the three temperatures, the Herschel Buckley and the Unified models are recorded the lowest error rates. The commonly used Power law and the Bingham models show 11% and 18 % error rates respectively. This shows that the Herschel Buckley and Unified models describe the behavior of the mud system very well. It is obvious that the Newtonian model doesn't describe the drilling fluid behavior at all.

Another observation is that increasing the temperature the prediction behavior the models are not influenced by the temperature.

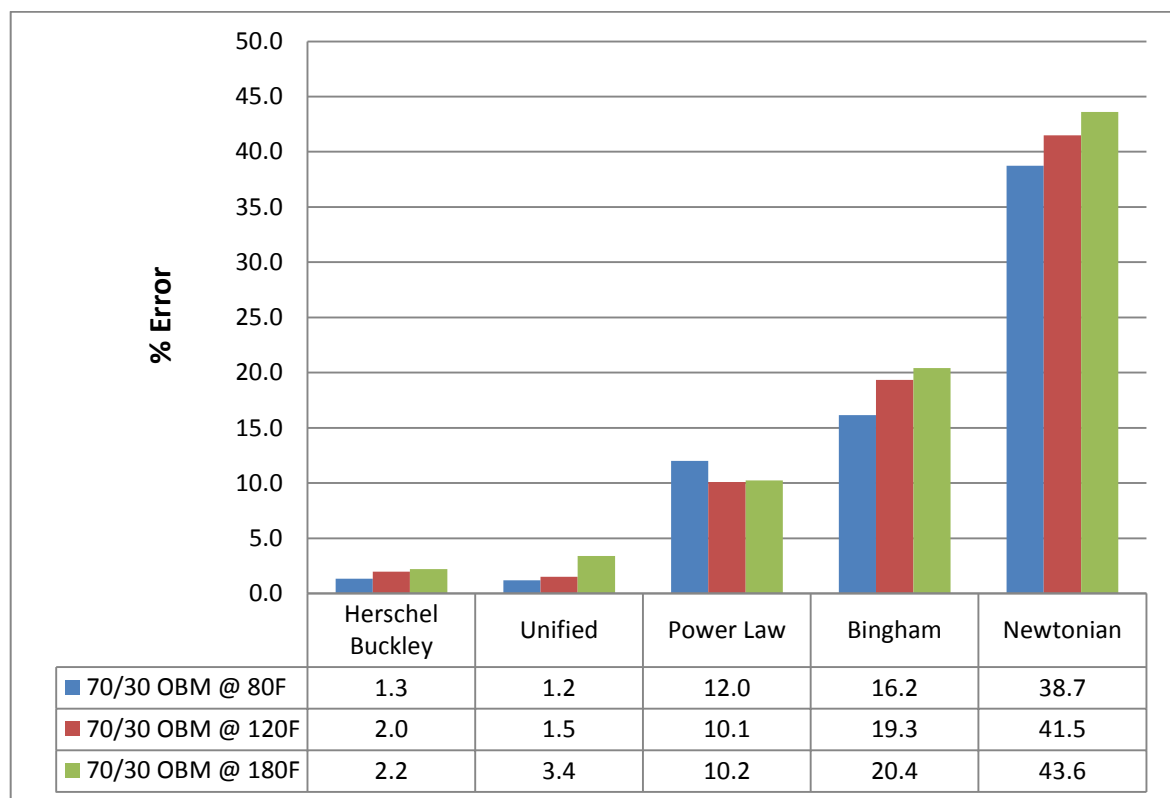


Figure 3.8: Comparison of the different rheology models errors of the 70/30 OWR at the 80, 120 and 180 °F

3.2.2 Rheology Modeling and Analysis of 90/10 OBM

The Rheology prediction of the 90/10 OBM at the normal temperature of 80°F is presented in the Figure 3.9. The figure shows that the comparison of the 80°F Fann data among rheology models with the modeled curves.

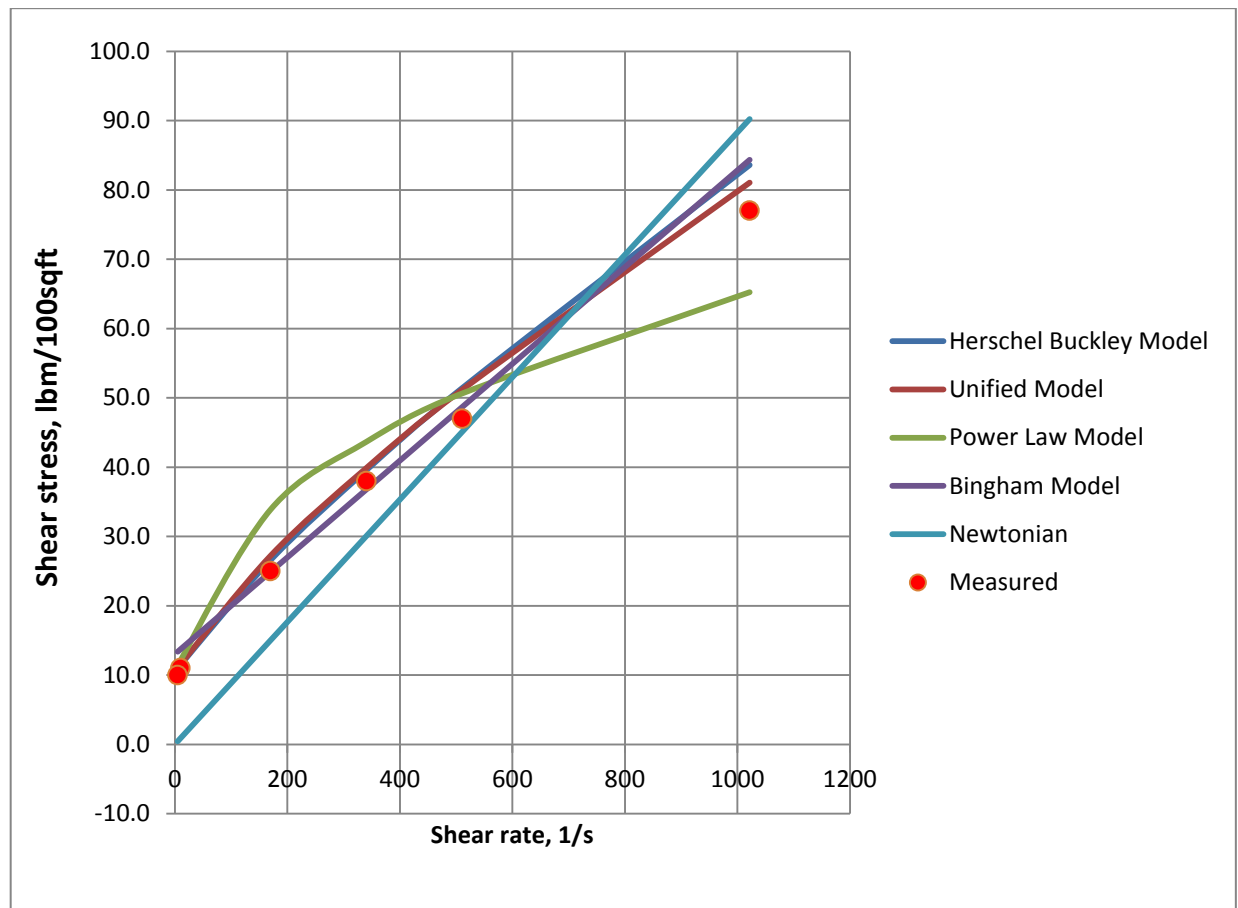


Figure 3.9: Comparison of different rheology models measurement of the 90/10 OWR at normal temperature (80 °F)

The comparison of errors obtained from the analysis among the models for the 90/10 OBM at the normal temperature (80°F) is shown in the Figure 3.10. The cumulative error between the models and the data for the three temperature data was calculated. The results are shown in figure 3.10 along with the tabulated data. As can be seen, the Unified and Herschel Buckley models exhibit lowest error rates compared with the other models. The Bingham and the power law models show similar error rates. The

result shows that the Newtonian model is not suitable to describe the behavior of the drilling fluid systems.

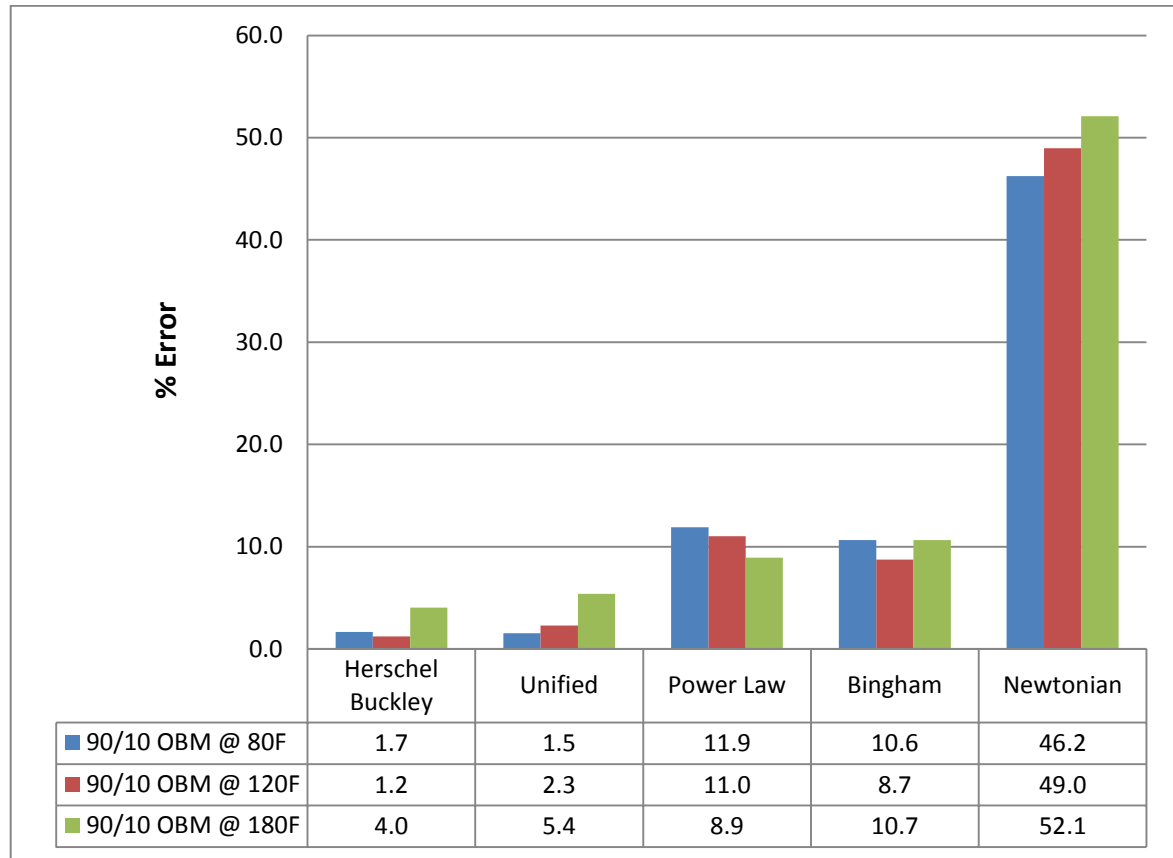


Figure 3.10: Comparison of the different rheology models errors of the 90/10 OWR at the 80, 120 and 180°F

3.2.3 Temperature Dependent Plastic Viscosity Modeling of 70/30 & 90/10 OBMs

The rheological data obtained from the experimental tests have been analyzed to generate correlations equation between the plastic viscosity of the drilling fluid and temperature. Figure 3.11 shows polynomial best fit equation.

As can be seen, the temperature has a significant influence on the plastic viscosity of the 70/30 than the 90/10 OBM systems. This shows that the behavior of the 90/10 in terms of hydraulics and cutting transport efficiency is not very much varies comparing

to the 70/30 OBM. Evaluation of hydraulics and cutting transport efficiency of two drilling fluids will be carried out later in the performance simulation.

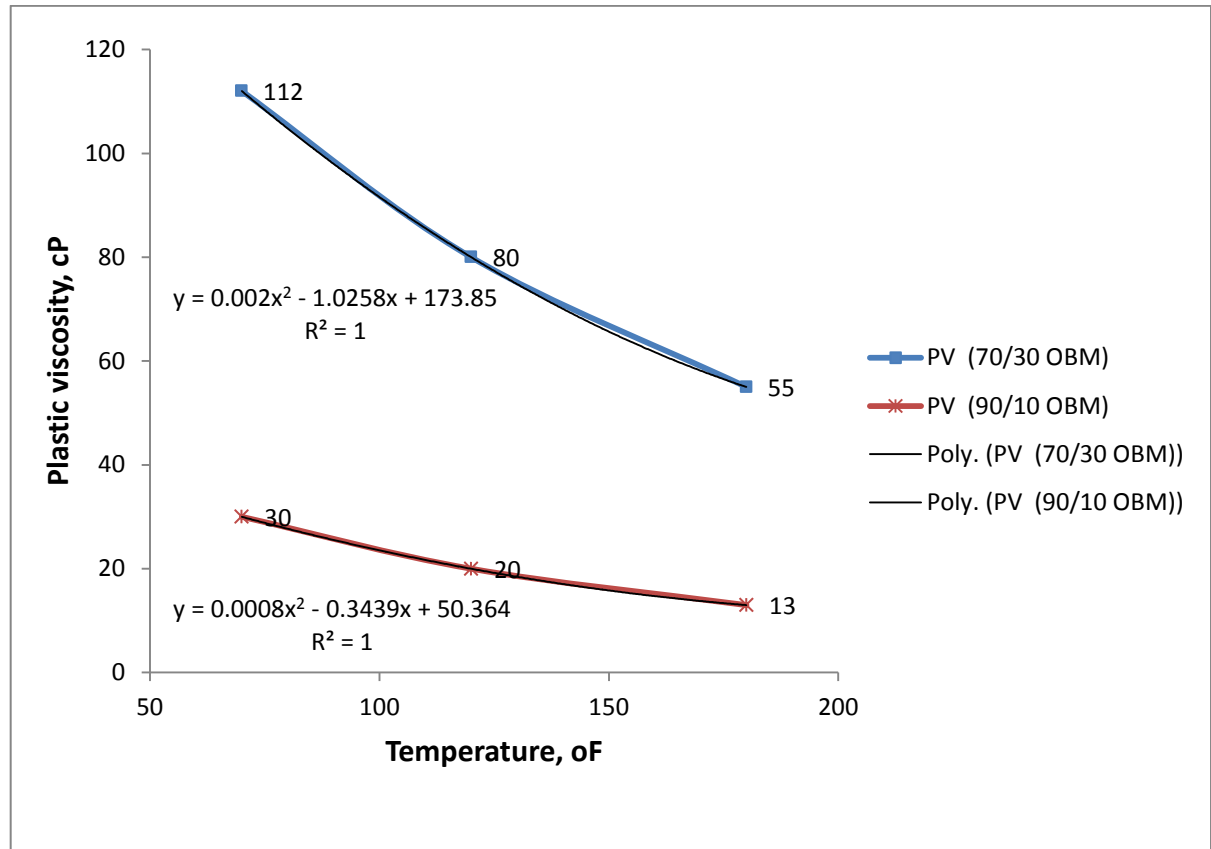


Figure 3.11: Comparison of the temperature effect on the Plastic Viscosity of the 70/30 and 90/10 OWR

Mud System	Plastic Viscosity Equation	R ²
73/30 OMB	PV = 0.002T ² - 1.0258T + 173.8	1
90/10 OMB	PV = 0.0008T ² - 0.3439T + 50.364	1

Table 3.1 Temperature dependent plastic viscosity models

3.2.4 Temperature Dependent Yield Stress Modeling of 70/30 & 90/10 OBMs

Similarly, temperature dependent yield stress correlations equation is developed. Figure 3.12 shows that polynomial equation fits the measured data. The 90/10 OBM shows a minimum value point between the 80°F and 180°F. On the other hand, the 70/30 OBM shows a decreasing trend as temperature increase. As can be seen at higher temperature, the yield stress values are getting closer than at the lower temperature.

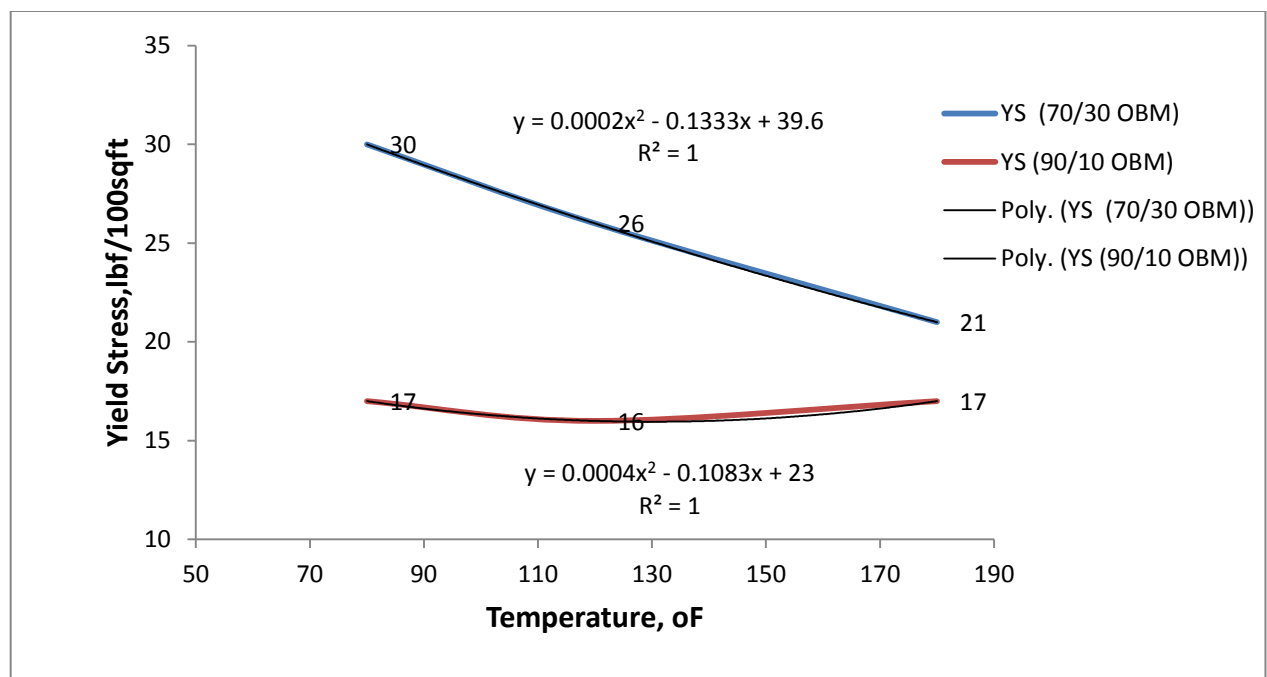


Figure 3.12: Comparison of the temperature effect on the Yield Stress of the 70/30 and 90/10 OWR

Table 3.2 shows the yield stress as a function of temperature. Please note that if the measurement had been done at different pressure and temperature the results would have been different.

Mud System	Yield Stress Equation	R ²
73/30 OMB	YS = 0,0002x ² - 0,1333x + 39,6	1
90/10 OMB	YS = 0,0004x ² - 0,1083x + 23	1

Table 3.2: Temperature dependent yield stress equations

3.2.5 Hydraulic Simulation and Analysis

For many operations, ECD is an important parameter. For instance well stability, cutting transport and stress in drill string are functions of the ECD. As mentioned in the introduction part, ECD is the sum of the static mud weight and the annular friction loss. The annular friction pressure loss is determined by hydraulics models. Therefore it is interesting to compare the hydraulic behavior of the 70/30 and 90/10 OBM systems at various temperatures.

In the industry, there are several hydraulic models available. However, in this thesis, the unified model is selected since the rheology model prediction shows a lower error rate (see section §3.2.1 & §3.2.2).

3.2.5.1 Experimental arrangement

For the hydraulic friction loss comparisons a vertical well with a total depth of 10000 ft well geometry was considered. The well has 9 5/8 in casing as the last casing and the casing shoe is set at the 8600 ft depth. Internal diameter of the casing is 8,755 in. The outer and inner diameters of the drill pipe are 5 in and 4,275 in respectively.

The drill collar is placed in the open hole and it has a length of 500 ft. And the drill collar is located 900 ft from the casing shoe. The outer and inner diameters of the drill collars are 8 in and 3 in respectively. Inner diameter of the open hole is the same as the casing hole that is 8,755 in.

Surface pressure is assumed to be zero. The drill bit has three nozzles of 28 in size.

The rheology measured data shown in Figure 3.1 are used in Figure 3.13 experimental well. Table 3.3 is the well construction geometry.

DP	Drill collar	Openhple	Casing	Nozzle
5'x4.275''	8x3''	8.755	9 5/8	3x28''

Table 3.3: Well construction geometry

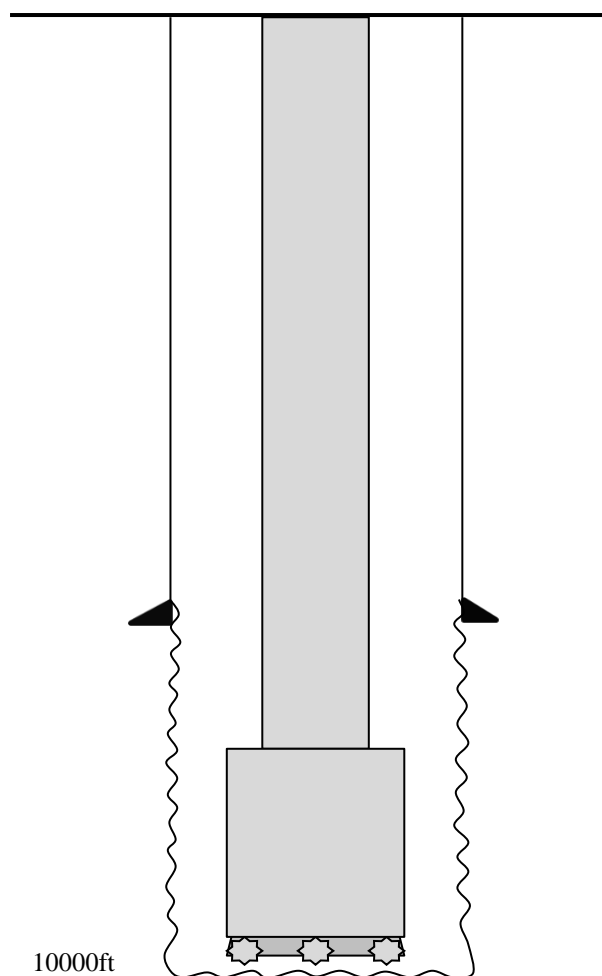


Figure 3.13: Simulation well for hydraulic analysis

3.2.5.2 Simulation result

As mentioned earlier, the Unified hydraulics model was used to compare the frictional pressure losses of the 70/30 and the 90/10 Oil-Based Mud systems. The simulation was performed the rheology data obtained from the 80, 120 and 180°F. During the simulation, the flow rate was varied from 50 to 300 gpm.

Figure 3.14 shows the simulation result. As can be shown the 70/30 OBM exhibits a higher friction loss in compared to the 90/10 OBM. This is directly associated with the higher density and the higher viscosities.

As can also observe from the 70/30 OBM that as temperature elevates from 80-120°F, the pressure loss higher than as temperature increases from 120-180°F. Similar behavior also can be observed on the Fann 35 data.

The relative change in the 90/10 is lower than the 70/30 as temperature changes. This behavior can also be observed in the Fan 35 data.

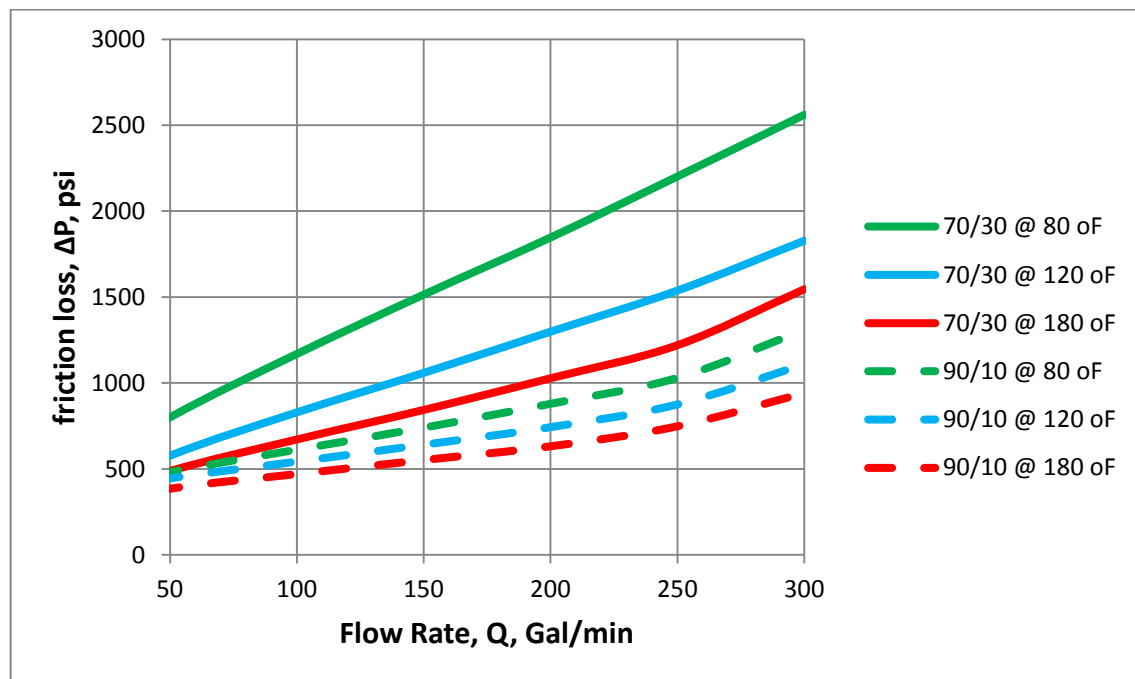


Figure 3.14: Comparison of the frictional pressure losses of the 70/30 and 90/10 OWR at the 80, 120 and 180°F based on the Unified Hydraulics model

Comparisons between the two mud systems were performed based on error analysis. Figure 3.15 shows the results of the error analysis. As can be seen the trends more or less show as a power law curves up to 250gpm and then begun reducing. At the 80°F, the error between the 70/30 and 90/10 OBM's shows 40% and 53% at 50gpm and 250 gpm respectively. However the error reduces to 47% at the 300gpm.

For an elevated temperature, i.e 120°F and 180°F, one can observe that both drilling fluid shows the same error rates at 50gpm and 300gpm. However, the difference in error rates shows almost constant between 100 and 250gpm, which is about 4-5 %.

The error rate is lower when the temperature is higher, as shown for the 180°F. One can also learn that the 70/30 OMB at 180°F nearly behaves like the 90/10 OBM at 80°F.

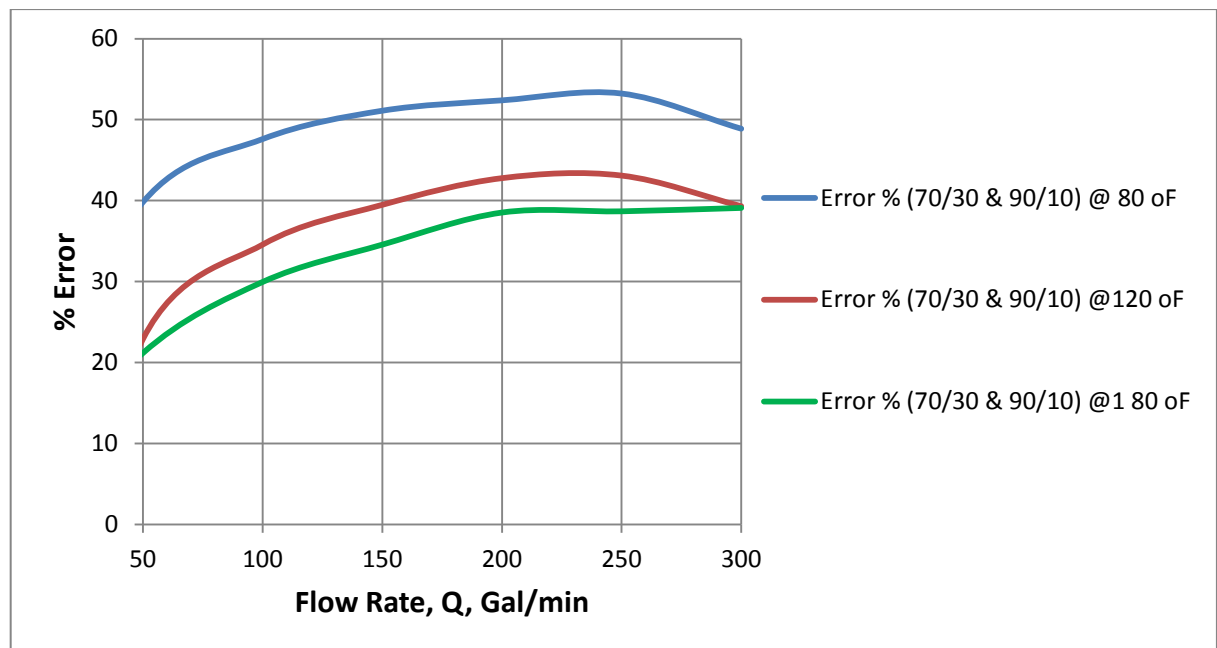


Figure 3.15: Comparison of the error% for the 70/30 and 90/10 OWR based on temperature differences

Similarly, the relative change or % error among three difference temperatures for two drilling fluids is evaluated. The results are shown in Figure 3.16.

For the 70/30 OBM as the temperature elevated from 80°F to 120°F, the hydraulics relative % difference increases from 28 to 30% as flow rate increases from 50 to 250 gpm respectively. The error % increases from 39 to 45% as the temperature elevated from 80°F to 180°F.

During the temperature elevated from 80°F to 120°F, the hydraulics relative % difference for the 90/10 OBM increases from 8 to 15% as flow rate increases from 50 to 250 gpm respectively. The error % increases from 20 to 28% due to the temperature elevated from 80°F to 180°F.

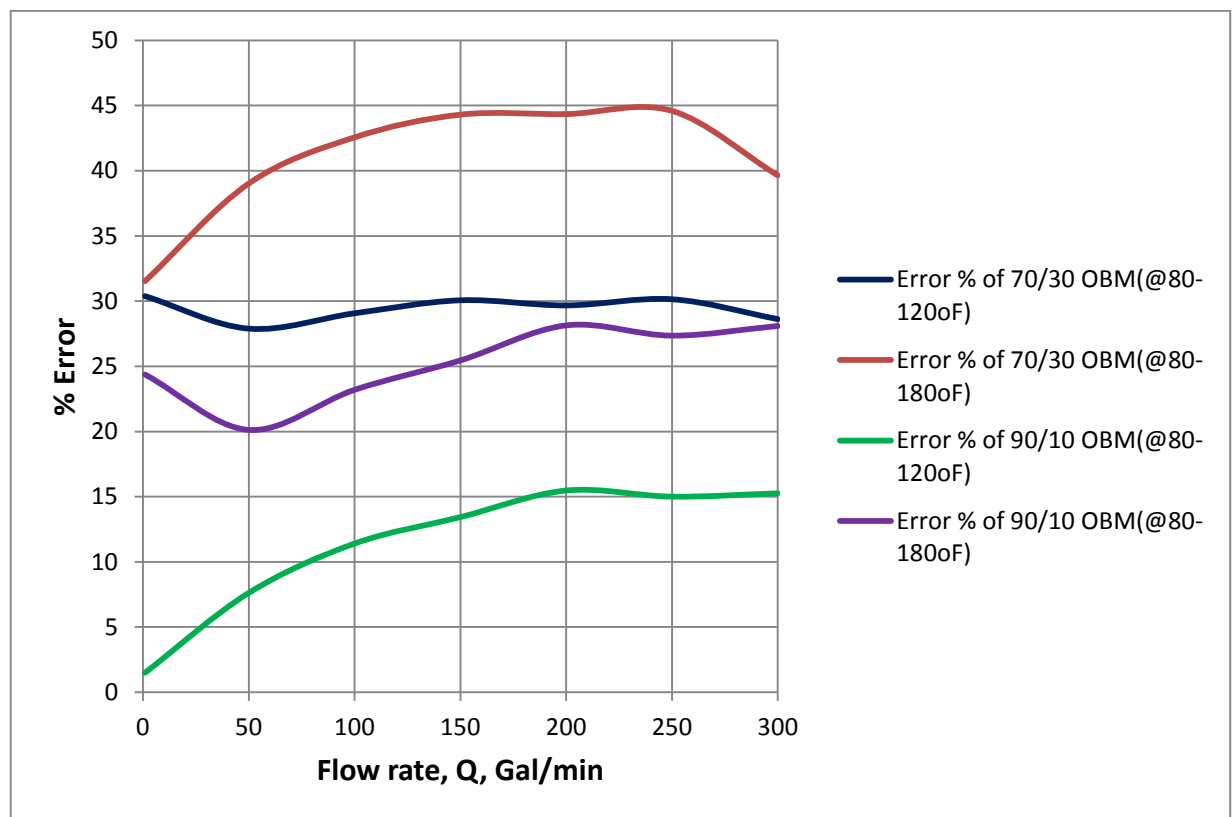


Figure 3.16: Comparison of the error% for the 70/30 and 90/10 OWR based on temperature elevated from 80-120°F and 80-180°F

The overall analysis shows that the appropriate knowledge of the thermodynamics states of drilling fluid rheology and physical properties is very important for the appropriate prediction of the hydraulic in the drilling formation. For this, it is important to derive a model which predicts the behavior of the drilling fluid at any temperature and pressure.

3.3 Flow in Sand Pack Porous Media of 70/30 & 90/10 OBMs

In this study, the rate of the two drilling mud filtrate invasion into porous media is investigated. The porous media is one sized homogeneous sand packs of 24% porosity.

Though the two mud system have different densities, the depth fluid column is calculated in order to have the same bottom hole pressure at the top of the sand pack.

The depth of drilling fluid flow into the porous sand pack was measured every 30min until the flow rate become stable.

Flow in 70/30 OBM

Figure 3.17 shows the diffusion test process during filling of mud and after 150min testing period. The first measurement of diffusion rate for 70/30 OBM is carried out after 30min, and the diffusion depth of drilling mud is recorded as 2,8 cm. The depth of invasion finally stabilizes after 150min reaching to 3,8cm.

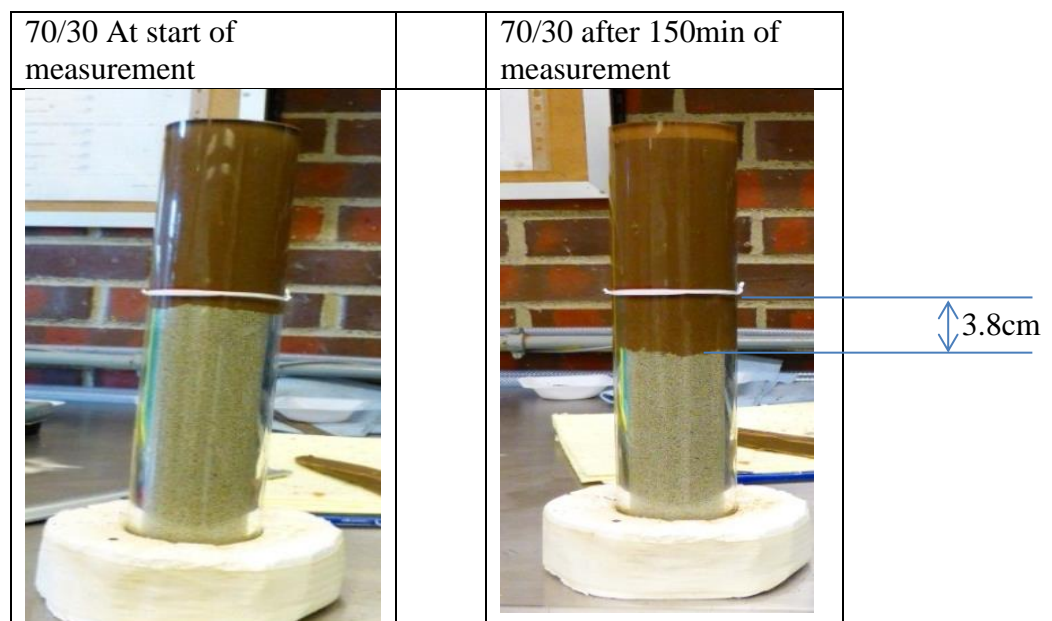


Figure 3.17: Illustration of diffusion of 70/30 OBM in Sand pack

Flow in 90/10 OBM

Unlike the 70/30 OBM system, an instant diffusion (spurt loss) of the 90/10 drilling fluid is observed as shown in the picture. Figure 3.18 shows the process of fluid invasion into the sand pack.

After 30 min the depth of invasion recorded was 4,5cm. The rate of diffusion gradually decreases after 150min. The invasion stopped after 150min recording 4,87cm.

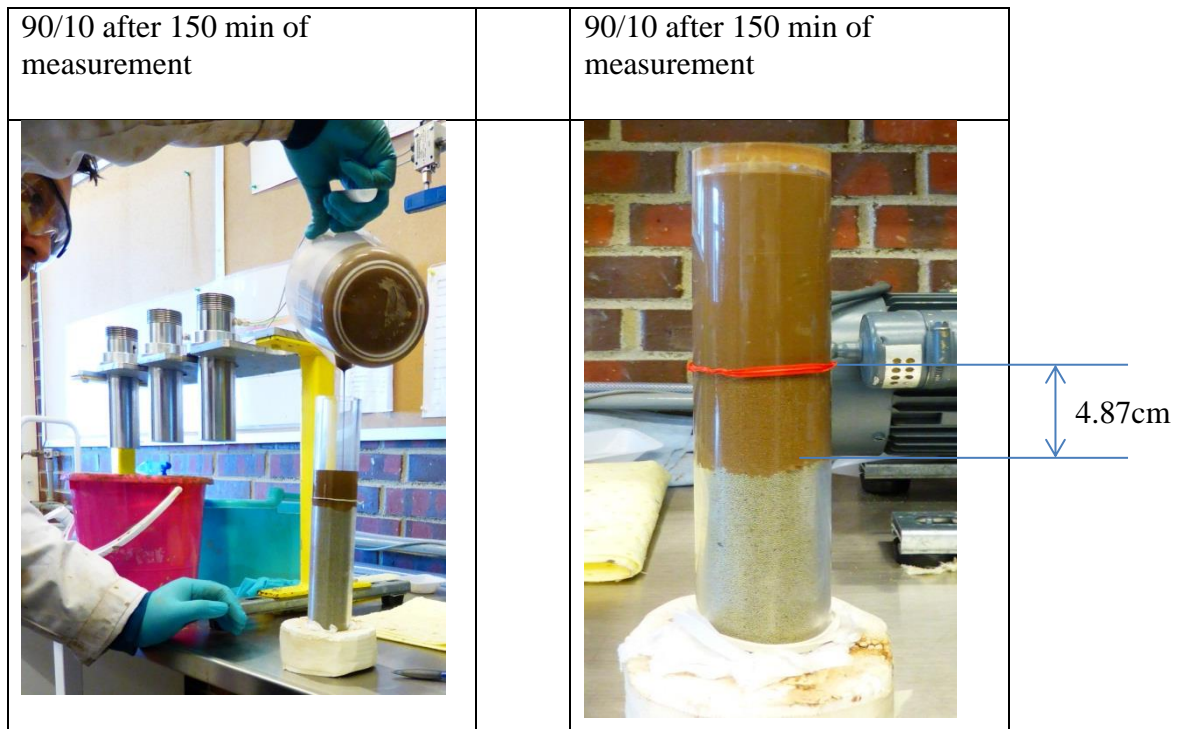


Figure 3.18: Illustration of diffusion of 90/10 OBM in Sand pack

Figure 3.19 shows the depth of mud invasion measured in time. Comparing with 70/30 OBM, the 90/10 OBM exhibits a quick fluid invasion rate into the sand pack due to fact that the 90/10 OWR is less viscous than the 70/30 OWR.

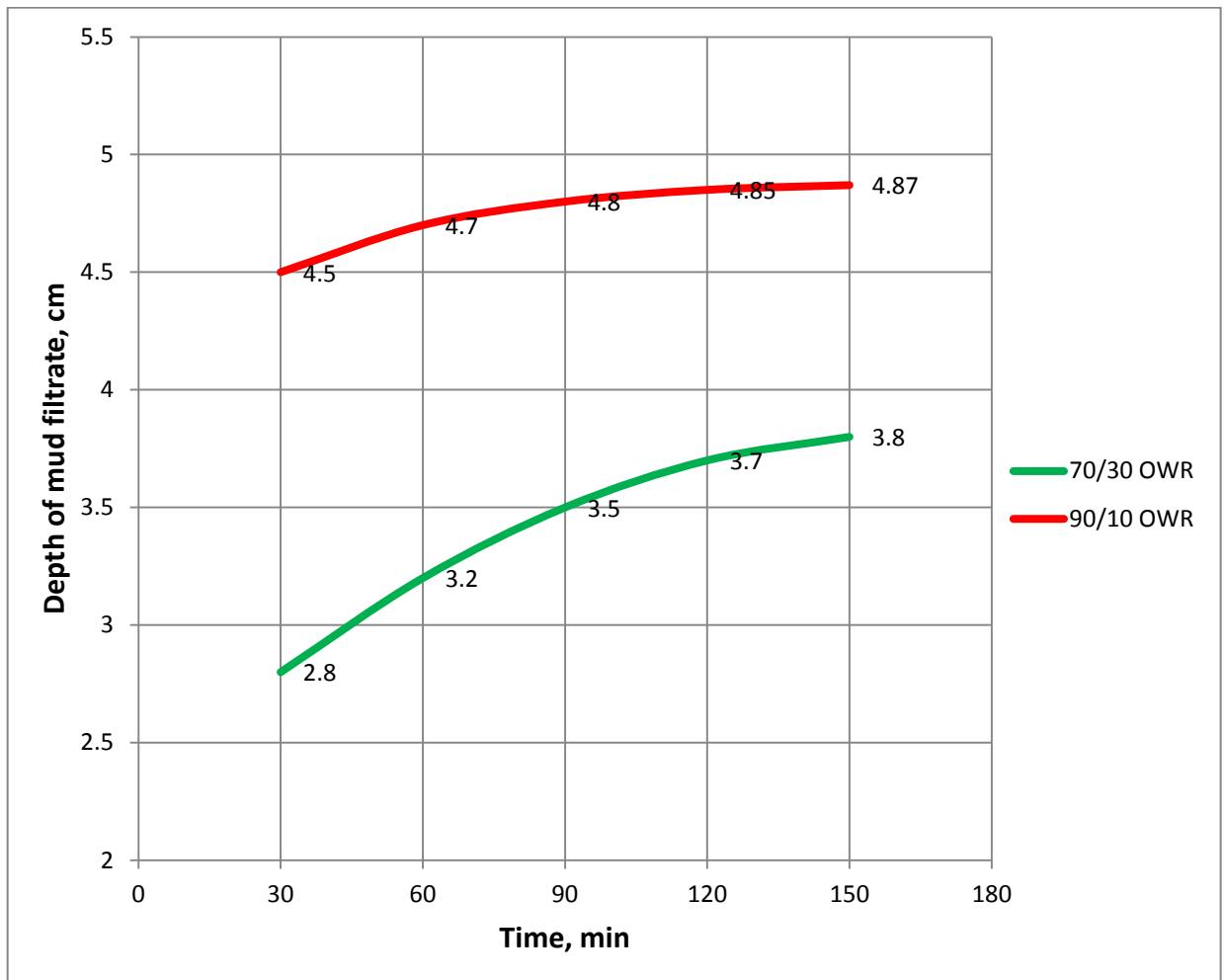


Figure 3.19: Diffusion of the 70/30 and 90/10 OBMs against Time

3.4 Visco-elasticity Test

Viscoelastic behaviors of the two mud systems were investigated by using Anton Paar MCR 301 Rheometer, which include Oscillatory Amplitude Sweep and Oscillatory Frequency Sweep Test. The tests were performed at 22°C. The experiment was conducted in parallel plate. Figure 3.20 shows the picture of Anton Paar MCR 301 Rheometer.

A repeat test was performed. It was observed that the behavior was changing due to gelation. In main part of the report presented only one of the selected.



Figure 3.20: Illustration of the Anton Paar MCR 301 Rheometer

3.4.1 Oscillatory Amplitude Sweep Tests-70/30 OBM and 90/10 OBM

This test is the first test conducted to determine the linear viscoelastic range, the range of strain (or stress) where G' and G'' are constant. It is also used to detect structural stability, strength and dynamic yield point of drilling fluids.

Test parameters and Test result

The first experiment in dynamic tests is the oscillatory amplitude sweep test to define the linear viscoelastic range. Amplitude sweep tests were conducted with a constant frequency of 10 s^{-1} and a strain ramp from 0,001 to 1000%.

Figure 3.21 shows the comparisons of the amplitude sweep test results. As can be shown the storage and the loss modulus of the 90/10 OBM system is higher than the 70/30 OBM system. At a frequency about lower than 0,3% strain the 70/30 OBM dominates which indicates the stable gel structure or solid like property. This indicates the viscoelasticity of the fluid system such that the fluid deformation is dominated by elastic behavior. After the crossing point the fluid behaves viscoelastic fluid since the loss modulus greater than the storage modulus

Similarly until about lower than 0,7% strain, the 90/30 OBM dominates which indicates the stable gel structure or solid like property. This system is viscoelastic solid. It is interesting to observe a transitional system that behaves like a mixture of viscoelastic solid and viscoelastic fluid within the range of 0,7-10% strain. The system then dominated by viscoelastic fluid since the loss modulus became large than the storage modulus.

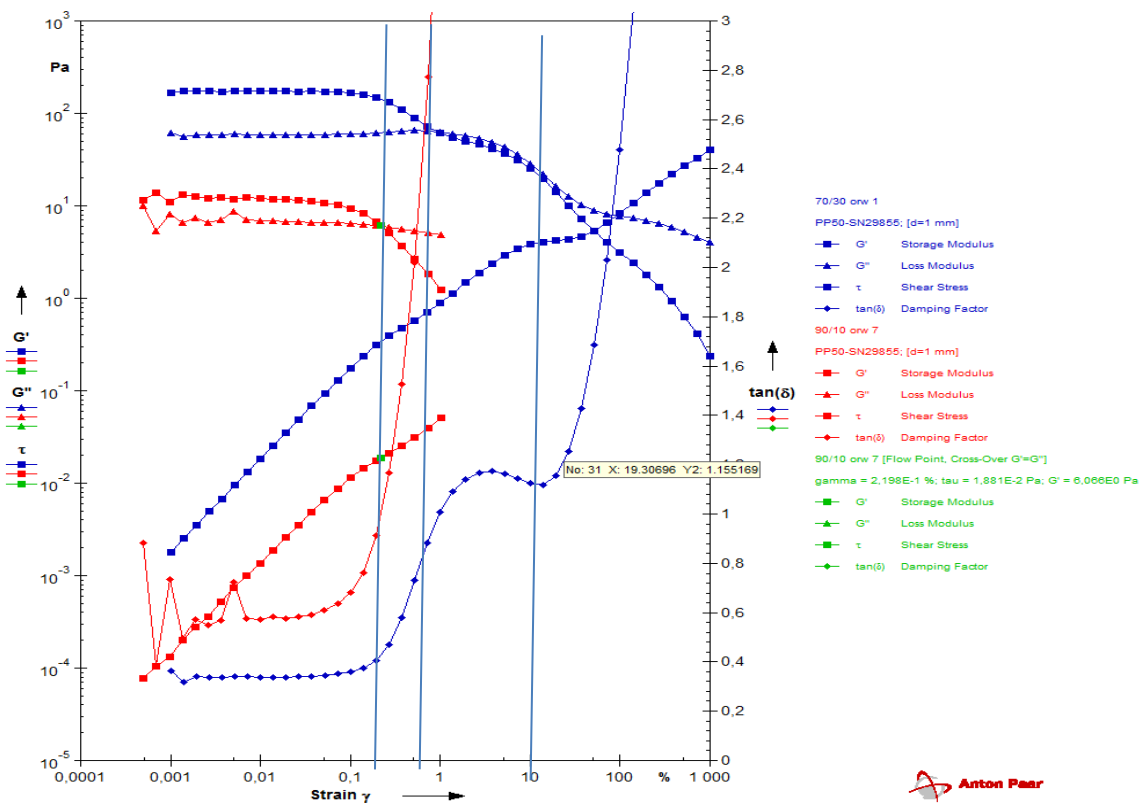


Figure 3.21: Amplitude sweep test of the 70/30 and 90/10 OBM systems

3.4.2 Oscillatory Frequency Sweep Test 90/10 OBM

The frequency sweep test was performed based on the result obtained from the amplitude sweep test.

The test was also conducted in the linear viscoelastic range. In this study, strains of 0,05% and the frequency ramps from 100 to 0,01 in a log scale were used.

Figure 3.22 shows the test results. As can be shown throughout the test period the G' and G'' modulus are frequency dependent and oscillating up and down. This event is interpreted as the fluid system behaves unstable gel structure or solid like property since the storage modulus is higher than the loss modulus. It is also observed that complex viscosity is also a frequency dependent. As can be seen the viscosity profile follows the storage modulus profile. This indicates that probably there is a direct relationship between these two profiles.

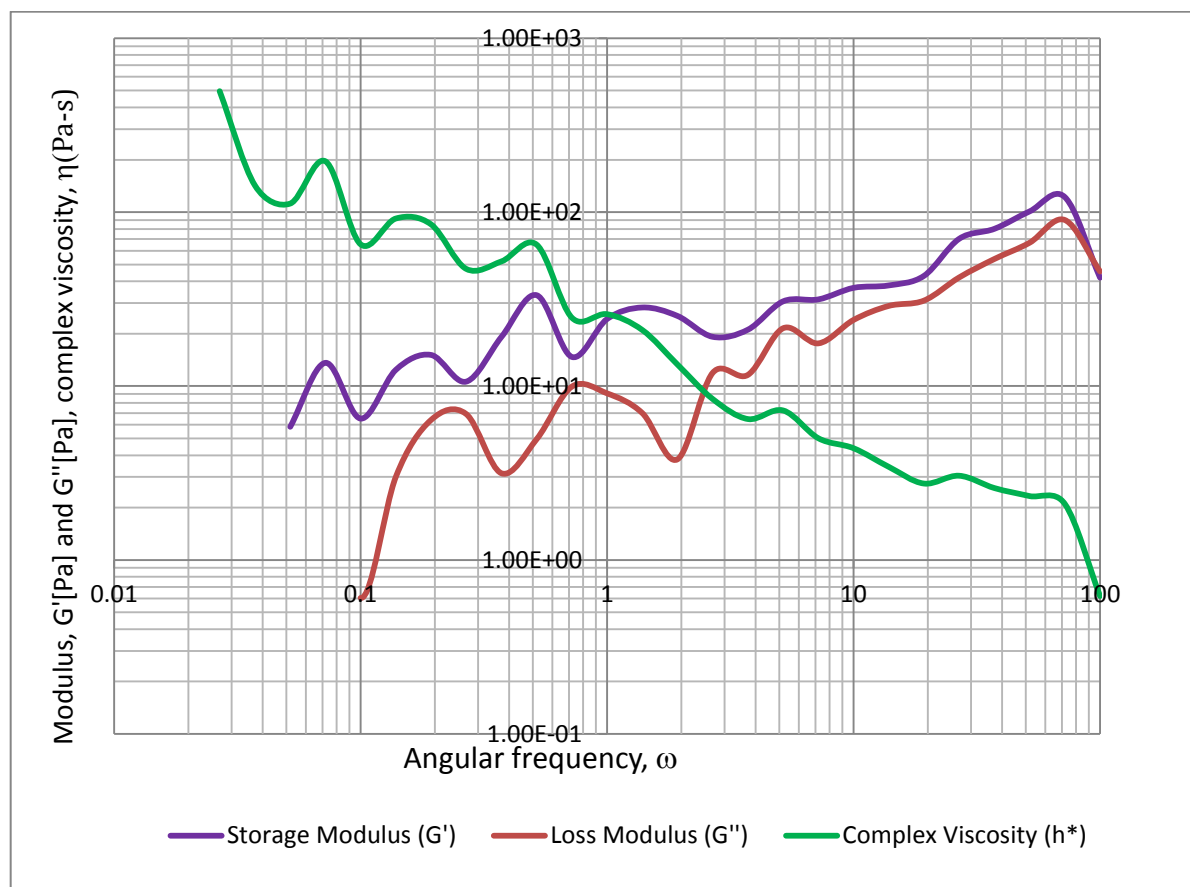


Figure 3.22: Sweep frequency test for 90/10 OBM system

4 Drilling Fluid Performance Evaluations

The 70/30 and 90/10 OMB mud systems will be compared through their performance in drilling operations. The performance of the drilling fluids will be investigated through experimental and simulation works. These are bridging, cutting transport efficiency, and hydrodynamic force effect on Hook Load.

4.1 Bridging Experimental Study

The behavior of the 70/30 and the 90/10 Oil-Water Ratio two mud systems are characterized in terms of their bridging performance. The 70/30 mud system is more viscous in compared to the 90/10 mud system. The viscosity properties of the drilling fluid may have a relation with the particle stability at the mouth of a fracture. Therefore, for the comparisons purpose a loss circulation experimental test has been performed. From the test result the parameters used for comparison of the two mud systems includes the average pressure, the maximum pressure and the peak of the pressure.

The question to be raised is that is there any correlation between bridging with fluid behavior?

4.1.1 Experimental Arrangements and Test Procedure

Figure 4.1 shows the static bridging experimental setup. Mud systems is mixed with particles and filled in the cylindrical mud holder (5) having 35mm and 64mm for the inner and outer diameters, and 150mm long. A single line-opening slot is designed to simulate a fracture in the formation. The suspensions-settling process is affected by gravitational force and buoyancy force. The maximum pumping capacity of the pump is 50MPa. The openings used for testing are 200 μ m, 300 μ m, 400 μ m, and 500 μ m. The depth of the slots is 10mm and the length is 24,4mm. Drilling fluid with suspension is filled in (5) and forms a filter cake at (4). As the cake collapses, it passes through the opening slot cell (7), and the fluid collects in the graduated cylinder (8). The volume of mud loss can be measured to evaluate the efficiency of particles in the mud cake.

The pressure response compressed by Gilson pump is recorded in the PC-control Lab-View (1). Valves (3) and (6) control fluid (air) and mudflow respectively [7].

The experiment was carried out at room temperature and pressure. Before the actual testing began, the test preparations were performed by closing valve (6) and opening valve (3). The water is injected by Gilson pump until water began flowing out through (9). This ensured the avoidance of undesired air from the system. Once the system was ready, the test was then initiated by closing valve (3) and opening valve (6) throughout the 30-minute duration. The injection rate during testing was 2ml/min.

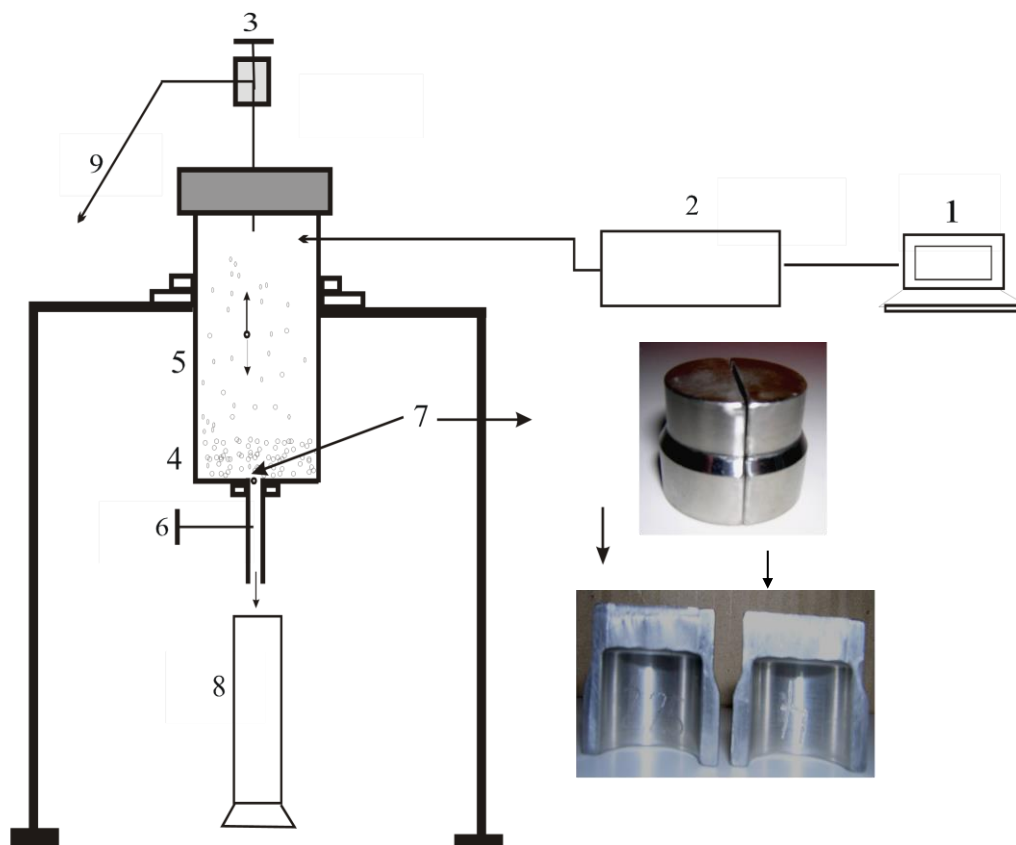


Figure 4.1: Schematic particle bridging testing experimental set-up (1) Lab-View (2) Gilson pump (3) Valve to control air/fluid flow (4) Cake (5) Drilling fluid with suspension (6) Valve to control mudflow (7) Opening slots (8) Cylinder (9) Fluid/air outflow [7]

4.1.2 Description of Drilling Fluids

In this experiment, two types of oil-based mud have been obtained from MI-SWACO. These are 70/30 oil-water ratio and another type with 90/10 oil-water ratio. The two different types of fluids have both different densities and different rheology.

Figure 4.2 shows rheological properties of the drilling mud systems used for bridging experiments. .

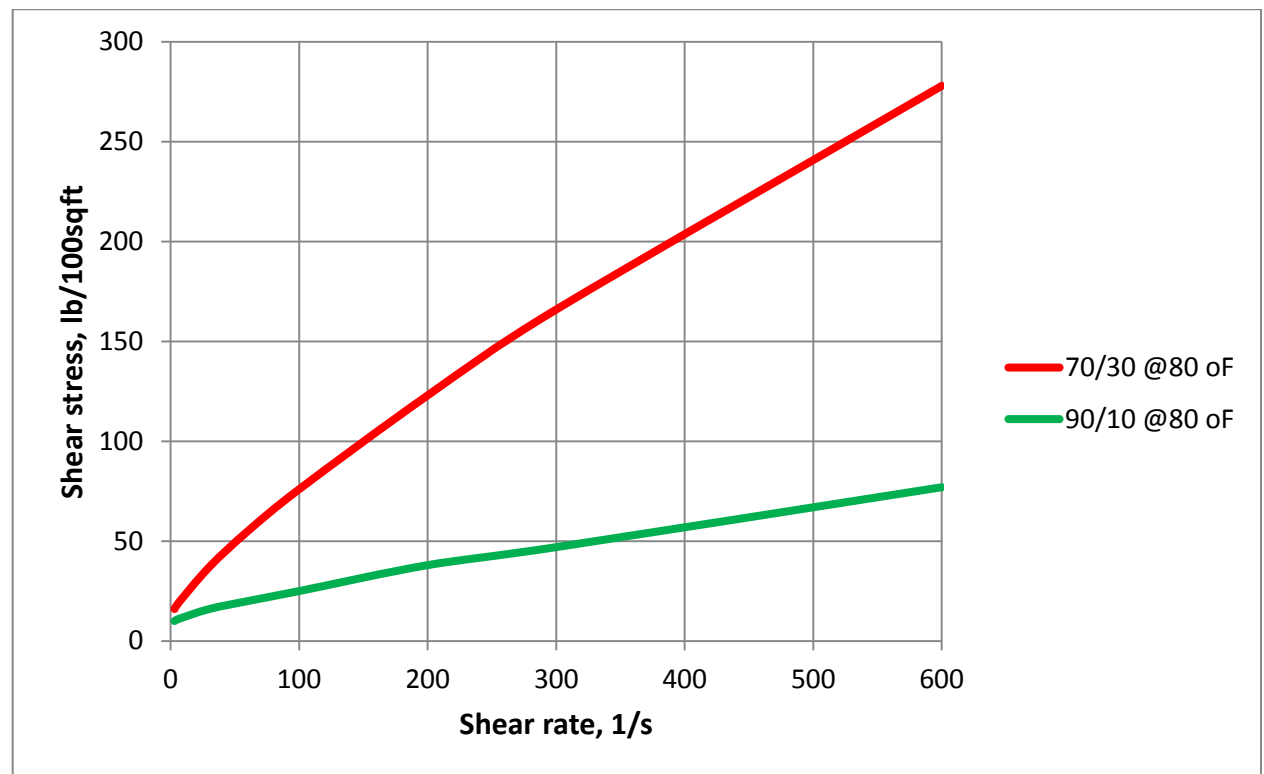


Figure 4.2: Drilling fluid rheology for 70/30 and 90/10 OBM

Parameters	70/30 OBM at 80F	90/10 OBM at 80F
Plastic Viscosity	121	38
Yield Stress	88	16
Density	1.77	1.65

Table 4.1: Calculated viscosity and measured density of drilling fluids

4.1.3 Description of Particle – LC-lube

LC-lube particle was used as bridging material in the two drilling fluid. The LC-lube is the product of Baker Hughes. Basically the LC-lube is graphite. At first the particle is sieved in order to find out both the sizes of the particle and the percentage of the mass of each particle size Figure 4.3. Then the cumulative particle size distribution was generated as shown in Figure 4.4. As can be seen from the PSD, the D50 value is at about 300 micron. The D10 and the D90 are about 150 and 500 microns respectively. For the experiment, 200, 300 400 and 500 microns have been selected.

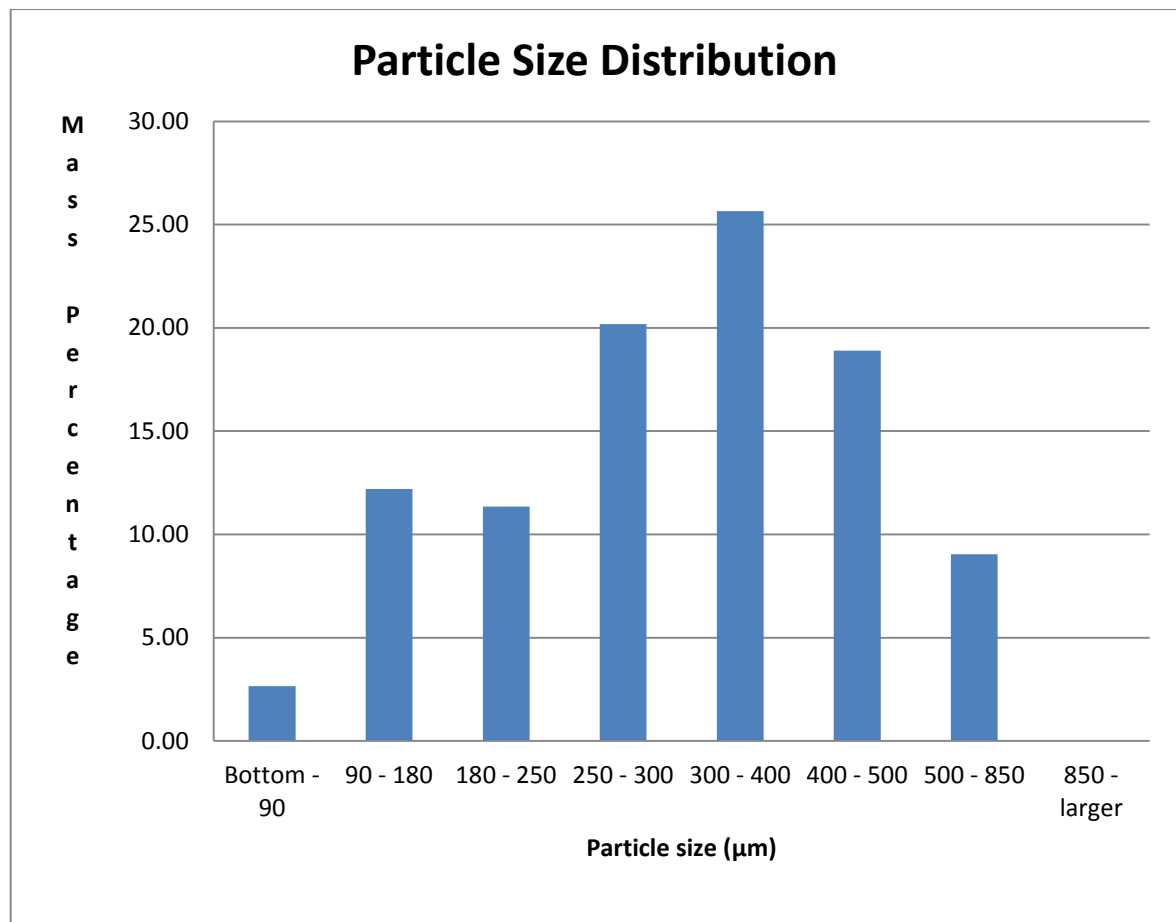


Figure 4.3: LC-Lube particle size distribution

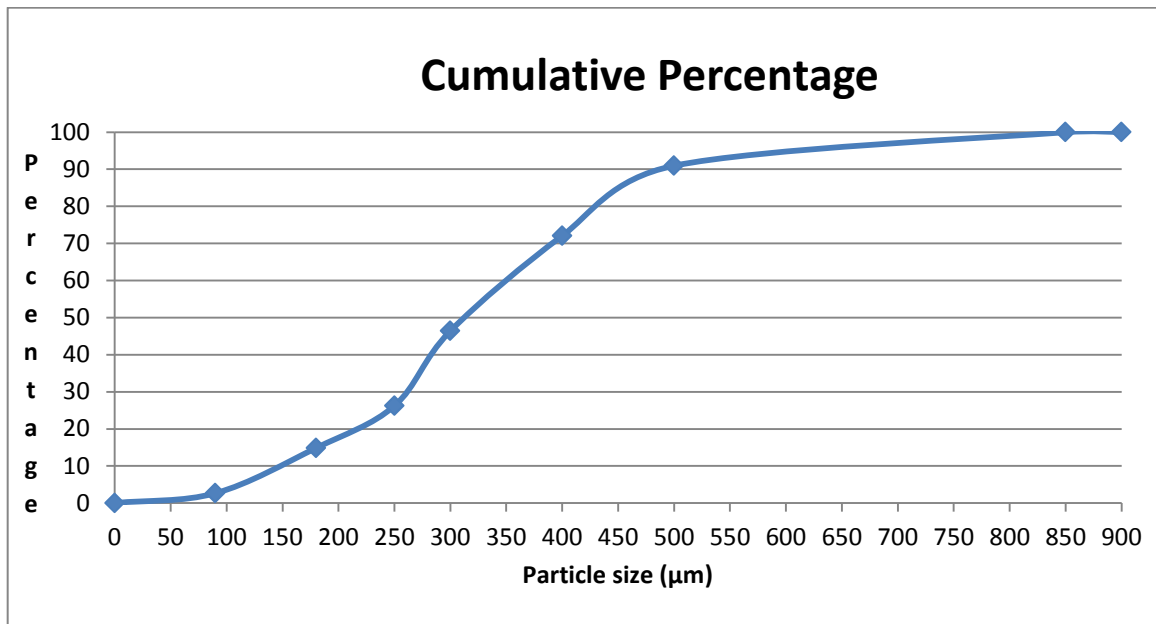


Figure 4.4: Cumulative Percentage of LC-Lube

SEM

To have a better insight of the structure of the particles Scan electron picture of the particle is taken Figure 4.5. As can be seen the LC lube is an irregular shape and having a longer length than the width. Mechanically on the Mohs scale the scratching is 4.

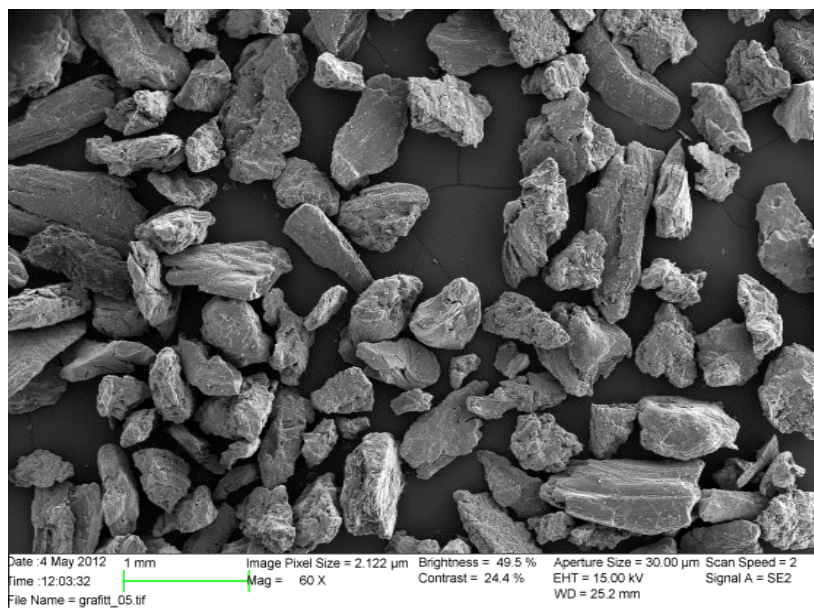


Figure 4.5 SEM picture of LC-lube at magnification of 60x

4.1.4 Bridging Test Results and Analysis

4.1.4.1 Bridging Test Result Summary

In the 70/30 and 90/10 OBM systems a 16,85 ppb LC lube was mixed for testing. The experiment was carried out at the 200, 300, 400 and 500 microns. Table 4.2 shows the test matrix and average bridging pressure obtained from test results.

Mud and additives	Slot μm	Average Pressure/20min
70/30 OBM + 16,85 LC Lube	200	10,1 MPa
70/30 OBM + 16,85 LC Lube	300	4,74 MPa
70/30 OBM + 16,85 LC Lube	400	2,81 MPa
70/30 OBM + 16,85 LC Lube	500	4,23 MPa
90/10 OBM + 16,85 LC Lube	200	13,99 MPa
90/10 OBM + 16,85 LC Lube	300	2,64 MPa
90/10 OBM + 16,85 LC Lube	400	0,57 MPa
90/10 OBM + 16,85 LC Lube	500	0,11 MPa

Table 4.2: Test matrix and average bridging pressure

The bridging test results obtained from 70/30 and 90/10 OBMs are plotted together in order to show a better comparisons.

4.1.4.2 Test with 70/30 OBM vs 90/10 OBM

The bridging performance of the 70/30 and 90/10 OBM are plotted for each opening slots. Figure 4.6 shows the comparisons of the two mud systems at 200 micron. As can be seen, during the first 10min testing period the bridging of the two systems shows equal strength. However after the 10min testing, the 90/10 OBM system shows a better performance. Figure 4.7-4.9 shows the test result at 300, 400 and 500 microns slots respectively. The results show that the performance of the 70/30 is better than the 90/10 OBM. One of the possible reasons why 70/30 is better bridging performance could be due to the high viscosity and the lower filtrate behavior of the

mud system allows good bridge stability. The overall results indicate the fluid barrier effect on wellbore strengthening.

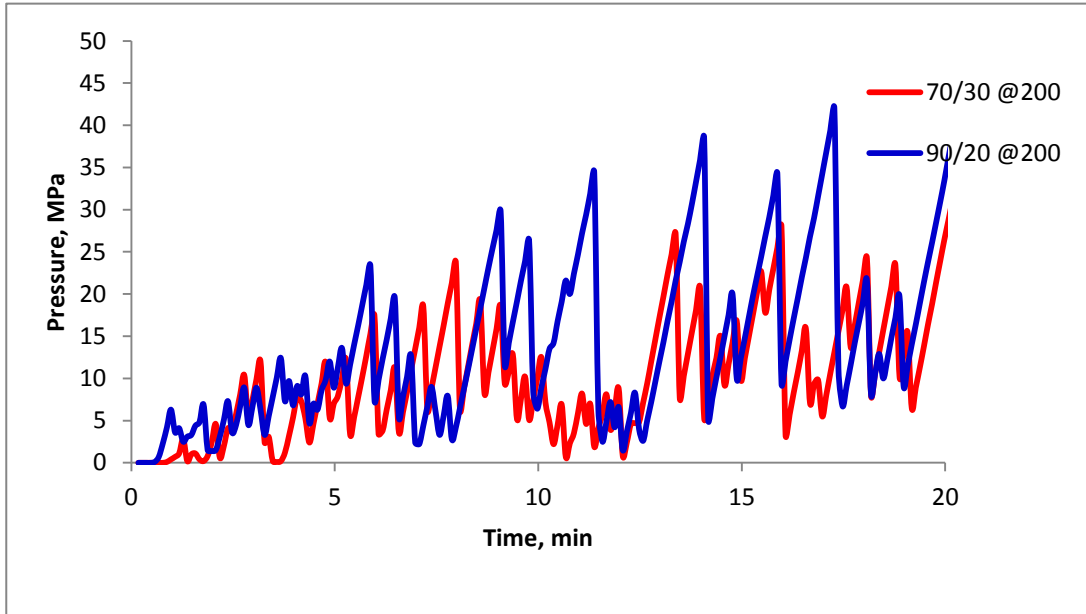


Figure 4.6: Pressure Profile of the 70/30 and 90/10 OBM for Bridging Test with 200 slot opening

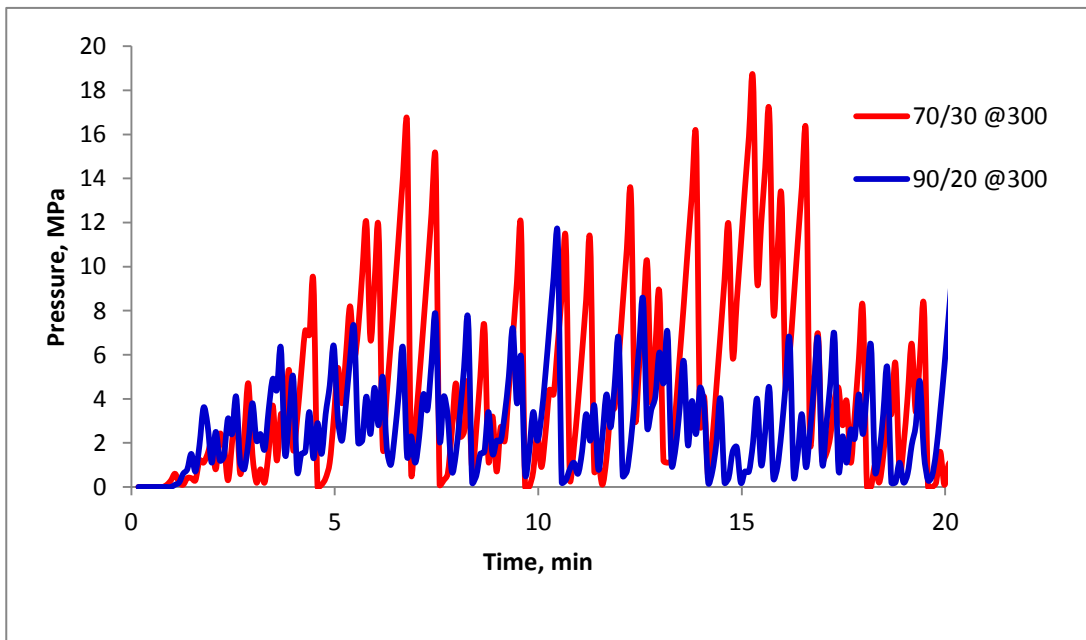


Figure 4.7: Pressure Profile of the 70/30 and 90/10 OBM for Bridging Test with 300 slot opening

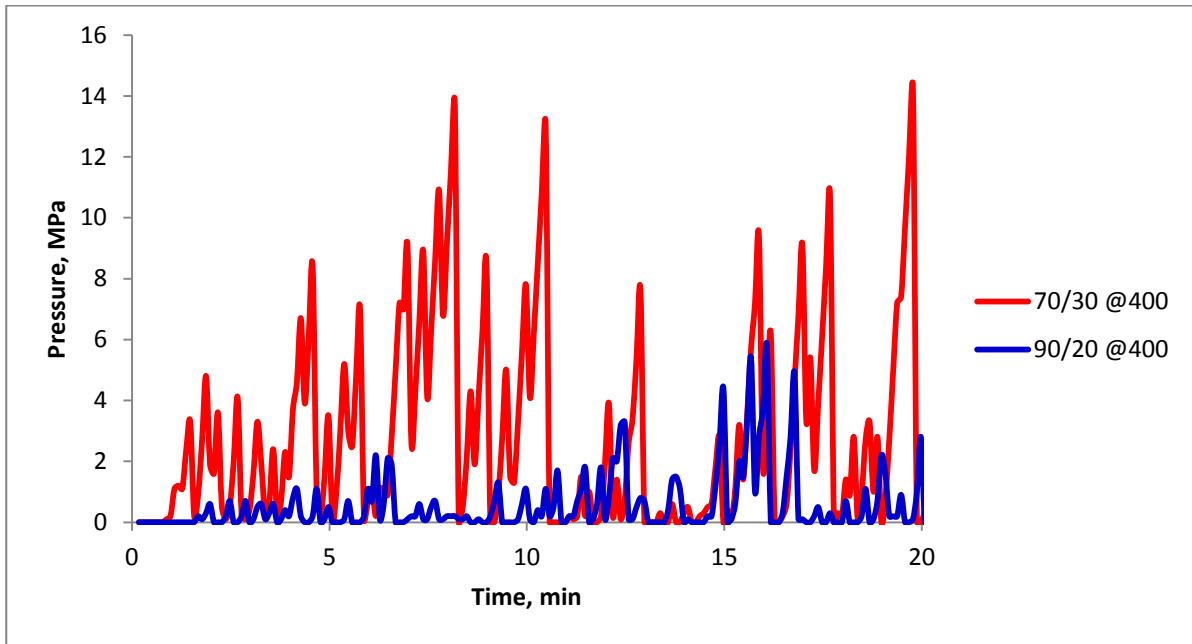


Figure 4.8: Pressure Profile of the 70/30 and 90/10 OBM for Bridging Test with 400 slot opening

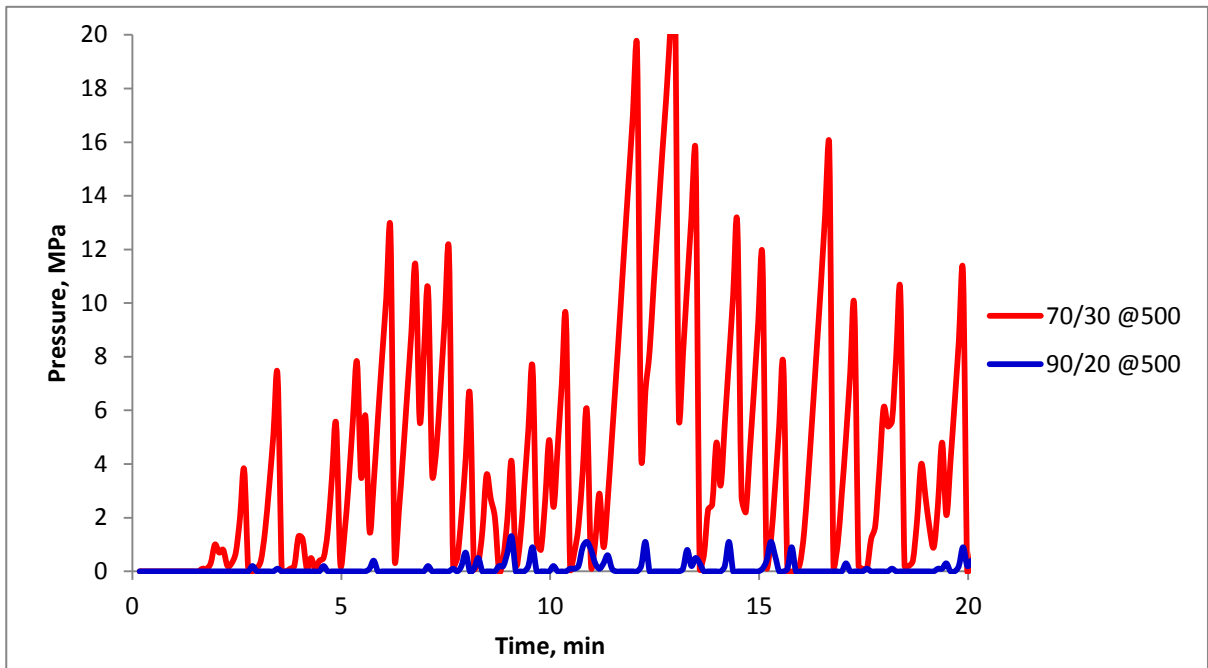


Figure 4.9: Pressure Profile of the 70/30 and 90/10 OBM for Bridging Test with 500 slot opening

4.1.4.3 Comparison and Analysis of the Experimental data

The experimental data analysis is based on the method presented by Mostafavi, V. [14].

Figure 4.10 shows the maximum Pressure in the cell (P_{max}) during the 20min testing duration. This magnitude describes the maximum strength of the bridging tolerate to carry the load. As can be shown the bridging in the 70/30 OBM records a higher maximum pressure than the 90/10 except at the 250 microns opening.

Figure 4.11 shows the average bridging pressure (P_{avg}) during the 20min testing duration. The result shows that very similar trend to the peak pressure shown in Figure 4.10. This pressure considers both pressure build-up and collapse pressures, which actually reflects the sealing capacity of the bridge.

Figure 4.12 shows the average of peak bridging pressures. The peak pressure is the pressure build-up right before bridge collapse. The magnitude describes the strength of the bridging performance of the system at the given slot during the testing period. The result shows similarly that the 70/30 OBM is better sealing performance than the 90/10 OBM system.

Figure 4.13 shows the number of pressure build-up before collapse is counted during testing period. The number of bridge (N) corresponds to the number of peaks as new bridge forms. However, comparing with the other figures, there is no direct correlations. Comparing the two mud systems, the 70/30 shows higher number of bridge than the 90/10 OBM. This means that as the bridge collapse, it forms new bridge by building the pressure.

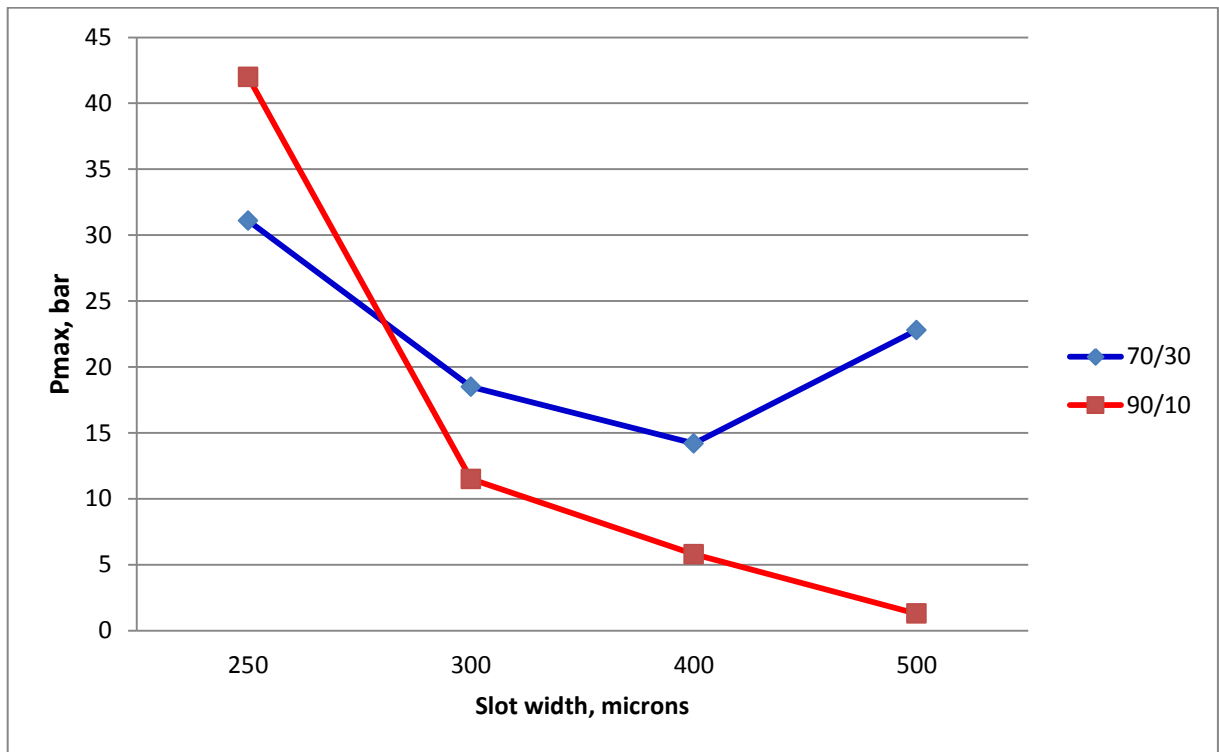


Figure 4.10: Maximum Pressure in tests with various Slot widths

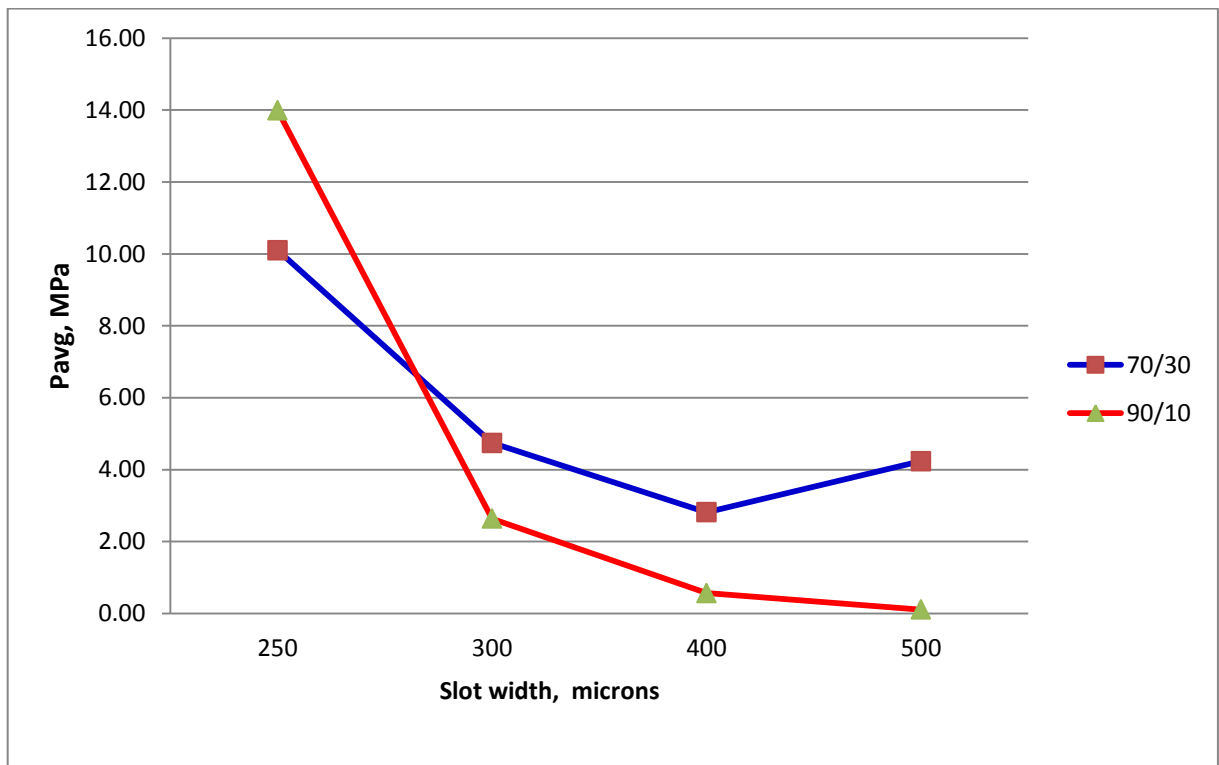


Figure 4.11: Average Pressure in tests with various Slot widths

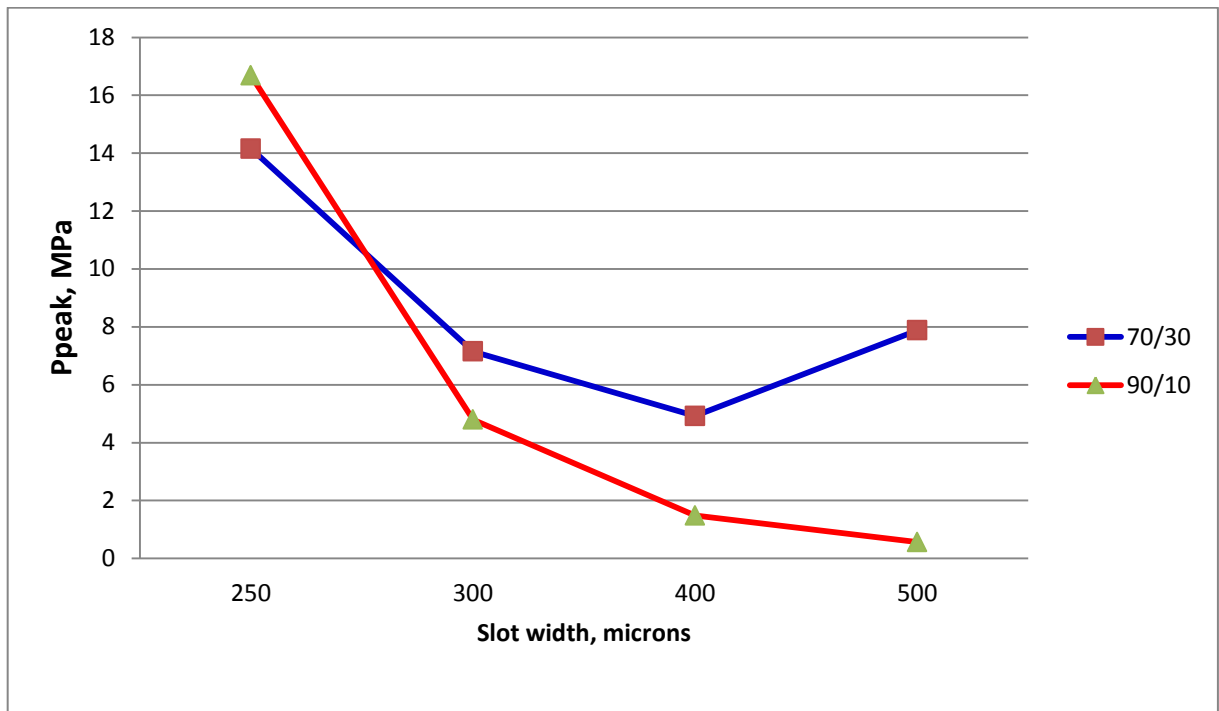


Figure 4.12: Average Peak Pressure in tests with various Slot widths

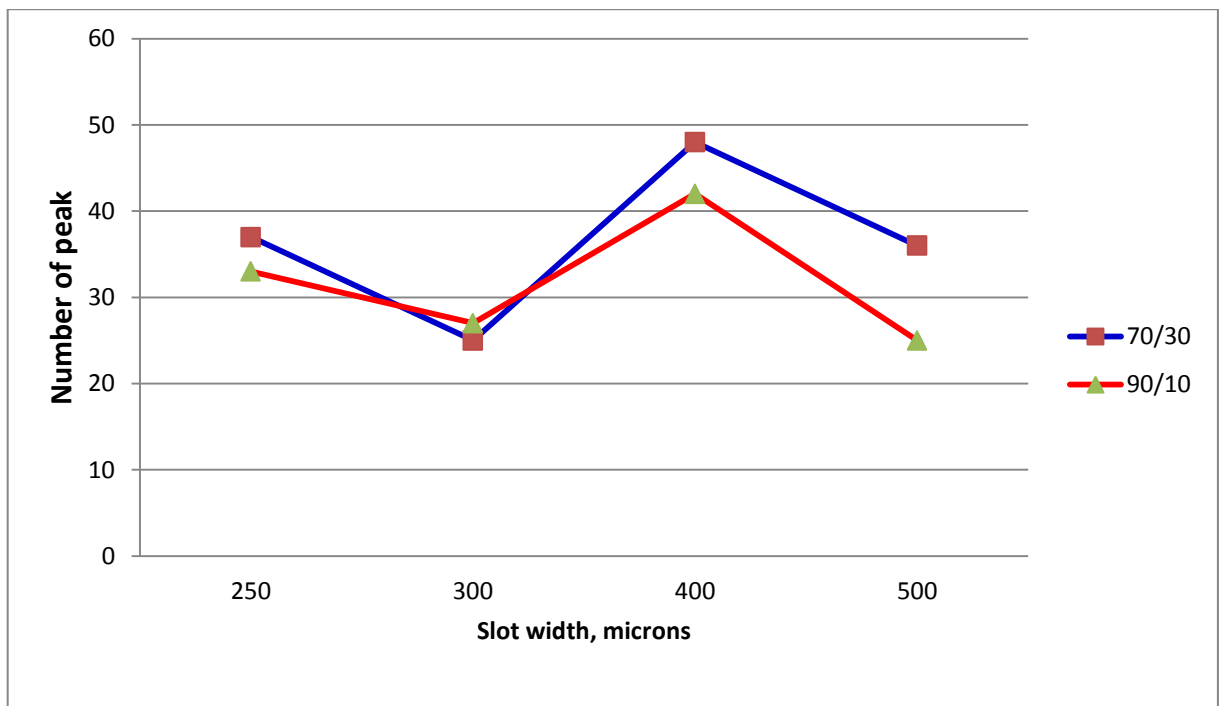


Figure 4.13: Number of peak as a function of Slot width

4.2 Hole Cleaning Efficiency of the 90/10 and 73/30 OBM systems

The cutting transport phenomenon is influenced by forces acting on particles such as: Forces acting on the particle determine the transport, deposition and suspension mechanism of cutting. Different types of loading acting on the particle when the cuttings are transported through the annulus. The forces can be categorized as hydrodynamic forces, static forces and colloidal forces. In addition sticking force due to the stagnation of the mud system [33].

The mud systems are characterized based on their hole cleaning performances. The comparisons are made at three temperatures conditions. The Fann 35 data shown in section § 3.1 are used for the evaluation.

The cutting lifting ability of fluid system is an important aspect for effective hole cleaning. There are several parameters that influence cutting transport efficiency. They are fluid properties, cutting properties and operational parameters [19][34][35]. In this section assuming that the cutting and well and operational parameters are constant, the two mud systems will be evaluated. The simulation experiment is performed in a real well geometry which consists of vertical and bend and inclined sections.

4.2.1 Simulation Setup

The experimental well is 11003ft measure depth long. The well is constructed with 12,26'' casing and 12,22'' open hole. A drill string which consists of drill pipe (OD=5'') and BHA are used in the simulation well. The detail of the well and string data is shown in Appendix E. Figure 4.14 shows the simulation experimental well. The simulation is performed with Well-PlanTM software [20] and Power Law rheology model is chosen for the simulation. Figure 4.15 shows the well inclination of the simulation.

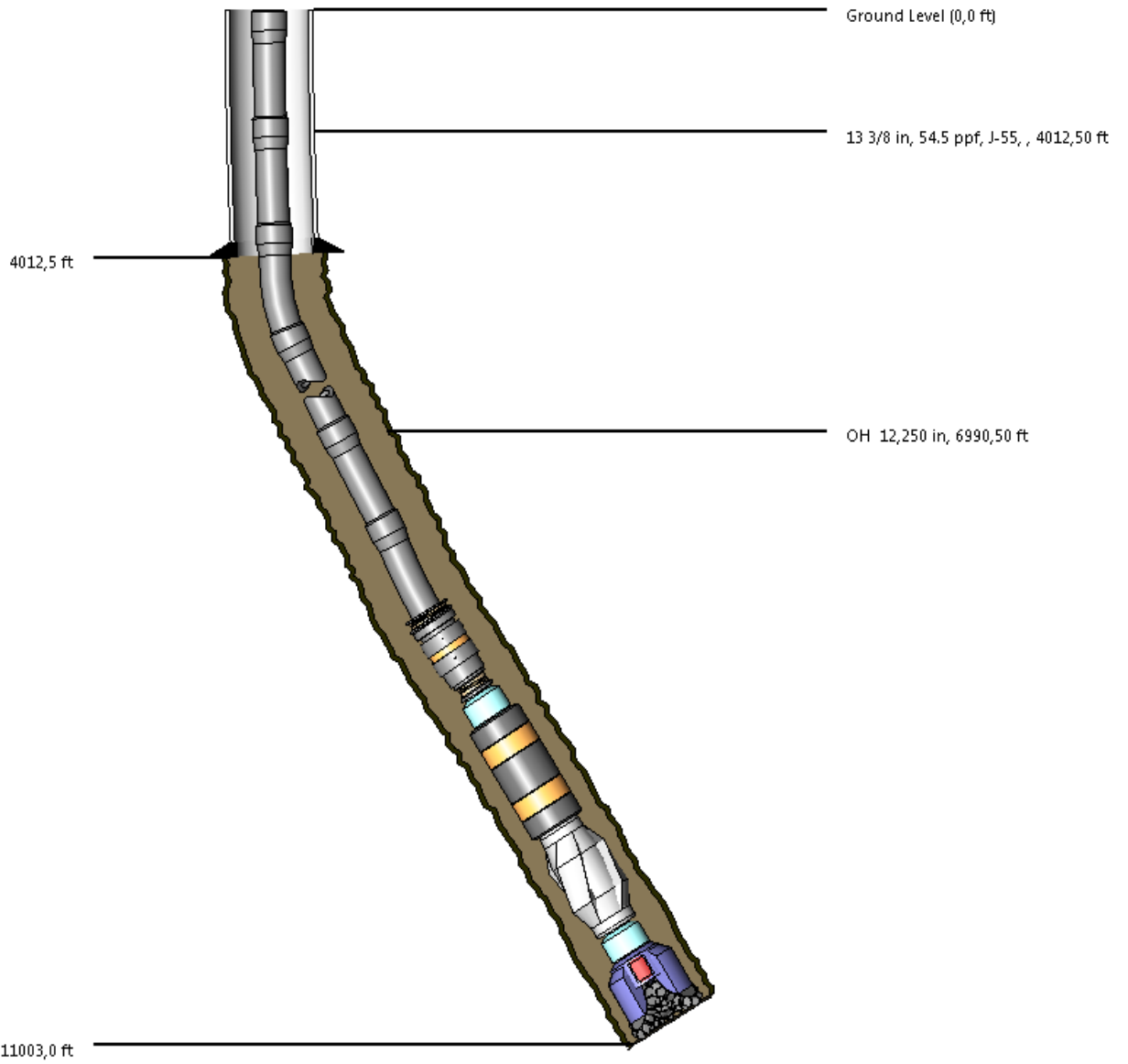


Figure 4.14: Simulation experimental well

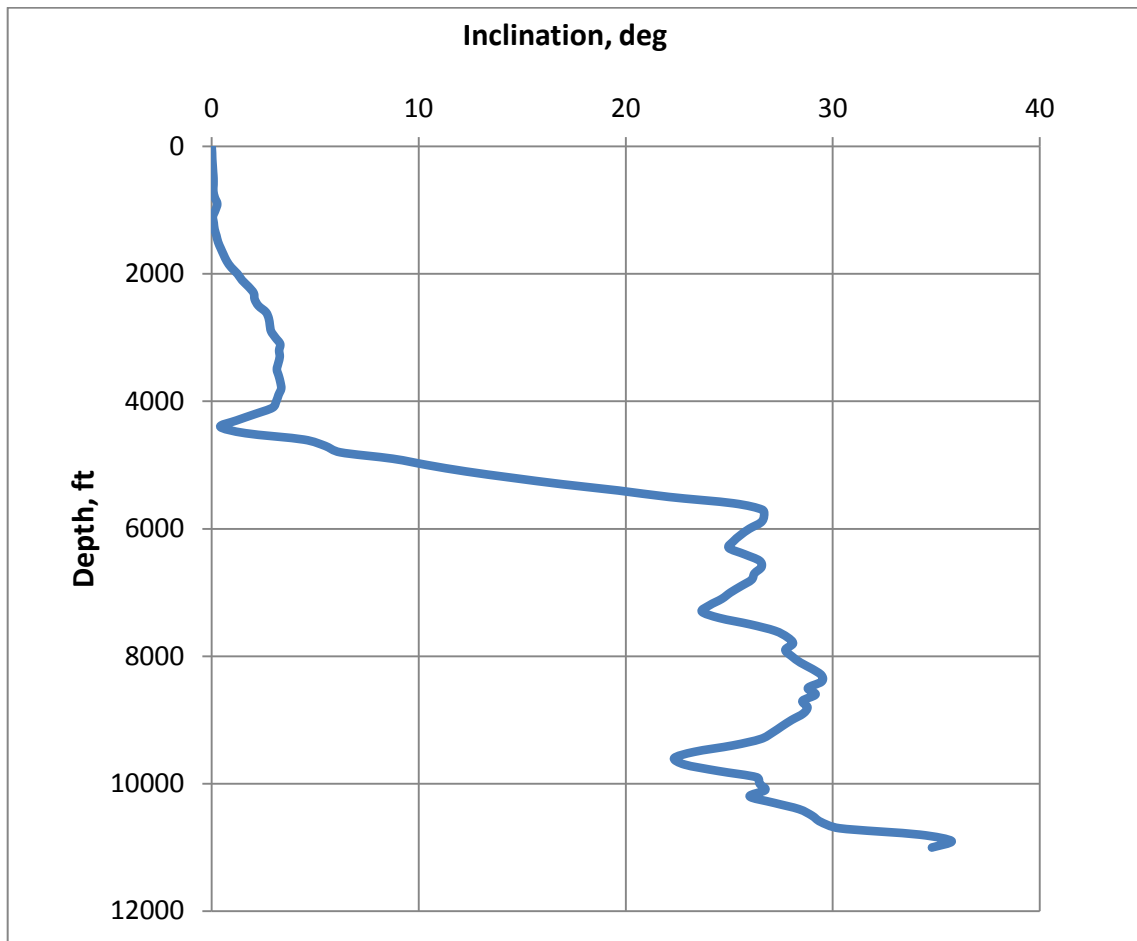


Figure 4.15: Well inclination of the simulation

4.2.2 Simulation Performance Result and Analysis

The cutting carrying capacity of the 70/30 and the 90/10 OBMs at different temperatures was investigated through the bed height deposition. For the analysis, the drilling fluid was allowed to circulate at 400gpm, which is the typical circulation rate. Bed height is deposition of cuttings on the bottom of the well. Poor hole cleaning results a higher bed height which can cause several undesired operational effect. These are drill string sticking, increase hydraulic pressure and hence increase ECD and increase torque and drag [35]. Through the experimental well, the cutting transport performances are simulated and the results are shown in Figure 4.16. As shown on the figure, the 70/30 shows good performance than the 90/10 in terms of the bed height with a maximum bed height difference of 0,5inch.

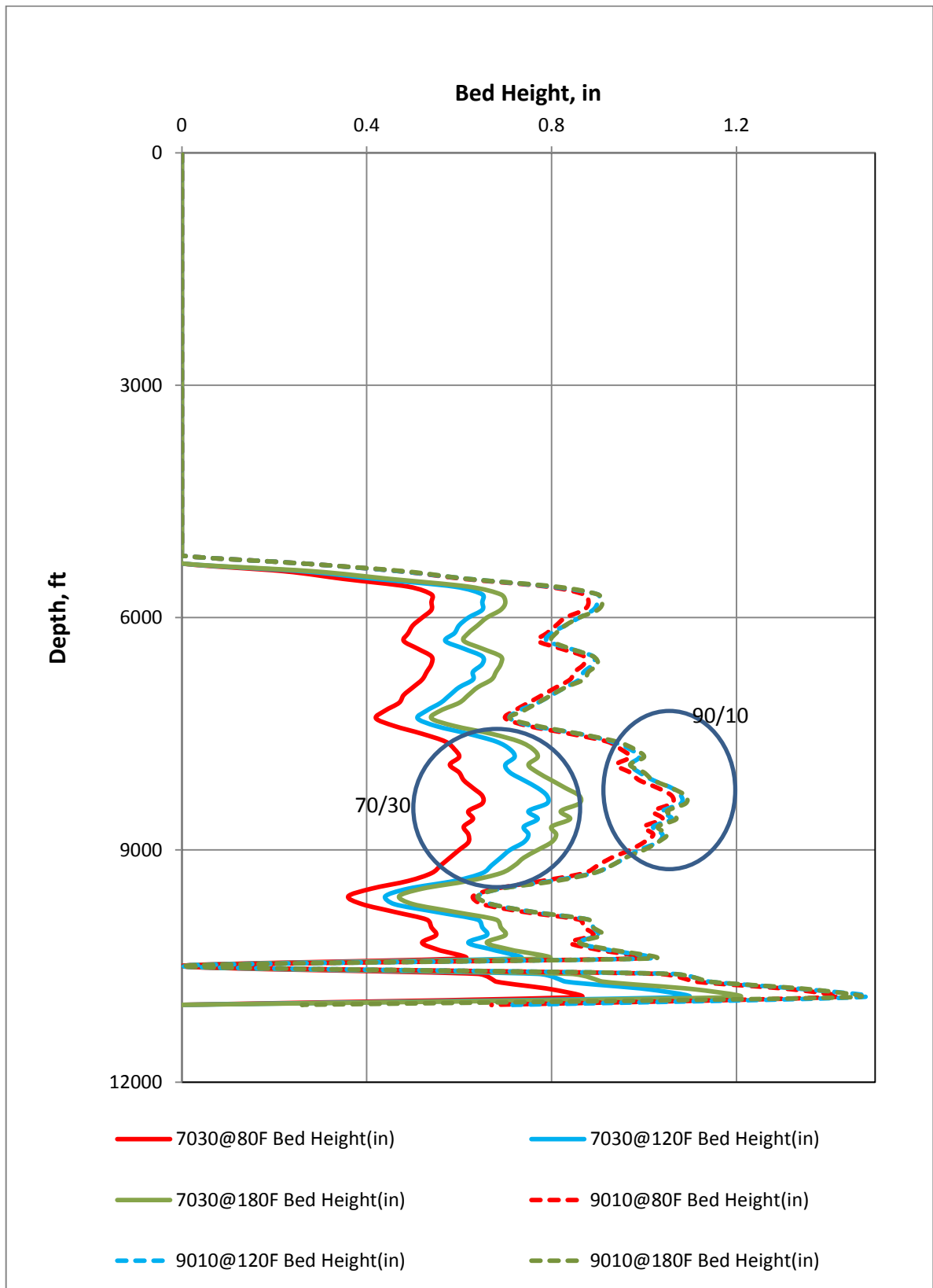


Figure 4.16: Comparison of the Bed Height between two mud systems with difference temperatures

The cutting bed deposited in the Figure 4.16 shows that the profile follows the trends of the well inclination. In vertical section up to 5000t, the figure obviously exhibits that no sign of cutting deposit and intuitively this is correct. Increment of well inclination from vertical to horizontal to about 600ft results dramatically increased of the cutting deposited to about 0.45 to 0.9in bed height. The well inclination shows quite inclined but quite varied until the 1000ft MD.

For better comparisons of the simulation results, the analysis of the relative errors between the two mud systems individually was performed. Figure 4.17 shows the calculated % error between the mud systems.

As shown on the figure, for the 70/30 OWR drilling fluid, the average error % of bed height ranges between 21-28% and 15-18% when the temperature increases from 80-120°F and 80-180°F respectively.

For the 90/10 OBM mud system, the average bed height error% ranges between 1,4-3,7% and 1,0-3,3% when the temperature is increased from 80-120°F and 80-180°F respectively.

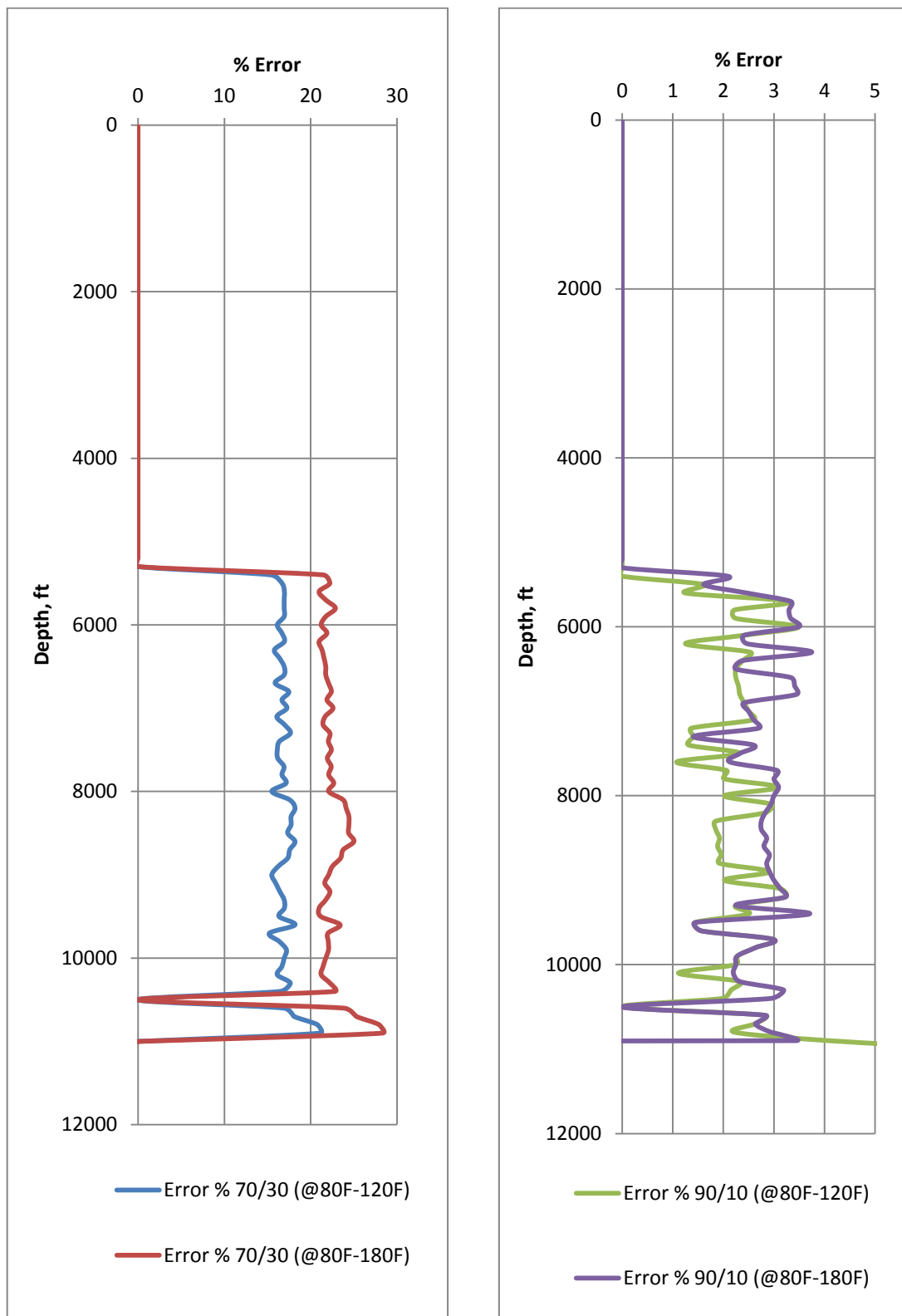


Figure 4.17: % Error comparisons of bed height between two drilling fluids

4.3 Hydrodynamic Force Effect of 90/10 & 73/30 OBM Systems on Hook Load

Before drilling operation, the design of torque and drag is one of the most important operations which need to be simulated. The torque and drag are a function of mainly drilling string geometry, length and weight. However, the hydrodynamic force due to fluid properties and flow also do have effects on the torque and drag. In addition, the density of the drilling fluid and the friction coefficient between the drill string and the wellbore/casing are the main factors.

In this thesis, the friction coefficient of the drilling fluid systems were planned, but due to time the measurement were not be able to perform. However, the analysis of the hydrodynamic force effect was carried out under some assumptions. The simulation is performed with Well-PlanTM software [20] and Power Law rheology model is chosen for the simulation.

Since the densities of the drilling fluids at various temperatures were not measured, it is assumed that the 120 and 180°F decrease the density by 5 and 10% respectively. Table 4.3 below shows the calculated result of density % decrease due to the elevated temperatures.

Temperature	Density	
80F	13,74	Reference (measured)
120F	13,053	5% Decrease Density (assumed)
180F	12,366	10% Decrease Density (assumed)

Table 4.3: Measured and assumed drilling fluid densities used for hook load simulation

Simulation was performed in Figure 4.15. For the simulation, 0 and 400gpm drilling fluid flow rates were used. For the given fluid systems, the Hook Load was computed.

In the main report the effect of the tripping out comparisons presented. The effect of the tripping in comparisons is shown in the Appendix-D.

Temperature/% density decrease	Hook Load (tons) when Flow rate =0 gpm	Hook Load (tons) when Flow rate =400 gpm	Increase in tons (Flow rate=0gpm)	Increase in tons (Flow rate=400gpm)
80F (Reference)	115	114		
120F (5% density Decrease)	117	116	1,6	2,1
180F (10% Decrease)	118	117	3,1	3,8

Table 4.4: Tripping Out of 70/30 OBM for 0 and 400gpm flow rates

As shown in the Table 4.4 above, during tripping out the hydrodynamic force effect of the 70/30 OBM on Hook Load due to temperature elevated from 80-120°F and from 80-180°F are calculated. At 0gpm flow rate, the hook load increases from 1,6 tons to 3,1 tons due to the temperature increased from 80°F to 120°F and 180°F respectively. As the flow rate increased to 400gpm, the Hook Load also increases from 2,1 tons and 3,8 tons when the temperature elevates from 80°F to 120°F and 180°F respectively.

Temperature/% density decrease	Hook Load (tons) when Flow rate =0 gpm	Hook Load (tons) when Flow rate =400 gpm	Increase in tons (Flow rate=0gpm)	Increase in tons (Flow rate=400gpm)
80F (Reference)	117	116		
120F (5% Decrease)	119	118	1,4	0,8
180F (10% Decrease)	120	119	2,9	2,3

Table 4.5: Tripping Out of 90/10 OBM for 0 and 400gpm flow rates

For the 90/10 OBM, the simulation result of the hydrodynamic force effect of tripping out at the flow rate of 0gpm and 400gpm due to temperature elevation is shown in the Table 4.5 above. At the flow rate of 0gpm, the Hook Load increases from 1,4 tons to 2,9 tons due to the temperature increased from 80°F to 120°F and 180°F respectively. The simulation running at the flow rate of 400gpm, the Hook Load is increased from 0,8 tons to 2,3 tons when the temperature increases from 80°F to 120°F and 180°F.

5 Simulation and Analysis of Mud Systems

5.1 Numerical Bridging Simulation

Several bridging experimental study have been carried out at the UoS [7] [11] [12]. The result shows that particle forming bridging at the mouth of a fracture hinders fluid loss. In addition, well fracturing experimental results have also shows that the addition of particles in drilling fluid increase both fracturing pressure and re-fracturing pressure. During re-fracturing test particles plugged at the mouth of the fracture increase the strength of the well.

The question to be asked

- Does bridging hinder the possible stress concentration increase at the fracture tip by disconnecting the communication between the fracture tip and the well?

Nowadays, the application of the finite element method (FEM) for stress and fracture analysis of a complex problem is widely used, and the result is believed to be reliable.

We have used ANSYS structural finite element simulator to understand the stress field at the tip and around a fracture [21].

In this thesis three scenarios were analyzed to describe the interpretation presented in section § 2.4.1 [9] and section § 2.4.2 [13].

The result of simulation may also describe the laboratory observations presented in section § 4.1.

5.2 Model Generation Loading and Material Properties

The geometrical model is built as a semi well with fracture at the center. A bridge is formed at the mouth of the fracture. The modeling procedure starts with the pre-processing stage, which includes geometry building, meshing, loading, material properties, problem type and boundary conditions as specified. The post-processing includes deformed meshes, stress and strain contours. ANSYS has no defined geometry dimension that the MKS system is used in this experiment that the unit used in this geometry model dimension is meter or mm [21].

- **Meshing:** The bilinear Q8 element with 8 degree of freedom gives a better solution and is chosen for meshing the model.
- **Loading:** The well is loaded with constant pressure on the bridge, on the wellbore and on wall of the fracture.
- **Boundary condition:** Around the external side of the model, we assume no deformation along the x and y directions that the model is fixed. The assumption is based on that the formation is unable to move to any direction in reality.
- **Material properties:** The material properties are Young's modulus, Poisson's ratio and the thickness of the model. For the thin model, the plain stress problem is recommended. The plane stress thickness is set as "0,01 m (or) 0,01 mm".

The properties for the model in this experiment are chosen as Linear, Elastic and Isotropic.

5.2.1 Model Scenario 1-Refernce model

In this case, the model is assumed that the drilling fluid system doesn't make good mud cake. During well fracturing, the drilling fluid doesn't make bridging. Therefore the well pressure is communicating with the fracture and loads on the face of the fracture.

This scenario simulates the model presented in Figure 5.1. The face of the fracture can be permeable or non-permeable depending on the petro-physical properties of the formation.

The modeling parameters used for the analysis is obtained from reference [9]. The pressure on the wellbore and on the face of the fracture is 9200psi. The pressure of the minimum horizontal in-situ stress is 9000 psi and the pressure of the maximum horizontal in-situ stress is 9200 psi respectively. The model parameters are presented in the Table 5.1.

Length of the Formation	5 meter
Height of the Formation	5 meter
Radius of the Wellbore	1
Width or aperture at the mouth of the Fracture	0,6 meter
Length of the Fracture	1 meter
Formation Young's Modulus	1.09E+06 psi
Formation Poisson's ratio	0.225
Minimum Horizontal in- situ Stress	9000 psi
Maximum Horizontal in-situ Stress	9200 psi
Wellbore Pressure	9200 psi
Pressure inside the Fracture	9200 psi

Table 5.1: Geometry of the Scenario 1

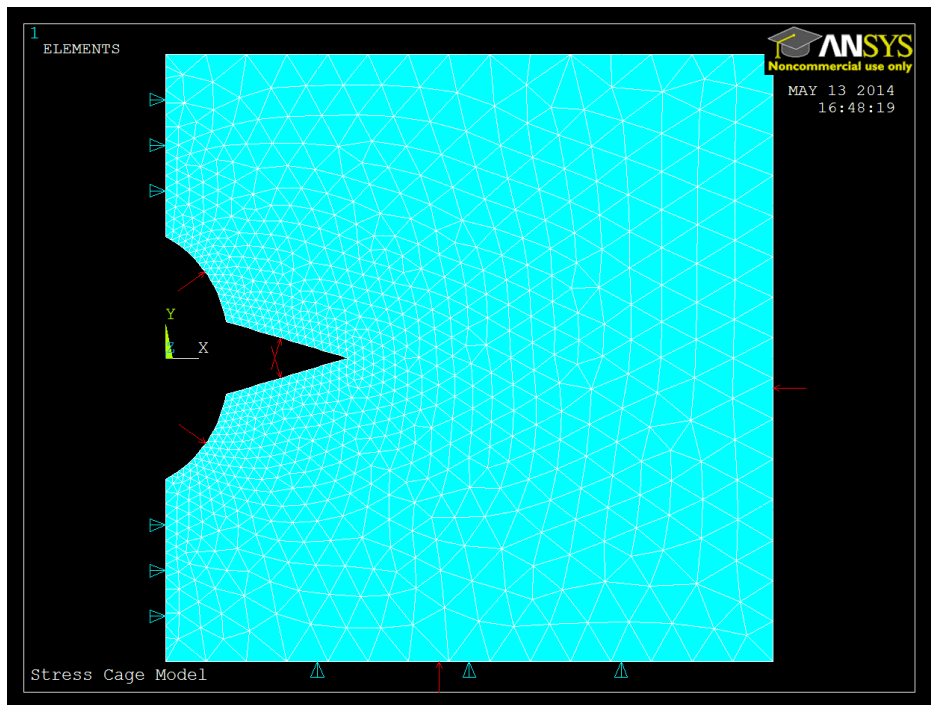


Figure 5.1: Illustration of loads and boundary conditions for scenario 1

Results:

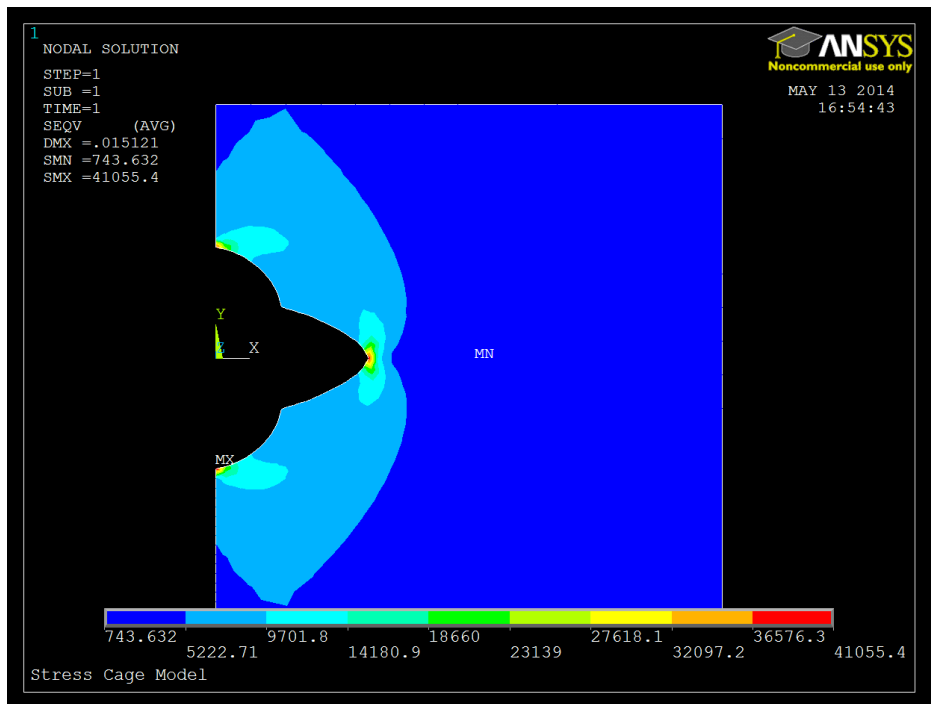


Figure 5.2: Deformation and Stress Distribution results by Von Mises of scenario 1

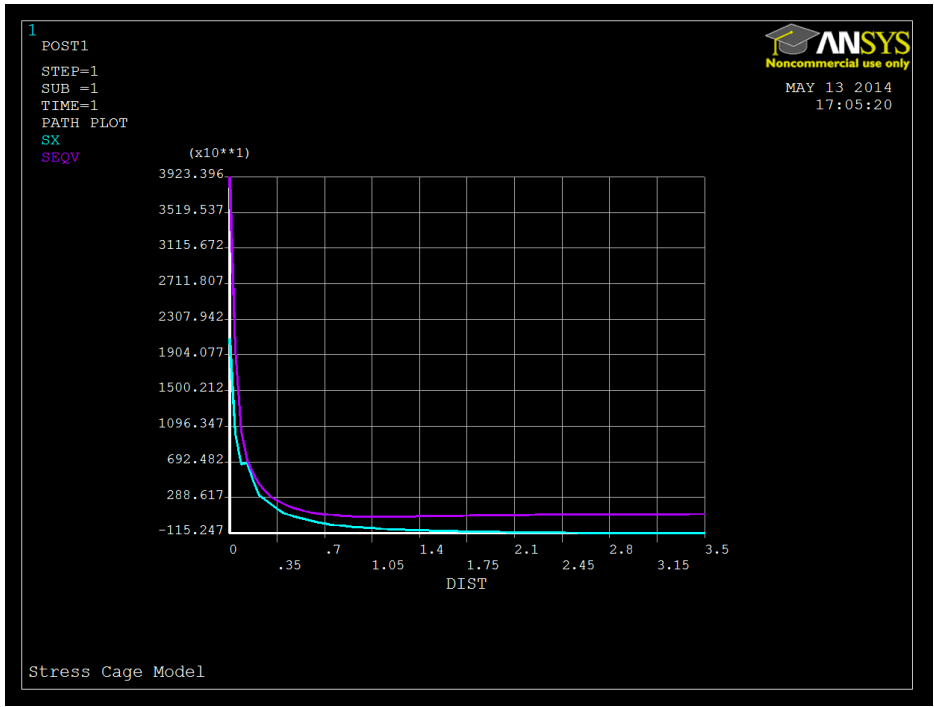


Figure 5.3: Line plot of Von Mises and Stress component along the X-direction (σ_x) for scenario 1

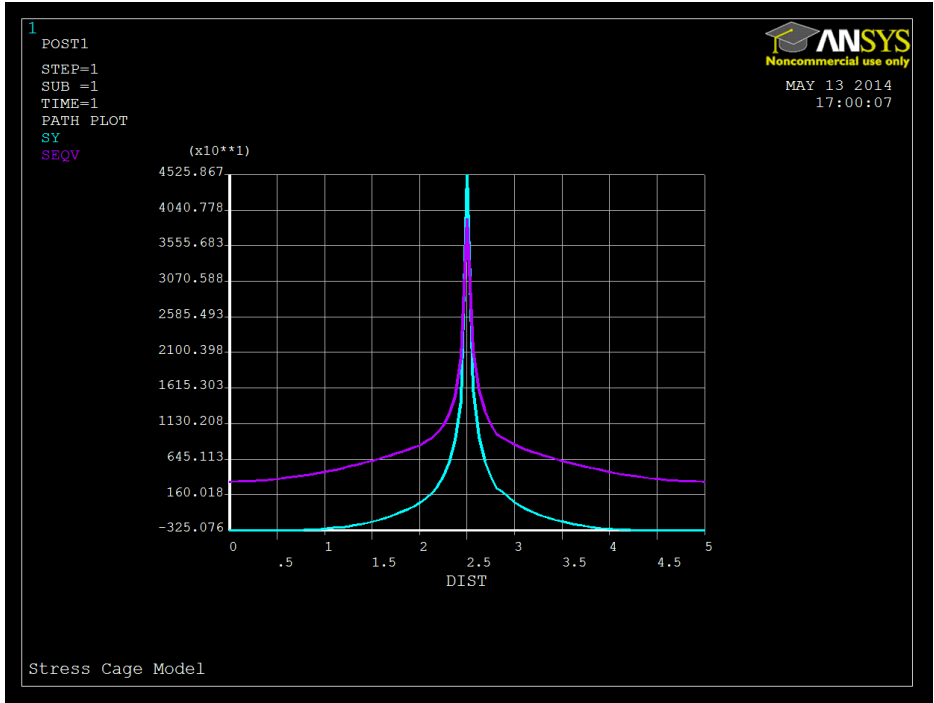


Figure 5.4: Line plot of Von Mises and Stress component along the Y-direction (σ_y) for scenario 1

Figure 5.2 shows the deformation and Von-Mises stress distribution. As can be seen at the tip of the fracture the loading induce higher tensile strength. When the strength reaches to the tensile strength the fracture will propagate and in a real operation mud flows into a formation.

To better understand the stress fields along the direction and perpendicular to the fracture, path plots profiles are generated.

Figure 5.3 is the path plot of Von-Misses (S_{von}) and the stress component in the X-direction (σ_x). The result shows that both the Von Mises stress and the x-components are higher at the fracture tip and exponentially decay out as going away from the tip. The stress magnitudes are about three times higher than the well pressure.

Figure 5.4 is the path plot of the Von-Mises (S_{von}) and the stress component in the Y-direction (σ_y). As can be seen, the stress at the tip of the fracture in the y-direction is higher than in the x-direction by about 54%. The stress fields decay exponentially as we go from the tip away.

From this huge stress concentration, if there is a well and fracture communication, the application pressure loading causes a continuous fracture growth and hence mud losses.

This simulation result suggest that the need to have fluid barrier at the mouth of the fracture in order to avoid the communication between the well and the fracture. In section §4.1, the bridging experimental result illustrates that good bridging hinder mud loss through opening slots.

5.2.2 Model Scenario 2-Model based on Alberty's interpretation

Scenario 2 developed based on the Alberty's [9] FEM simulation study. The model is shown in Figure 5.5. The loading is inside the fracture. Based on their loading, the following two cases try to describe the models.

The first interpretation of the model is that the drilling fluid system doesn't make good mud cake. During well fracturing, the drilling fluid doesn't make bridging. Therefore the well pressure is communicating with the fracture and loads on the face of the fracture. The second interpretation of the model is that the particles deposited at the mouth of the fracture width as illustrated in Figures 2.3-2.5. The pressure loaded on the particle is equally transferred the side contact surface area of the fracture. Therefore, the pressure in the well (i.e on the bridging) is the same as loading on the face of the fracture.

The face of the fracture can be permeable or non-permeable depending on the petro-physical properties of the formation. However, ANSYS cannot handle the diffusion and pore pressure build-up effects. The modeling parameters used for the analysis is obtained from reference [9]. The pressure on the wellbore and on the face of the fracture is 9200psi. The pressure of the minimum horizontal in-situ stress is 9000 psi and the pressure of the maximum horizontal in-situ stress is 9200 psi respectively. The model parameters are shown in Table 5.2. Figure 5.5 illustrates the meshed model geometry, and loading.

Length of the Formation	3 meter
Height of the Formation	3 meter
Radius of the Wellbore	1
Length of the Fracture	0,2 meter
Formation Young's Modulus	1.09E+06 psi
Formation Poisson's ratio	0.225
Minimum Horizontal in-situ Stress	9000 psi
Maximum Horizontal in-situ Stress	9200 psi
Wellbore Pressure	9200 psi
Pressure inside the Fracture	9200 psi

Table 5.2: Geometry of the Scenario 2

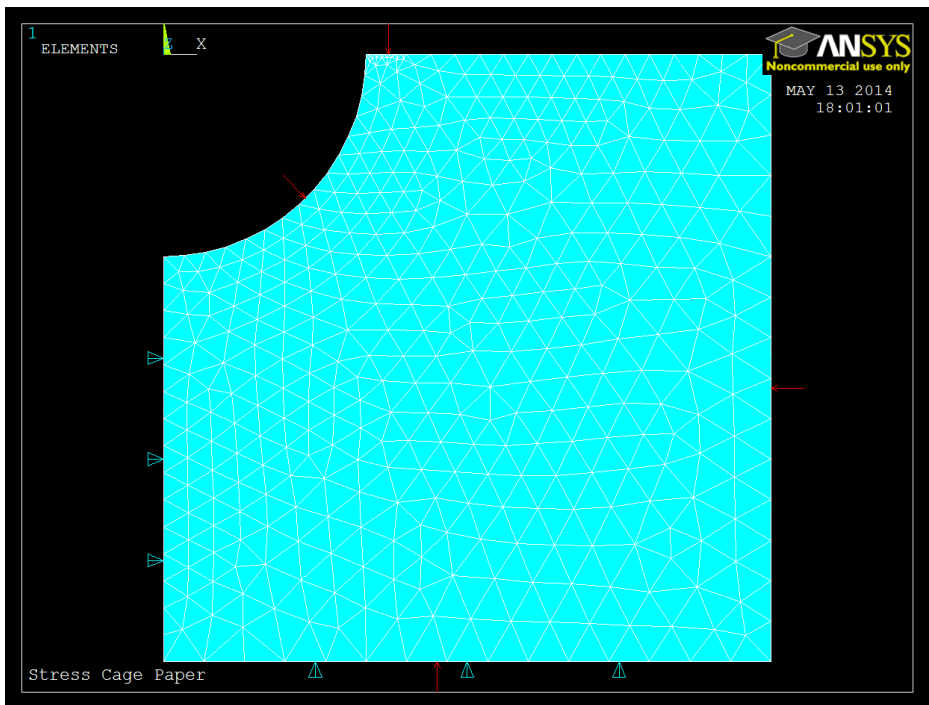


Figure 5.5: Illustration of loads and boundary conditions for scenario 2

Results:

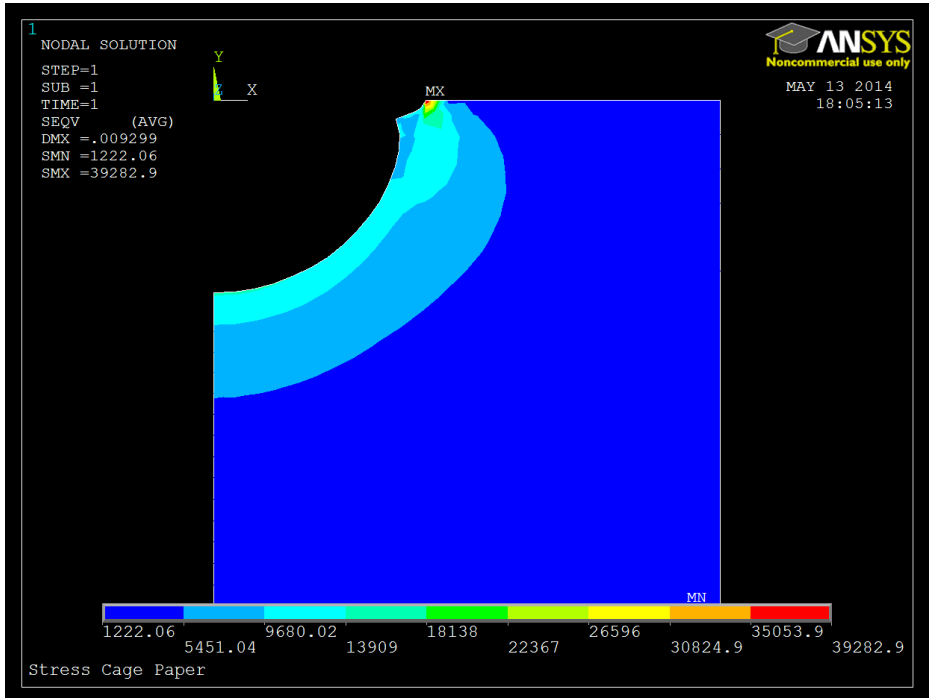


Figure 5.6: Deformation and Stress Distribution results by Von Mises of scenario 2

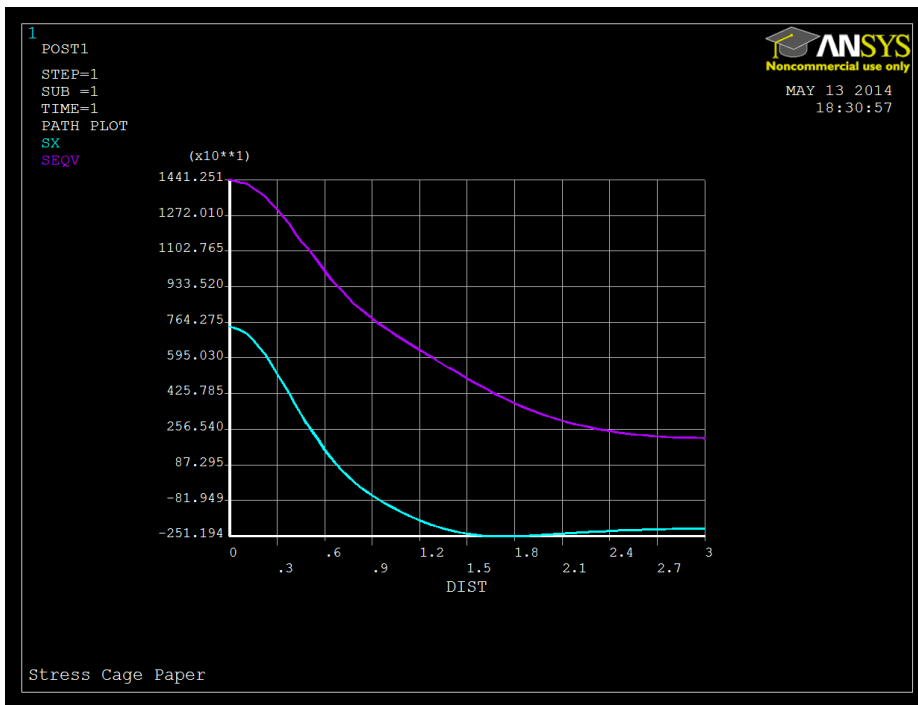


Figure 5.7: Line plot of Von Mises and Stress component along the X-direction (σ_x) for scenario 2

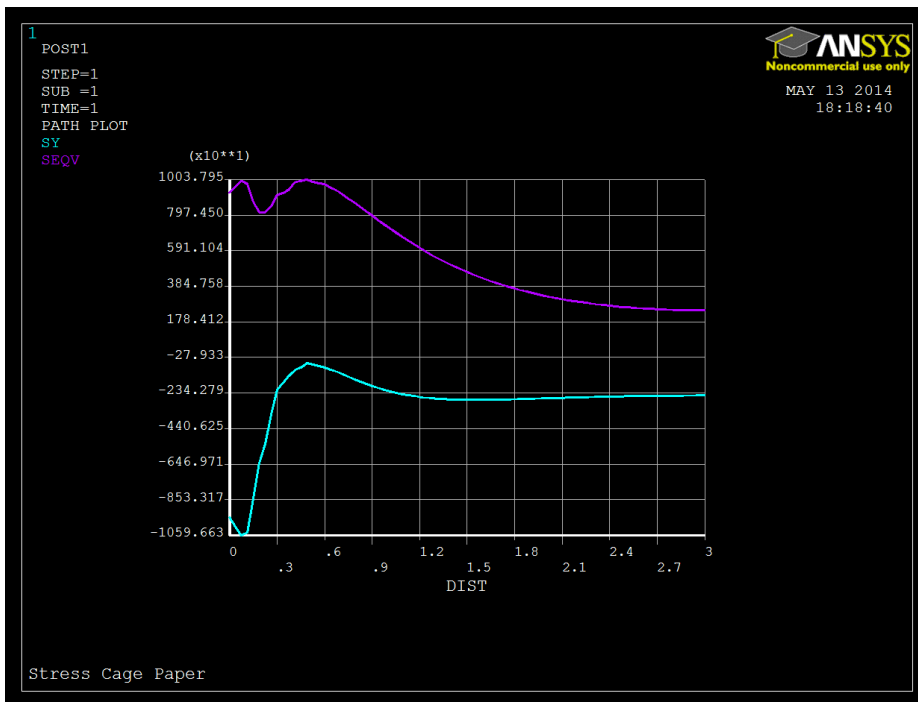


Table 5.8: Line plot of Von Mises and Stress component along the Y-direction (σ_y) for scenario 2

Figure 5.6 shows simulation result of the Von-Mises stress distribution. As can be seen, the maximum tensile stress located at the tip of the fracture. When the stress at tip of the fracture reaches to the tensile strength of the formation, it will open up the fracture and growth ahead. This observation is contrary to the interpretation of the Alberty, which says that the stress cage increase the strength of the wellbore.

Figure 5.7 is a line plot of VonMises (S_{von}) and (σ_x) along the X-direction of the fracture. The result shows that both stress are tensile and very high at the tip of the fracture and decay out as we go far from the fracture tip.

Figure 5.8 also shows the plot of VonMises (S_{von}) and (σ_y) along the Y-direction of the fracture. The result shows that the Von-Mises is tensile and the σ_y stress component is compressive. Both shows higher stress magnitudes the tip of the fracture. From the two stress line plots we can learn that the Von-Mises along and perpendicular to the fracture tip are higher and tensile. This stress is responsible for the fracturing provided that the magnitude reaches to the tensile strength of the formation.

This thesis simulation results support the interpretation presented by Aadnøy [12][13].

5.2.3 Model Scenario 3-Model based on Aadnøy's interpretation

In this case, the model is assumed that the drilling fluid system makes good mud cake. The bridge is a cylindrical shape at the mouth of the fracture and illustrated in Figure 5.9 [12][13]. The process of loading and bridging deformation and finally bridge collapse is illustrated on the figure. Based on this model interpretation, Model scenario-3 is developed. According to the model, since the bridge forms good cake, there will be no communication between the well pressure and the fracture. Therefore the loading will be on the bridge and on the wellbore. We will also assume that even if there is a bridge because of filtrate there will be pressure communication between the well and the fracture. .

The modeling parameters used for the analysis is obtained from reference [9]. The pressure on the wellbore and on the face of the fracture is 9200psi. The pressure of the minimum horizontal in-situ stress is 9000 psi and the pressure of the maximum horizontal in-situ stress is 9200 psi respectively. Table 5.3 shows the model parameters. Figure 5.9 illustrates the meshed model geometry, and loading.

Length of the Formation	5 meter
Height of the Formation	5 meter
Radius of the Wellbore	1
Width or aperture at the mouth of the Fracture	0,6 meter
Length of the Fracture	1 meter
Thickness of the Bridging	0,02 meter
Formation Young's Modulus	1.09E+06 psi
Formation Poisson's ratio	0.225
Minimum Horizontal in-situ Stress	9000 psi
Maximum Horizontal in-situ Stress	9200 psi
Wellbore Pressure	9200 psi
Pressure inside the Fracture	9200 psi

Table 5.3: Geometry of the Scenario 3

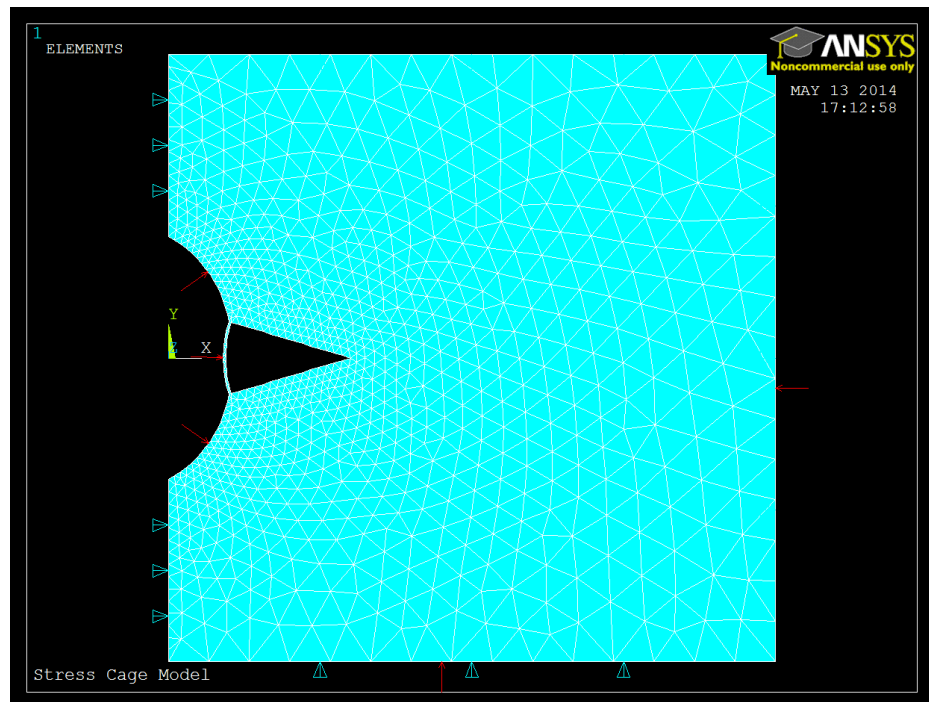


Figure 5.9: Illustration of loads and boundary conditions for scenario 3

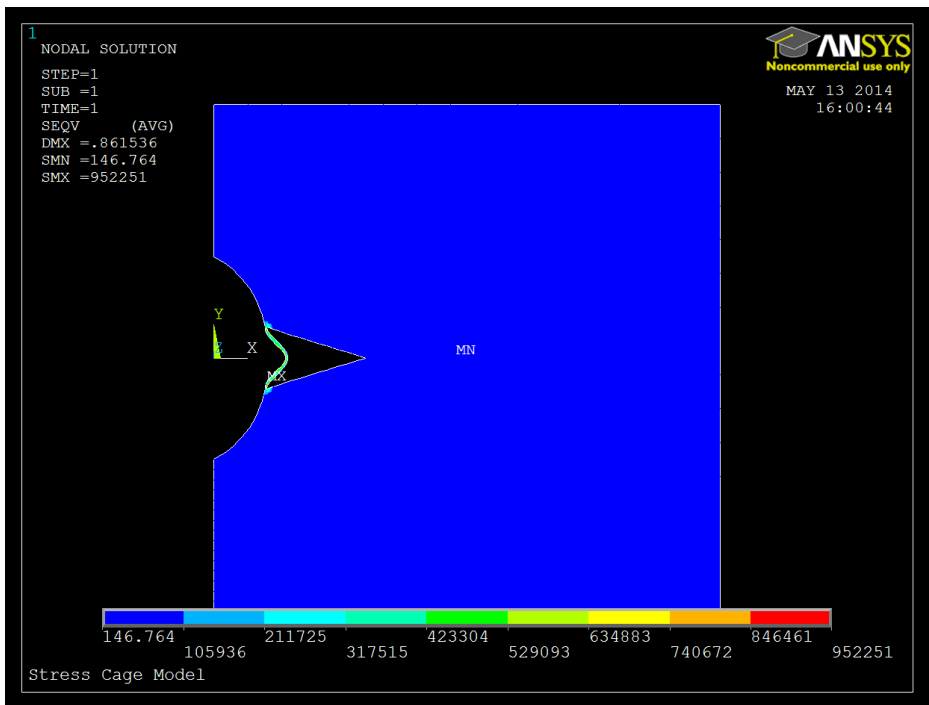


Figure 5.10: Deformation and Stress Distribution results by Von Mises of scenario 3

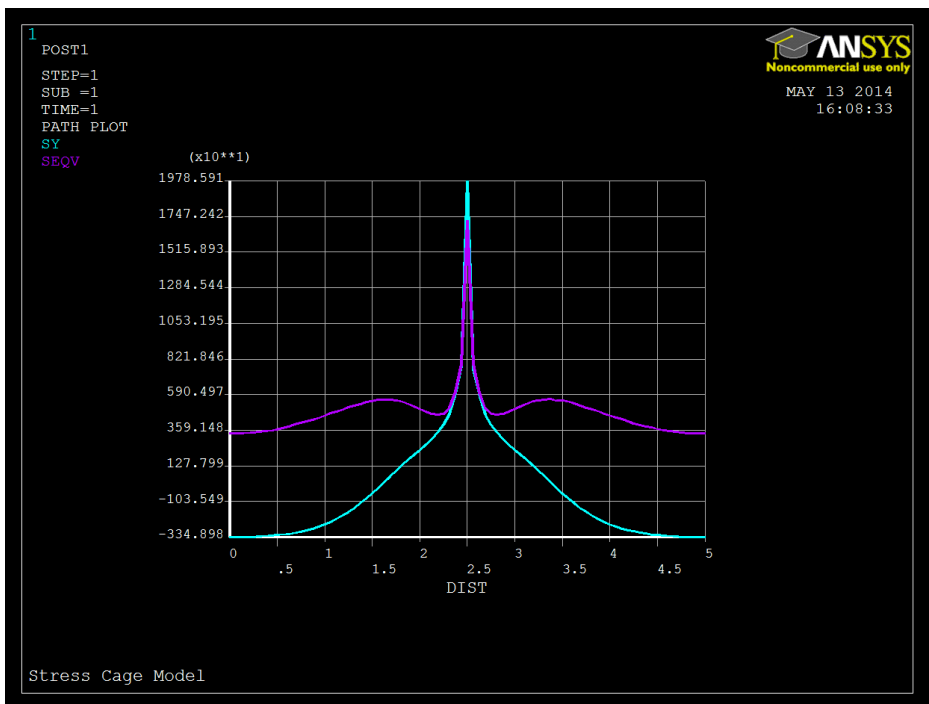


Figure 5.11: Line plot of Von Mises and Stress component along the Y-direction (σ_y) for scenario 3

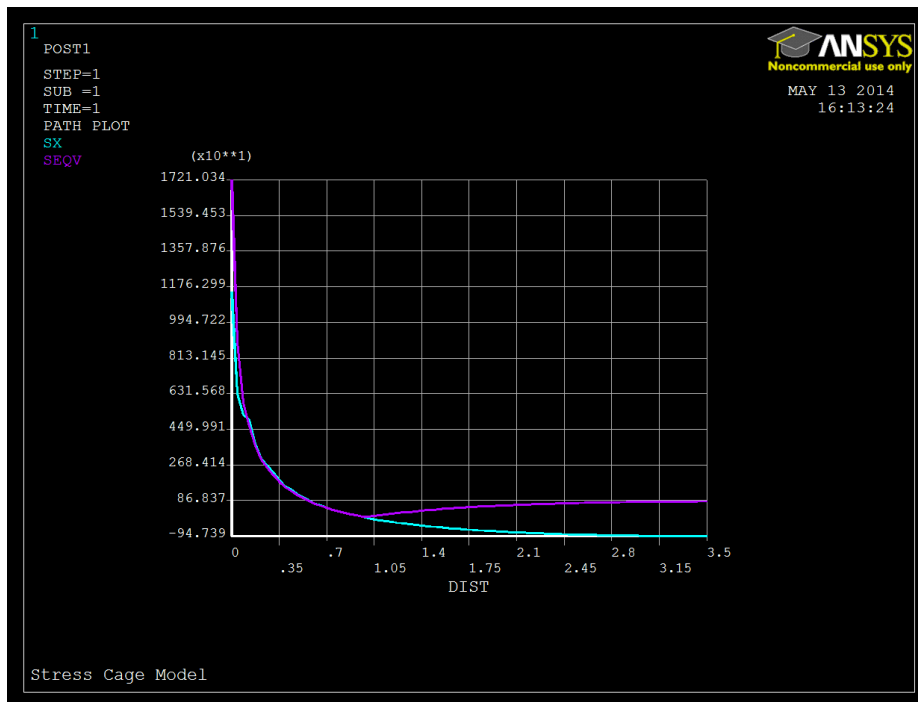


Figure 5.12: Line plot of Von Mises and Stress component along the X-direction (σ_x) for scenario 3

Figure 5.10 shows the Von Mises stress field after loading. As shown on the figure, due to loading the bridge is deformed. The stress fields are very low at the tip of the fracture as compared to scenario 1.

Figure 5.11 is the path plot of the Von-Mises (S_{von}) and the stress component in the Y-direction (σ_y). Similarly the path plot along the x-direction is shown in Figure 5.12. As can be seen, the stress at the tip of the fracture in the y-direction is higher than in the x-direction by about 44%. The stress fields decay exponentially as we go from the tip away.

The Von-Mises stress comparison between scenario 1 and 3 show that scenario 1 is higher than scenario 3 by 56%. Comparisons between the stress components show that scenario 1 is higher than scenario 3 by 48% and 56% along the x and y-direction respectively.

Comparing the interpretation of Aadnoy with the ANSYS simulation result, one can observe that the interpretation is in line with the numerical bridging deformation and stress field phenomenon. This is also supported by core well fracturing experiments and the bridging experimental result, which exhibits good bridging hinder mud losses since the bridging can carry well pressure and disconnect the communication with the fracture. The experimental results also show that the particle additives in a mud system regain the strength of a fractured wellbore [12] [7] [14].

6 Summary and discussion

This section presents the summary and discussion of the overall study. The main purpose of the thesis is to compare between 70/30 and 90/10 OBM systems. The investigation was through experimental, modelling and performance simulation and finite element numerical methods. These are Bridging test, Rheology test, HPHT filtration test, Viscoelasticity test, Hook Load and Cutting Transport simulations.

Temperature Effect on Plastic Viscosity and Yield Stress

The knowledge of the effect of the thermodynamic state on the drilling fluid is very important for accurate predictions of hydraulics. Most simulators do have empirical correlation equation which adjust the density and viscosity to the given temperature and pressure. In this thesis, the effect of temperature on the two mud systems were analyzed and compared. The results show that both fluid systems are sensitive to the temperature. As temperature increases from 80 to 180°F, the rheology of the both drilling fluids decreases. The effect is more significant on plastic viscosity (PV) than on the yield stress (YS). For instance:

- As temperature increases from 80 to 180°F, the PV of the 70/30 OBM system decreases from 112 to 55cP, while the PV of 90/10OBM decreases from 30 to 13cP.
- However it is interesting to observe that the YS of the 90/10 OBM doesn't shows a significant decreases (it is almost equal). The YS of the 70/10 OBM decreases from 30 to 21 lbf/100sqft.

The temperature dependent correlation equations developed in this thesis are valid for the given temperature ranges and at atmospheric pressure. For a realistic analysis, it would be interesting to study the problem at various temperature and pressure, which simulated the thermodynamics state of drilling formations.

HPHT Filtrate Test

One of the drilling challenges is drilling in a HPHT environments. The more the filtrate results in formation damage and modifying the properties of the drilling fluid since it losses the chemical, the fluid and particle solids. The lower the filtrate the thinner the mud cake is the better. The static HPHT filtrate test was performed on the two mud systems at 500psi and 100°C.

Initially the 70/30 OWR filtration test shows that the filtrate consists of 24% water phase. The Electrical Stability Test is required to investigate the oil-water ratio in the 70/30 OBM. The result of the ES measurement shows 360mV, which is very low voltage. This is an indication that the mud system has a poorly emulsified system. Later the mud systems were treated with emulsifiers (paramul and parawet) and lime in order to adjust the stability. After modification the HPHT filtrate results shows no water phases and record 2,25ml. In real operation, it is therefore important to test the stability and adjust the system before re-use it for drilling.

The ES of the 90/10 OWR was 678mV, which exhibits good emulsified system. The HPHT filtration test recorded 7,2ml which is 68,8 percent higher than the 70/30 OBM. One can also easily see from Figure 1.2 section §1.2. The filtrate phase of the 90/10 is almost three times higher than the 70/30OBM.

Based on Bridging Performance

Loss circulation is a critical problem for the industry. The loss circulation problem can occur through stress induced fracture and naturally fractured formations. Depending on the severity of the loss one can design a treatment to hinder further losses. The commonly used technique is to use loss circulation material. The bridging performance of the particles on the mouth of a fracture depends on the property of the drilling fluid. In this thesis, the bridging performance of the 16,85 ppb LC-lube in the 70/30 and 90/10 OBMs was evaluated. LC-Lube is graphite loss circulation material. The LC-lube treated drilling fluids were tested at slots width of 200, 300, 400 and 500 microns. The pressure profile the experimental results were analyzed by computing the maximum pressure, the average pressure and the peak of the pressure.

The result also shows that the bridging performance of the loss circulation material is better in the 70/30OBM than in the 90/10 OBM systems. The better stability of the 70/30 could be due to low filtrate and high viscosity of the fluid systems. The mobility of the 70/30 fluid in fracture system is slower than the 90/10 fluid as illustrated in Figure 6.1.

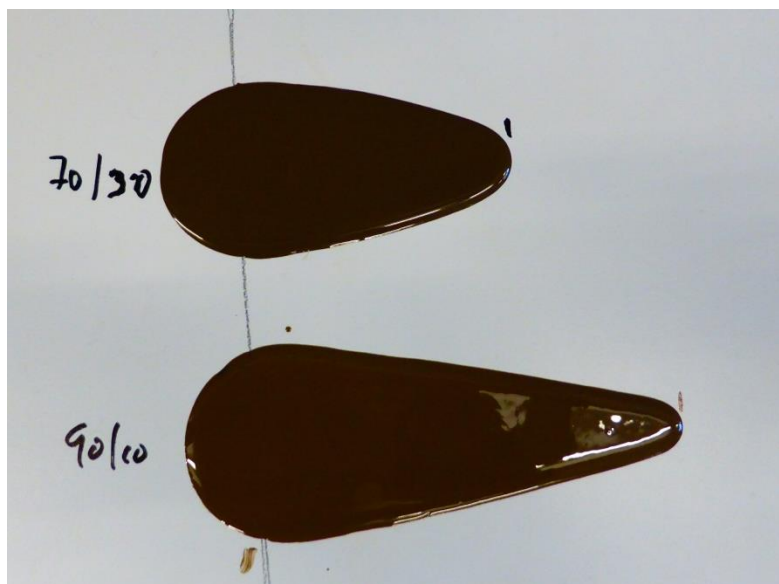
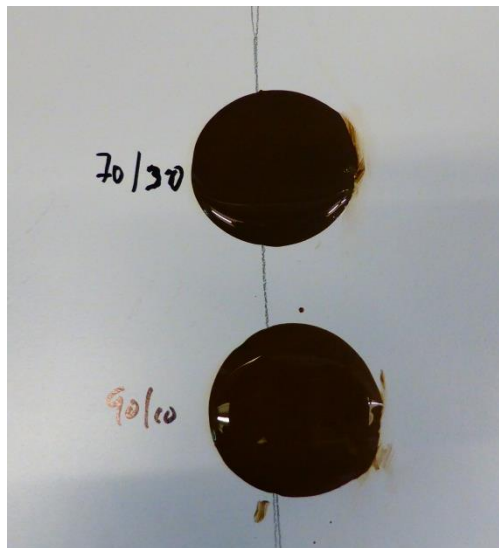


Figure 6.1: Illustration of mobility in 30sec

Hydraulic and Rheology Analysis

The hydraulics property of drilling fluid is very important for drilling operation such as ECD management, cutting transport, and pump performance determinations. In this thesis a simulation well was designed the hydraulics of the two mud systems evaluated through Unified yield power law model. Since temperature has a significant effect on the rheology and density of drilling fluid, the hydraulic effect in HPHT is also higher. The result shows that as temperature increase the pressure losses decrease. As RPM increase the pressure loss increases. It is therefore important to have a temperature and pressure dependent rheology and density models so that during simulation the laboratory measured data will be adjusted to the correct thermodynamic states. Comparing the two mud systems it is shown that the 70/30 OBM shows a higher pressure than the 90/10 OBM mainly due to the rheology and density parameter effects.

Cutting Transport capacity of the Fluid Systems

Hole cleaning is an important issue to be considered during drilling operation. The cuttings are transported to surface by the help of the return drilling fluid. The cutting transport capacity of the drilling fluid depends on several factors. These are the rheology, the density of drilling fluids, the cutting properties, the operational parameters (RPM and ROP) and flow rates. In this thesis the cutting lifting capacity of the two mud systems at three different temperatures were evaluated. For the evaluation an experimental well is constructed and the bed height depositions during 400gpm flow condition were simulated.

The result shows that the performance of the 70/30 OBM is better than the 90/10 OBM. The main reason here is that the higher the viscosity and the density holds cutting particles in suspension. This allows for the particles to be transported instead of being settled. The temperature effect on the cutting transport of the 90/10 shows lower than the 70/30 OBM.

Hydrodynamic Force Effect on Hook Load

Torque and drag are also very important issue for drilling operation. During designing phase accurate prediction of loads on drill string allows a safe operation both reaching to the desired measured depth and without drilling string failure. Among other the hydro-dynamic forces do have effects on the torque and drag. In this thesis, the effect of flow and rheology of the two drilling fluids systems on the Hook load was evaluated. For instance for 70/30 OMB as temperature increase from 80 to 180°F, the result shows that the hydrodynamic force increase the hook load up to 3,8 tons during tripping out operation.

Viscoelasticity Behavior

The knowledge of the viscoelastic properties drilling fluids is important. The viscoelastic properties of a drilling fluid allow evaluating gel structure, gel strength, barite sag, and hydraulic modeling. In this thesis amplitude and frequency sweep tests were carried out. The comparison of the amplitude sweep test results shows that the storage and the loss modulus of the 90/10 OBM system are higher than the 70/30 OBM system. The frequency sweep test results performed on the 90/10 OBM shows that loss modulus, the storage modulus and the complex viscosity are being frequency dependent. The fluid system behaves like unstable gel structure or solid like property during the testing period. It is also observed that complex viscosity follows the storage modulus profile, but not of the loss modulus.

ANSYS Simulation

Finite element simulation was carried out in order to study the stress fields around and away from fracture tip with and without bridging at the mouth of a fracture.

The motivation of the study is to describe the bridging experimental results and to compare the bridging interpretations documented in literature. The simulation results show that good bridging carries well pressure and disconnect the communication between the well and the fracture. The simulation results describe best the interpretation presented by Aadnøy et al [13].

7 Conclusion

The study in this thesis covers characterization and performance of the considered two oil based mud systems. The major investigations of the thesis work are summarized in the Table 7.1 below.

	Parameter	70/30 OBM	90/10 OBM
Rheology Measurement	Error % at temperature elevated from 80-120oF	Error range is between 21 and 35%	Error range is between 10 and 27%
	Error % at temperature elevated from 80-180oF	Error range is between 33 and 53%	Error range is between 10 and 44%
Hydraulic Measurement	Error % at the temperature elevated from 80-120oF	The hydraulics relative % difference increases from 28 to 30%	The hydraulics relative % difference increases from 8 to 15%
	Error % at the temperature elevated from 80-180oF	The hydraulics relative % difference increases from 39 to 45%	The hydraulics relative % difference increases from 20 to 28%
Bridging Test	Slot Width of 200 μm after running of 20 min	$P_{\text{avg}} = 10,1 \text{ MPa}$	$P_{\text{avg}} = 13,99 \text{ MPa}$
	Slot Width of 300 μm after running of 20 min	$P_{\text{avg}} = 4,74 \text{ MPa}$	$P_{\text{avg}} = 2,64 \text{ MPa}$
	Slot Width of 400 μm after running of 20 min	$P_{\text{avg}} = 2,81 \text{ MPa}$	$P_{\text{avg}} = 0,57 \text{ MPa}$
	Slot Width of 500 μm after running of 20 min	$P_{\text{avg}} = 4,23 \text{ MPa}$	$P_{\text{avg}} = 0,11 \text{ MPa}$
HPHT Filtration Test	Before Modification	4.6 ml of filtrate with containing of 24% water Phase come out	7.2 ml of pure filtrate come out
	After Modification	2.25 ml of pure filtrate without containing water phase come out	No re-measurement since the first test showed a good result
Cutting Transport	Error % at temperature elevated from 80-120F	The highest error% reached is 17%.	The highest error% is recorded as 3.2%.
	Error% at temperature elevated from 80-180F	Peak error% is extended to 21% in here.	Peak error% is slightly increased to 3.7%.
Flow in Porous Media	After 30 minutes	2,8 cm	4,5 cm
	After 120 minutes	3,7 cm	4,85 cm
	After 150 minutes	3,8 cm	4,87 cm
Hydrodynamic fluid force effect on Hook Load	Flow Rate = 0 gpm	80oF-120F (Density Decrease 5%)	Hook load increased by 1,6 tons during tripping out
		80oF-180F (Density Decrease 10%)	Hook load increased by 3,1 tons during tripping out
			Hook load increased by 1,4 tons during tripping out
			Hook load increased by 2,9 tons during tripping out

	Flow Rate = 400 gpm	80oF-120F (Density Decrease 5%)	Hook load increased by 2,1 tons during tripping out	Hook load increased by 0,8 tons during tripping out
		80oF-180F (Density Decrease 10%)	Hook load increased by 3,8 tons during tripping out	Hook load increased by 2,3 tons during tripping out
Visco-elastic	Loss modulus (G'') Storage modulus (G')		Cross point ($G'=G''$) at 0.3 % stain	Cross point ($G'=G''$) at 0.7% stain

Table 7.1: Summary of the major investigations

Based on the summarized table the following conclusion can be drawn

- The results of the rheology measurement present that both the Herschel Buckley and Unified models with lowest error rates can describe the best for both 70/30 and 90/10 OWR of mud systems.
- The HPHT filtration test shows that the 70/30 OBM with less volume of filtrate is better than the 90/10 OBM which losses significantly amount of filtrate. It is vital to measure the Electrical Stability and other properties of the return mud before re-use it back. If the drilling fluid lost it properties, modification should be made right at the spot.
- The result of the hydraulic calculation shows that the 70/30 OBM exhibits a higher friction loss in compared to the 90/10 OBM due to higher density and higher viscosity.
- For the bridging test, the 70/30 OBM with loss circulation material shows a better performance due to low filtrate and high viscosity.
- Both drilling fluids are sensitive to the temperature that temperature increase results the rheology of the drilling fluids decrease. The analysis shows that the effect of temperature is more significant on plastic viscosity than on the yield stress.
- In the cutting lifting simulation, the 70/30 OBM shows a better performance than the 90/10 OBM due to higher viscosity helped particles to be transported. In addition, temperature has a significant effect on the 70/30 OBM in compared to the 90/10 OBM.

-
- Results of hydrodynamic force effect on Hook Load show that both elevated temperature and increased flow rate have effect on the Hook Load during tripping out for both drilling fluids.
 - In the amplitude sweep test, the storage and the loss modulus of the 90/10 OBM is higher than the 70/30 OBM.
 - In the study of stress fields around the fracture tip, results of the ANSYS structural finite element simulator support the interpretation presented by Aadnøy et al [13].

8 Future Work

Due to the limited time, more were not able to perform. However, this thesis propose do more characterization and performance studies in the future. The following is proposal for future work:

- The performance of the Friction test for the 70/30 and 90/10 OBMs
- Dynamic HPHT filtration test
- More visco-elastic test at various temperature and using cylinder cup test
- HTHP rheology test
- Perform modelling and simulations based on the measured data

Reference

1. Darley, H.C.H., and Gray, G.R., “Composition and properties of Drilling and Completion fluids”, Fifth Edition 1988, (ISBN 0-87201-147-X)
2. Economides, M.J., Watters, L.T., and Dunn-Norman, S., “Petroleum Well Construction”, 1998 (ISBN 0-471-96938-9)
3. Fjær, E., HoIt, R.M., Horsrud, P., Raaen, A.M., Risnes, R., “Petroleum Related Rock Mechanics”, Elsevier (1992), (ISBN 978-0-444-50260-5)
4. Aston, M.S., Alberty, M.W., McLean, M.R., de Jong, H.J., and Armagost, K., “Drilling Fluids for Wellbore Strengthening”, Paper SPE 87130, 2004, Presentation at the IADC/SPE Drilling Conference held in Dallas, Texas, U.S.A., 2-4 March 2004
5. Aadnøy, B. S., and Looyeh, R., “Petroleum Rock Mechanics”, First Edition 2011, (ISBN 978-0-12-385546-6)
6. Aadnøy, B. S., and Chenevert, M.E., “Stability of Highly Inclined Boreholes”, Journal Paper SPE 16052-PA , SPE Drilling Eng. (1987)
7. Belayneh, M., “Experimental and Analytical Borehole Stability Study”, Stavanger University College. 2004
8. Aadnøy, B.S., “Geomechanical Analysis for Deep-water Drilling”, SPE 39339 paper presented at the IADC/SPE Drilling Conference, Dallas, TX, 3 - 6 March, 1998
9. Alberty, M.W., and McLean, M.R., “A Physical Model for Stress Cages” SPE 90493, BP Exploration (2004)
10. Whitfill, D(Halliburton)., “Lost Circulation Material Selection, Particle Size Distribution and Fracture Modeling with Fracture Simulation Software”, Paper IADC/SPE 115039, Proceedings of the IADC/SPE Asia Pacific Drilling Technology Conference and Exhibition held in Jakarta, Indonesia, 25-27 August 2008
11. Anton G., “Lost circulation experimental study in Oil Based mud and modeling experimental data”, MSc. Thesis for Faculty of Science and Technology at UiS 2012

-
12. Aadnøy B. S., and Belayneh M., “Elasto-plastic Fracturing Model for Wellbore Stability Using Non-penetrating Fluids”, Journal of Petroleum Science and Engineering, Volume 45, 3-4, Pages 179-192, December, 2004
 13. Aadnøy, B. S., Belayneh, M., Arriado, M., and Flateboe, R., “Design of Well Barriers To Combat Circulation Losses”, Journal of SPE Drilling & Completion Vol 23, Number 3, SPE 105449, 2008
 14. Mostafavi V.T., “ Experimental Analysis and Mechanistic Modeling of Wellbore Strengthening”, Phd. Thesis for Univeristy of Calgary 2011
 15. Binh Bui, Arild Saasen, Jason Maxey, Mehmet E. Ozbayoglu, Stefan Z. Miska, Mengjiao Yu, Nicholas E. Takach., “Viscoelastic Properties of Oil-Based Drilling Fluids,” Annual Transactions of the Nordic Rheology Society, Vol. 20, 2012
 16. Rheology : Technical Bulletin, Kelco Oil Field Group
<http://www.kofg.com/Technical%20Bulletins/E.%20Rheology/5.%20KOFGRheologyEnglish.pdf> (Accessed: 27th March 2014)
 17. Messenger, J.U., “Lost Circulation”, Pennwell Publishing Company. Tulsa, Oklahoma, 1981, (ISBN: 978-0878141753)
 18. Mitchell, R. F., Miska, S. Z. & Aadnoy, B.S., “Fundamentals of drilling engineering”, Society of Petroleum Engineers (2011) (ISBN: 978-1-55563-207-6)
 19. Bourgoyne, A.T. Jr., Millheim, K.K., Chenevert, M.E., and Young J, F.S., “Applied Drilling Engineering”, SPE Textbook Series Vol. 2, 1991. Richardson, Texas (ISBN: 978-1-55563-001-0)
 20. WellPlan (Landmark)TM Software, Halliburton
 21. ANSYS Release 13 Mechanical APDL Software
 22. Gucuyener, I.H., “A Rheological Model for Drilling fluids and Cement Slurries”, Middle East Technical U., (1983) SPE11487
 23. Olaf Skjeggstad., “Boreslam Teknologi”, 1989 (ISBN 82-419-0010-4)
 24. Marilyn Viloría Ochoa., “Analysis of Drilling Fluid Rheology and Tool Joint Effect to reduce Errors in Hydraulics Calculations”, PhD thesis, August 2006

-
25. Tehrani A., “Behaviour of Suspensions and Emulsions in Drilling Fluids”, Annual Transactions of the Nordic Rheology Society, Vol. 15, 2007
 26. Versan, M., and Tolga, A., “Effect of Polymers on the Rheological properties of KCl/Polymer Type Drilling Fluid,” Energy Sources, (2005) 27,405
 27. Zamora, M., and Power, D., “Making a Case for AADE Hydraulics and the Unified Rheological Model,” paper AADE-02-DFWM-HO-13 presented at the 2002 AADE Technical Conference, Houston, 2-3 April.
 28. Zamora, M., Roy, S. and Slater, K., “Comparing a Basic Set of Drilling Fluid Pressure-Loss Relationships to Flow-Loop and Field Data,” Paper AADE-05-NTCE-27 presented at the AADE 2005 National Technical Conference and Exhibition, Houston, 5-7 April.
 29. Whitfill, D.L., Jamison, D.E., Wang, M., and Thaemlitz, C., “New Design Models and Material Provide Engineered Solutions to Lost Circulation”, SPE 101693 paper presented at the SPE Russian Oil and Gas Technical Conference and Exhibition held in Moscow, Russia, 3-6 October 2006
 30. Growcock F.B., Ellis C.F., and Schmidt D.D., “Electrical Stability, Emulsion Stability, and Wettability of Invert Oil-Based Muds”, SPE Annual Technical Conference and Exhibition in New Orleans, 23-26 September 1990
 31. RP 13B, Recommended Practice for Standard Procedure for Field Testing Drilling Fluids, 12th edition, API, Dallas (1988)
 32. <http://www.wee-solve.de/English/Rheologie/Methoden/Frequenztest.htm>
(Accessed: 18th April 2014)
 33. Mingqin Duan, Stefan Miska, Mengjiao Yu, Nicholas Takach, and Ramadan Ahmed, SPE, University of Tulsa; and Claudia Zettner, SPE, ExxonMobil., “Critical Conditions for Effective Sand-Sized Solids Transport in Horizontal and High-Angle Wells”, SPE 106707-PA SPE Drilling & Completion Volume 24, Number 2 June 2009

-
34. Larsen T.I., Pilehvari A.A., and Azar J.J., “Development of a New Cuttings Transport Model for High-Angle Wellbores Including Horizontal Wells”, SPE Rocky Mountain Regional/Low Permeability Reservoir Symposium, Denver, 12-14 April, SPE-25872-MS
 35. Nazari T., Hareland G., and Azar J.J., “Review of Cuttings Transport in Directional Well Drilling: Systematic Approach”, SPE 132372, SPE Western Regional Meeting, 27-29 May 2010, Anaheim, California, U.S.A
 36. Horsrud P., Bostrøm B., Sønstebø, E.F, and Holt, R.M., “Interaction between shale and water-based drilling fluids: Laboratory exposure tests give new insight into mechanisms and field consequences of KCL contents”, SPE 48986 paper prepared for presentation at the SPE Annual Technical Conference and Exhibition held in New Orleans, Louisiana, 27-30 September 1998
 37. Aadnoy, B.S., and Ong, S., “Introduction to special issue on Borehole Stability”, Petroleum Science and Engineering, (2003)
 38. Haimson, B., and Fairhurst, C., “Hydraulic fracturing in porous-permeable materials”, SPE 2354 paper presented at SPE 43rd Annual Fall Meeting held in Houston, Tex., September 29-October 2, 1968
 39. Thomas G. Mezger., “The Rheology Handbook”, 2002, (ISBN 3-87870-745-2)
 40. <http://people.sju.edu/~phabdass/physics/nonN.gif> (Accessed: 11th February 2014)

Appendix

Appendix A: Rheology Models and Model Parameters

Based on different rheology model, shear stress were calculated and compared with experimental data. From the best fit, the rheology parameters are determined. The sum of the average % error between the models and the experimental measured data are calculated and shown in the tables.

Rheology Measurement of 70/30 OWR at Normal Temperature (80F)

Model	Equation	Parameters			Error
Herschel Buckley	$0,5235*\gamma^{0,8767}+14,26$	$\tau_0=14.26$	$k=0,5235$	$n=0,8767$	1,35
Unified	$13,871+0,5385*\gamma^{0,8721}$	$\tau\gamma=13.871$	$k=0,5385$	$n=0,8721$	1,21
Power Law	$4,5917*\gamma^{0,5385}$		$k=4,5917$	$n=0,5385$	12,00
Bingham	$0,2176*\gamma+17,461$		$\mu\rho=104.19$	$\tau\gamma =17,461$	16,16
Newtonian	$0,2423*\gamma$		$\mu=116.01$		38,73

For Bingham : $\mu\rho = 0.2176 \times 47880 / 100 = 104.1869$ cp.

For Newtonian, $\mu = 0.2423 \times 47880 / 100 = 116.0132$ cp.

Rheology Measurement of 70/30 OWR at 120F

Model	Equation	Parameters			Error
Herschel Buckley	$0,5209*\gamma^{0,8125}+14,26$	$\tau_0=14.26$	$k=0,5209$	$n=0,8125$	1,99
Unified	$13,871+0,6407*\gamma^{0,7794}$	$\tau\gamma=13.871$	$k=0,6407$	$n=0,7794$	1,52
Power Law	$3,7588*\gamma^{0,507}$		$k=3,7588$	$n=0,507$	10,11
Bingham	$0,1387*\gamma+14,287$		$\mu\rho=66.41$	$\tau\gamma =14,287$	19,35
Newtonian	$0,159*\gamma$		$\mu=76.13$		41,50

For Bingham : $\mu\rho = 0.1387 \times 47880 / 100 = 66.4096$ cp.

For Newtonian, $\mu = 0.159 \times 47880 / 100 = 76.1292$ cp.

Rheology Measurement of 70/30 OWR at 180F

Model	Equation	Parameters			Error%
Herschel Buckley	$0,3751*\gamma^{0,8147}+14,26$	$\tau_o=14.26$	$k=0,3751$	$n=0,8147$	2,21
Unified	$13,871+0,2796*\gamma^{0,8618}$	$\tau_{yl}=13.871$	$k=0,2796$	$n=0,8618$	3,40
Power Law	$3,4449*\gamma^{0,4743}$		$k=3,4449$	$n=0,4743$	10,25
Bingham	$0,0989*\gamma+12,469$		$\mu p=47.35$	$\tau_y =12,469$	20,43
Newtonian	$0,1166*\gamma$		$\mu=55.83$		43,60

For Bingham : $\mu p = 0.0989 \times 47880 / 100 = 47.3533$ cp.

For Newtonian, $\mu = 0.1166 \times 47880 / 100 = 55.8281$ cp.

Rheology Measurement of 90/10 OWR at Normal Temperature (80F)

Model	Equation	Parameters			Error
Herschel Buckley	$0,2393*\gamma^{0,827}+20,96$	$\tau_o =20,96$	$k=0,2393$	$n=0,827$	1,67
Unified	$21,34+0,3185*\gamma^{0,7812}$	$\tau_{yl} = 21.34$	$k=0,3185$	$n=0,7812$	1,54
Power Law	$5,1835*\gamma^{0,3655}$		$k=5,1835$	$n=0,3655$	11,91
Bingham	$0,0698*\gamma+13,024$		$\mu p=33.42$	$\tau_y=13,024$	10,65
Newtonian	$0,0883*\gamma$		$\mu=42.28$		46,23

For Bingham : $\mu p = 0.0698 \times 47880 / 100 = 33.4202$ cp.

For Newtonian, $\mu = 0.0883 \times 47880 / 100 = 42.2780$ cp.

Rheology Measurement of 90/10 OWR at 120F

Model	Equation	Parameters			Error
Herschel Buckley	$0,2381*\gamma^{0,7705}+20,96$	$\tau_o =20,96$	$k=0,2381$	$n=0,7705$	1,21
Unified	$21,34+0,3695*\gamma^{0,7007}$	$\tau_{yl} = 21.34$	$k=0,3695$	$n=0,7007$	2,30
Power Law	$5,8836*\gamma^{0,3018}$		$k=5,8836$	$n=0,3018$	11,00
Bingham	$0,0478*\gamma+12,594$		$\mu p=22.89$	$\tau_y=12,594$	8,73
Newtonian	$0,0657*\gamma$		$\mu =31.49$		48,97
k (lbfsec ⁿ /100sq ft) $\tau_{yl} = \text{lbf}/100\text{sqft}$, $\tau_o = \text{lbf}/100\text{sqft}$ $\tau_y = \text{lbf}/100\text{sqft}$					

For Bingham : $\mu p = 0.0478 \times 47880 / 100 = 22.8866$ cp.

For Newtonian, $\mu = 0.06578 \times 47880 / 100 = 31.4955$ cp.

Rheology Measurement of 90/10 OWR at 180F

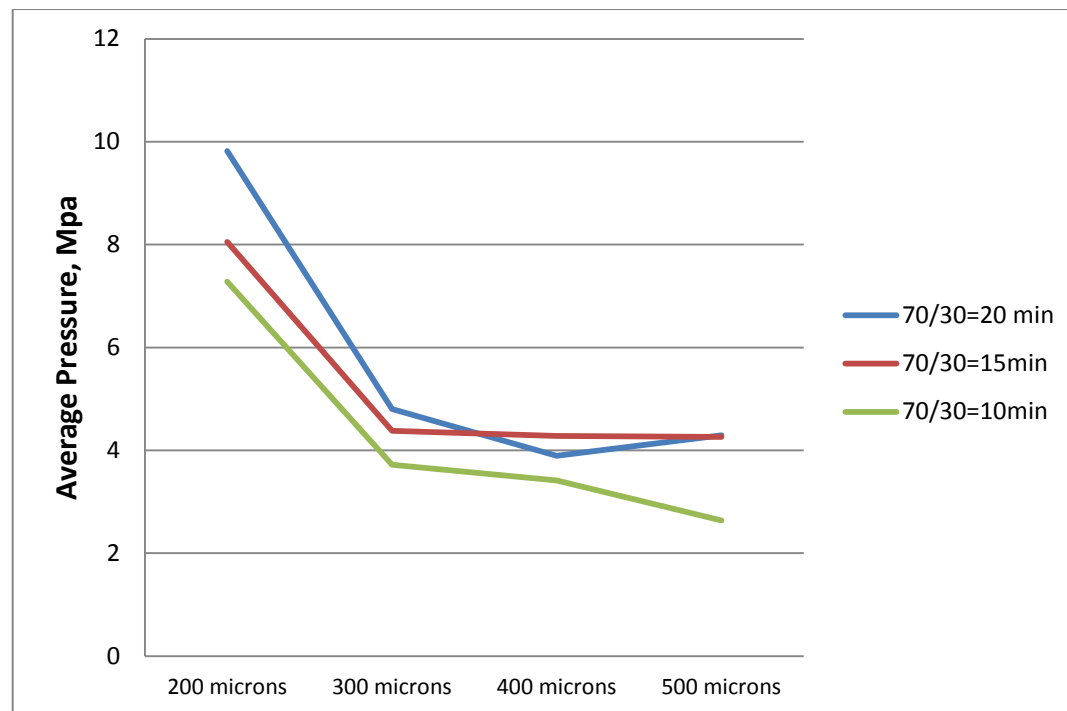
Model	Equation	Parameters			Error
Herschel Buckley	$0,5834 \cdot \gamma^{0,5938} + 20,96$	$\tau_o = 20,96$	$k = 0,5834$	$n = 0,5938$	4,05
Unified	$21,34 + 1,0786 \cdot \gamma^{0,5003}$	$\tau_{y1} = 21.34$	$k = 1,0786$	$n = 0,5003$	5,39
Power Law	$6,0054 \cdot \gamma^{0,2675}$		$k = 6,0054$	$n = 0,2675$	8,93
Bingham	$0,0347 \cdot \gamma + 12,289$		$\mu p = 16.6144$	$\tau y = 12,289$	10,65
Newtonian	$0,0521 \cdot \gamma$		$\mu = 24.9455$		52,08

For Bingham : $\mu p = 0.0347 \times 47880 / 100 = 16.61436$ cp.

For Newtonian, $\mu = 0.0521 \times 47880 / 100 = 24.94548$ cp.

Appendix B: Bridging Tests 70/30 & 90/10 OBMs after 10, 15 & 20 min

The average pressure trend shows a declination from lower micron to higher micron for almost all time measurements. The highest average pressure reaching is 9,8 MPa at 20 minutes running of 200 microns. The declination of average pressure trend is almost the same from 200 microns to 300 microns for all time measurements. The declination trend also continues from 300 microns to 400 microns for the time of 10- and 20-minutes. But the average pressure from 300 microns to 500 microns is almost stable for the time of 15-minutes. The reason of the stable average pressure trend could be the suspension of particle settling that it takes more time to settle down the particles on the mouth of the fracture due to the viscous drilling fluid.

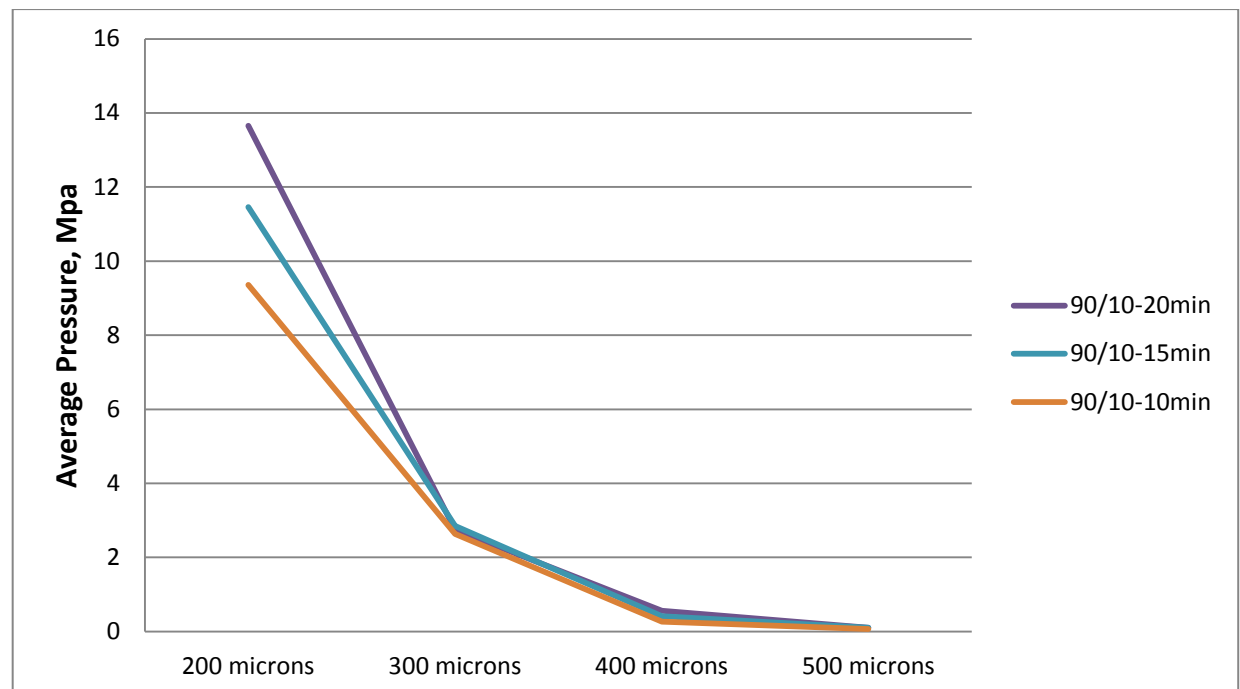


We can assume that most particles settle down across the slot opening around the time of 15-minutes for the 70/30 OBM.

The declination of average pressure trend is perfect for the time of 10-minutes that the highest average pressure with 7,3 MPa at 200 microns and the lowest average pressure with 2,6 MPa at 500 microns.

90/10 OWR after 10 min, 15 min and 20 min

The decreasing average pressure trend from lower to higher slot openings shows a reasonable assumption for a less viscous Oil-Based Mud like 90/10. The highest pressure gap is occurred at the 200 microns and the highest average pressure reaching is 13,65 MPa at 20 minutes running of 200 microns. The lowest average pressure reaching is 9,35 MPa at 10 minutes running of 200 microns. The reason of the increment of average pressure during the time increased is that the bridge development is gradually better after time. In the end the bridge is perfectly form and the slot is totally plugged after the time of 22 minutes



From this point, the average pressure variation is almost identical for 300 microns, 400 microns and 500 microns in different time measurements. The reason of the identical average pressure trend occurrence is because of the effect of the viscosity of the drilling fluid and wider slot opening. In the experiment with 400 microns, the average pressure varies from 0,27 to 0,56 MPa in different time measurements that almost no pressure build-up is achieved during the test. And the result with the experiment with 500 micron shows more obvious that the average pressure is almost 0 MPa throughout the test in different time measurements.

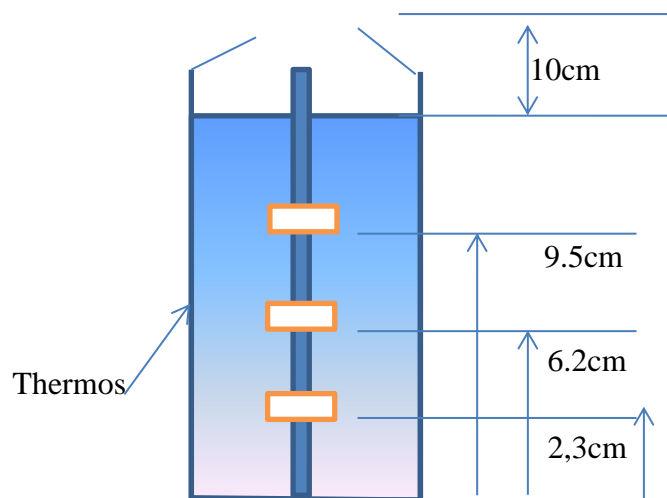
Appendix C: Thermal conductivity of drilling fluid

In this thesis, the measurement of the thermal conductivity of the two mud systems is performed. Since the measurement technique is new and we are not sure if it actually describes the physics, we only outline how we made the experiment and the results.

70/30 OWR Drilling Fluid

The cooked drilling fluid is put into the thermos cup and thermometers was tied wooden stick is also put into the cup. The height of the drilling fluid in the cup is about 10,0 cm.

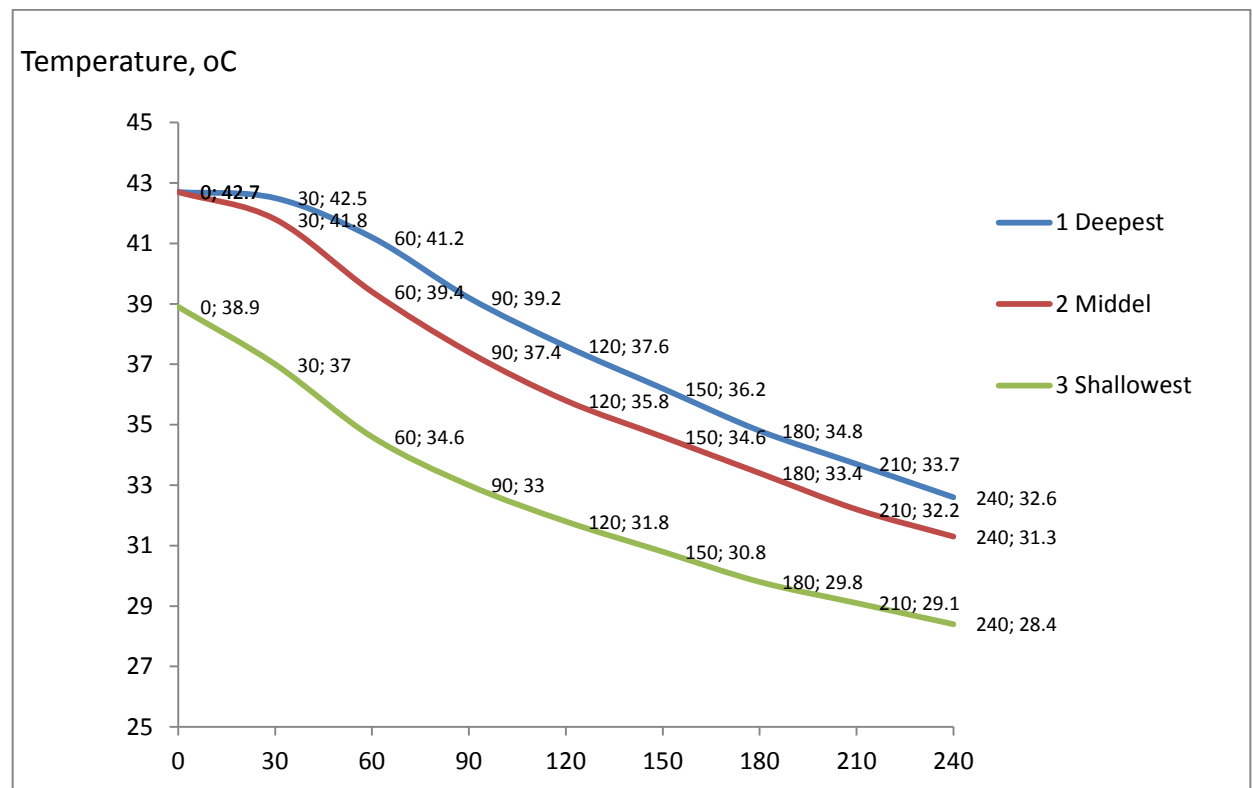
- 1. Temperature Measurement – 2,3 cm from the bottom of the cup (Deepest)
- 2. Temperature Measurement – 6,2 cm from the bottom of the cup (Middle)
- 3. Temperature Measurement – 9,5 cm from the bottom of the cup (Shallowest)



The 70/30 Oil-Based Mud was boiled until the temperature of the drilling fluid reached at 43C (or 109F).

Even if we measured the temperature in different depths, we assume that the heat capacity is the same due to the exponent of all three temperature points is the same as

-0,001. It can also be assumed that we measured one drilling fluid in different depths that we got a common exponent value.



Experimental Data Modelling

Based on the experimental data trend, we can assume that the temperature decay can be as exponential. This can be modeled as:

$$dT/dt \propto T$$

where α is temperature decrease by time. The slop of the decay is defined as $\Delta T/\Delta t$ where ΔT is temperature ... and Δt is time

Solving:

$$dT/dt = - \alpha T$$

$$T_s \int^T dt/T = - \alpha \int_0^t dt$$

$$\ln (T/T_s) = - \alpha t$$

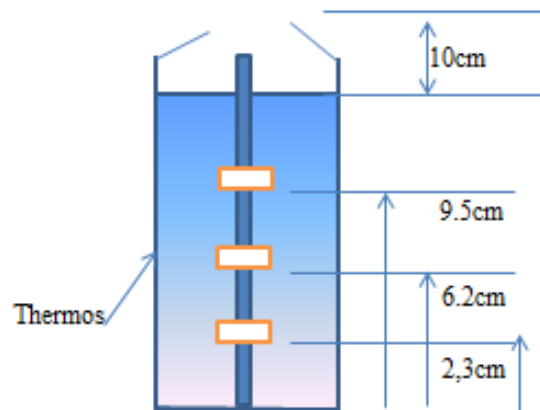
$$T = T_s e^{-\alpha t}$$

- $T = 43,593e^{-0,001t}$ (Deepest Point Measurement)
- $T = 42,703e^{-0,001t}$ (Middel Point Measurement)
- $T = 37,918e^{-0,001t}$ (Shallowest Point Measurement)

90/10 OWR Drilling fluid

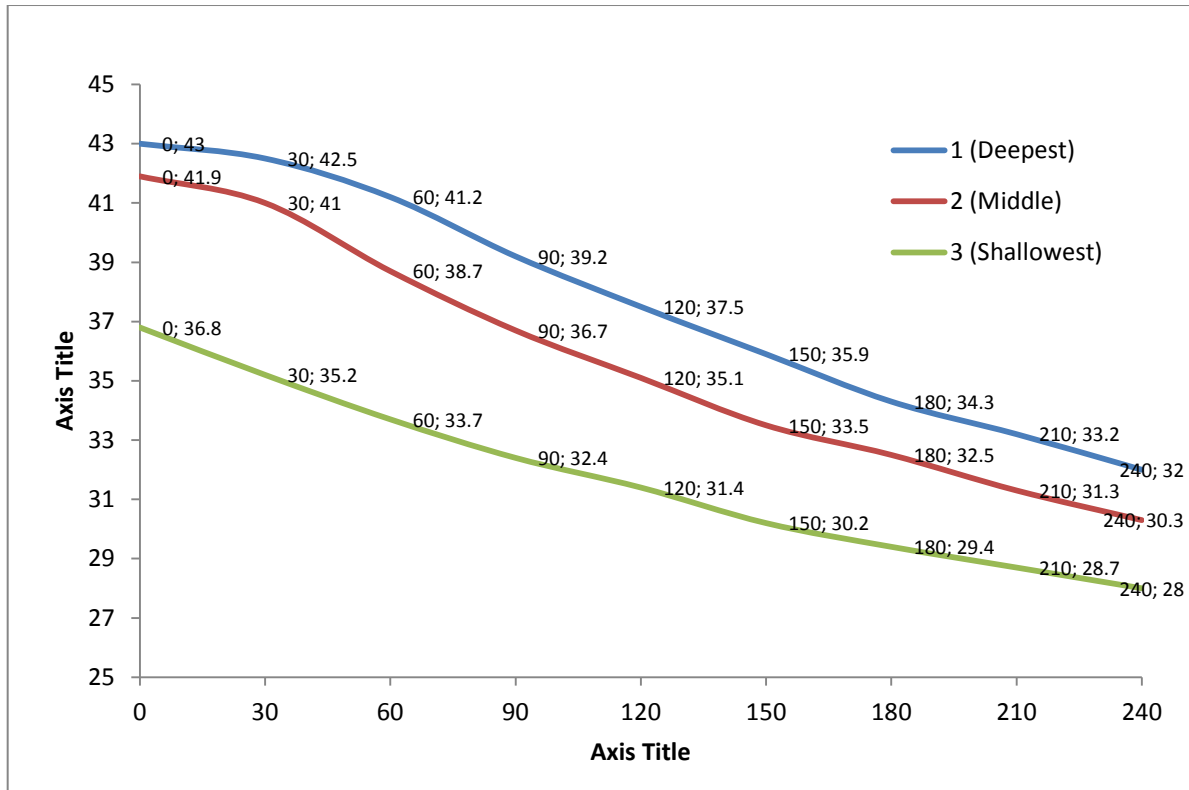
Similarly the cooked drilling fluid is put into the thermos cup and thermometers was tied wooden stick is also put into the cup. The height of the drilling fluid in the cup is about 10,0 cm.

- 1. Temperature Measurement – 2,3 cm from the bottom of the cup (Deepest)
- 2. Temperature Measurement – 6,2 cm from the bottom of the cup (Middle)
- 3. Temperature Measurement – 9,5 cm from the bottom of the cup (Shallowest)



The 90/10 Oil-Based Mud was cooked until the temperature of the drilling fluid reached at 43C (or 109F).

Measurement of the immediate temperature of the drilling fluid in the cup was performed at 13:05 but the temperature was unstable in the beginning. The temperature was inclining until it reached the highest point. It took over 12 minutes to reach the highest temperature point for all three measurements (at 13:18). The highest temperature reached for point 3 (Shallowest) was 36,8 C at 13:10 hr. The temperature of the point 3 was started to decrease to 36,7 C at 13:13 hr. The temperatures of other two points were not stable and continued to incline at that time.



We get the same exponential number for 90/10 OWR drilling fluid as for 70/30 OWR drilling mud. The common exponential number is $-0,001$ and the exponential number is the same for all three different points.

Experimental Data Modelling

Based on the experimental data trend, we can assume that the temperature decay can be as exponential. This can be modeled as:

- $T = 43,593e^{-0,001t}$ (Deepest Point Measurement)
- $T = 42,703e^{-0,001t}$ (Middel Point Measurement)
- $T = 37,918e^{-0,001t}$ (Shallowest Point Measurement)

Appendix D: Hydrodynamic Force Effect on Hook Load – Tripping In

The Hook Loads of the two drilling fluids during tripping in are computed for elevated temperature. Since the densities of the drilling fluids at various temperatures were not measured, it is assumed that the 120 and 180°F decrease the density by 5 and 10% respectively. Two different flow rates of 0 and 400gpm are used for the simulation.

Tripping in of 70/30 OBM for 0 and 400gpm flow rates

Temperature/ % density decrease	Hook Load (tons) when Flow rate =0 gpm	Hook Load (tons) when Flow rate =400 gpm	Increase in tons (Flow rate=0gpm)	Increase in tons (Flow rate=400gpm)
80F (Reference)	73	72		
120F (5% density Decrease)	74	74	1,0	1,4
180F (10% Decrease)	75	75	1,9	2,4

As shown in Table above, the calculation of the hydraulic force effect on the Hook Load during tripping in for the 70/30 OBM is performed. At the 0gpm flow rate, the Hook Load increases from 1.0 tons to 1.9 tons when the temperature increases from 80oF to 120oF and 180oF respectively. At the flow rate of 400gpm, the Hook Load increases from 1.4 tons to 2.4 tons due to the temperature elevated from 80oF to 120oF and 180oF respectively.

Tripping in of 90/10 OBM for 0 and 400gpm flow rates

Temperature/ % density decrease	Hook Load (tons) when Flow rate =0 gpm	Hook Load (tons) when Flow rate =400 gpm	Increase in tons (Flow rate=0gpm)	Increase in tons (Flow rate=400gpm)
80F (Reference)	74	74		
120F (5% Decrease)	75	75	0,9	0,9
180F (10% Decrease)	76	76	1,8	1,9

The simulation result of the hydraulic force effect on Hook Load for the 90/10 OBM is shown in the Table above. At 0gpm flow rate, the Hook Load increases from 0.9 tons to 1.8 tons due to the temperature elevated from 80oF to 120oF and 180oF respectively. As flow rate increased to 400gpm, the Hook Load increases from 0.9 tons to 1.9 tons due to the temperature increased from 80oF to 120oF and 180oF respectively.

Appendix E: Hole and drill string data for simulating §4.2 & §4.3

Hole data (Casing + Open hole)

	Section type	Measured Depth (ft.)	Length (ft.)	Shoe Measured Depth (ft.)	Id (In)	Drift (In)	Effective Hole Diameter (In)	Friction factor	Linear Capacity (bbl/ft)	Excess (%)	Item Description
1	Casing	4012.5	4012.5	4012.5	12.250	12.459	12.615	0.25	0.1458		13 3/8in, 54.5ppf, J-55
2	Open Hole	11003.0	6990.50		12.250		12.250	0.30	0.1458	0.00	

Table E.1: Hole data (Casing + Open hole)

Drill String data (Drill pipe + BHA)

Type	Length (ft)	Depth (ft)	Body OD (in)	Stabilizer/tool joint					Weight (ppf)	Material	Grade	Class
				ID (in)	Avg. joint Length (ft)	Length (ft)	OD (in)	ID (in)				
Drill pipe	10445	10445.00	5.0	4.276	30.00	1.42	6.406	3.75	22.26	CS_API 5D/7	E	P
Heavy weight Drill pipe	120.0	10565.0	6.625	4.5	30.00	4.00	8.25	4.5	70.50	CS_1340 MOD	1340 MOD	
Hydraulic Jar	32.00	10597	6.5	2.75					91.79	CS_API 5D/7	4145H MOD	
Heavy weight Drill pipe	305.0	10902	5.0	3.0	30.00	4.00	6.50	3.063	49.7	CS_1340 MOD	1340 MOD	
Bit sub	5.00	10907	6.0	2.4					79.51	CS_API 5D/7	4145H MOD	
MWD tool	85.00	10992	8.0	2.5					154.36	SS_15-15LC	15-15LC MOD	
Integral blade stabilizer	5.00	10997	6.25	2.0		1.00	8.453		93.72	CS_API 5D/7	4145H MOD	
Bit sub	5.00	11002	6.0	2.4					79.51	CS_API 5D/7	4145H MOD	
Tri-cone bit	1.00	11003	10.625						166.0			

Table E.2: Drill String data (Drill pipe + BHA)

List of figures

Figure 1.1: Illustration of the 70/30 & 90/10 Oil Based Mud systems

Figure 2.1: Non-penetrating borehole

Figure 2.2: Penetrating borehole and possible pore fluid distribution

Figure 2.3: Stress cage concept to enhance wellbore strength

Figure 2.4: Fracture sealing in permeable rocks

Figure 2.5: Fracture sealing in low-permeability rocks

Figure 2.6 A: Cylindrical bridge at the mouth of the fracture

Figure 2.6 B: Description of the fracture process

Figure 2.7: Amplitude Test G' and G'' moduli plotted against the deformation

Figure 2.8: The Frequency Sweep Test

Figure 2.9: Types of Lost Circulation

Figure 2.10: Rheology Model for different fluids

Figure 2.11: Diagram of the drilling fluid circulating system

Figure 3.1: Rheology data for 70/30 and 90/10 OBMs in different temperatures

Figure 3.2: Comparison of Error % for the 70/30 and 90/10 OBMs at the 80, 120 and 180 °F temperatures

Figure 3.3: Comparison of the individual mud systems at the 80, 120 and 180 °F temperatures

Figure 3.4: Comparison of the HPHT filtration for the 70/30 and 90/10 OBMs

Figure 3.5: ES measurement of Before and After Modification for the 70/30 and 90/10 OBMs

Figure 3.6: Volume of filtration test for the 70/30 OBM (Before & After Modification) and 90/10 OBM

Figure 3.7: Comparison of different rheology models measurement of the 70/30 OWR at normal temperature (80 °F)

Figure 3.8: Comparison of the different rheology models errors of the 70/30 OWR at the 80, 120 and 180 °F

Figure 3.9: Comparison of different rheology models measurement of the 90/10 OWR at normal temperature (80 °F)

Figure 3.10: Comparison of the different rheology models errors of the 90/10 OWR at the 80, 120 and 180 °F

Figure 3.11: Comparison of the temperature effect on the Plastic Viscosity of the 70/30 and 90/10 OWR

Figure 3.12: Comparison of the temperature effect on the Yield Stress of the 70/30 and 90/10 OWR

Figure 3.13: Simulation well for hydraulic analysis

Figure 3.14: Comparison of the frictional pressure losses of the 70/30 and 90/10 OWR at the 80, 120 and 180°F based on the Unified Hydraulics model

Figure 3.15: Comparison of the error% for the 70/30 and 90/10 OWR based on temperature differences

Figure 3.16: Comparison of the error% for the 70/30 and 90/10 OWR based on temperature elevated from 80-120°F and 80-180°F

Figure 3.17: Illustration of diffusion of 70/30 OBM in Sandpack

Figure 3.18: Illustration of diffusion of 90/10 OBM in Sand pack

Figure 3.19: Diffusion of the 70/30 and 90/10 OBMs against Time

Figure 3.20: Illustration of the Anton Paar MCR 301 Rheometer

Figure 3.21: Amplitude sweep test of the 70/30 and 90/10 OBM systems

Figure 3.22: Sweep frequency test for 90/10 OBM system

Figure 4.1: Schematic particle bridging testing experimental set-up

Figure 4.2: Drilling fluid rheology for 70/30 and 90/10 OBM

Figure 4.3: LC-Lube particle size distribution

Figure 4.4: Cumulative Percentage of LC-Lube

Figure 4.5 SEM picture of LC-lube at magnification of 60x

Figure 4.6: Pressure Profile of the 70/30 and 90/10 OBM for Bridging Test with 200 slot opening

Figure 4.7: Pressure Profile of the 70/30 and 90/10 OBM for Bridging Test with 300 slot opening

Figure 4.8: Pressure Profile of the 70/30 and 90/10 OBM for Bridging Test with 400 slot opening

Figure 4.9: Pressure Profile of the 70/30 and 90/10 OBM for Bridging Test with 500 slot opening

Figure 4.10: Maximum Pressure in tests with various Slot widths

Figure 4.11: Average Pressure in tests with various Slot widths

Figure 4.12: Average Peak Pressure in tests with various Slot widths

Figure 4.13: Number of peak as a function of Slot width

Figure 4.14: Simulation experimental well

Figure 4.15: Well inclination of the simulation

Figure 4.16: Comparison of the Bed Height between two mud systems with difference temperatures

Figure 4.17: % Error comparisons of bed height between two drilling fluids

Figure 5.1: Illustration of loads and boundary conditions for scenario 1

Figure 5.2: Deformation and Stress Distribution results by Von Mises of scenario 1
Figure 5.3: Line plot of Von Mises and Stress component along the X-direction (S_x) for scenario 1
Figure 5.4: Line plot of Von Mises and Stress component along the Y-direction (S_y) for scenario 1
Figure 5.5: Illustration of loads and boundary conditions for scenario 2
Figure 5.6: Deformation and Stress Distribution results by Von Mises of scenario 2
Figure 5.7: Line plot of Von Mises and Stress component along the X-direction (S_x) for scenario 2
Table 5.8: Line plot of Von Mises and Stress component along the Y-direction (S_y) for scenario 2
Figure 5.9: Illustration of loads and boundary conditions for scenario 3
Figure 5.10: Deformation and Stress Distribution results by Von Mises of scenario 3
Figure 5.11: Line plot of Von Mises and Stress component along the Y-direction (S_y) for scenario 3
Figure 5.12: Line plot of Von Mises and Stress component along the X-direction (S_x) for scenario 3

List of Tables

Table 2.1: Summary of Unified hydraulics model
Table 3.1 Temperature dependent plastic viscosity models
Table 3.2: Temperature dependent yield stress equations
Table 3.3: Well construction geometry
Table 4.1: Calculated viscosity and measured density of drilling fluids
Table 4.2: Test matrix and average bridging pressure
Table 4.3: Measured and assumed drilling fluid densities used for hook load simulation
Table 4.4: Tripping Out of 70/30 OBM for 0 and 400gpm flow rates
Table 4.5: Tripping Out of 90/10 OBM for 0 and 400gpm flow rates
Table 5.1: Geometry of the Scenario 1
Table 5.2: Geometry of the Scenario 2
Table 5.3: Geometry of the Scenario 3
Table 6.1: Summary of the major investigations

Nomenclature

OWR – Oil Water Ratio

OBM – Oil Based Mud

Lb/bbl (ppb) – Pounds per barrel

ECD – Equivalent Circulating Density